Andrea Ehrmann · Tomasz Blachowicz

Examination of Textiles with Mathematical and Physical Methods

Examination of Textiles with Mathematical and Physical Methods

Andrea Ehrmann • Tomasz Blachowicz

Examination of Textiles with Mathematical and Physical Methods

Andrea Ehrmann
Bielefeld University of Applied
    Sciences
Bielefeld, Germany

Tomasz Blachowicz
Silesian University of Technology
Gliwice, Poland

Preface

Several books are available on the market dealing with well-known physical test methods which are typical for textile fibers, yarns, and fabrics, most of them necessitating expensive test equipment which is not always available to students and researchers.

This book communicates basic knowledge on the examination of textile materials, from fibers to yarns and knitted or woven fabrics, using mathematical and physical methods. Besides typical textile test procedures, defined by well-known standards, the book aims at showing new ways to examine textile materials and giving an overview of the possibilities as well as problems occurring when methods from other areas are transferred into the examination of textiles. The contents range from apparently simple measurements, such as resistance of conductive coatings on woven fabrics, to diffraction measurements on woven fabrics, to optical examination of knitted fabrics by mathematical approaches to study yarn hairiness and cover factor.

While some chapters focus on the easy realization of self-built, inexpensive lab equipment according to defined test standards, others provide new ideas to test textile materials with novel methods. The combination of textiles and mathematics, for example, cannot be found in a book yet; apparently mathematical methods have not yet been adopted in many cases from other areas into the examination of textiles.

Alternatively, measurements can be adopted from other scientific areas. In this case, the deviations of measurements on textiles from tests on rigid materials are described to avoid useless measurements and resulting interpretation errors.

The measurements described here include (but are not limited to) optical examinations of fibers, yarns, and fabrics by different microscopic techniques; optical evaluation using a focused (laser) beam for diffraction images; image processing techniques for investigation of textile materials; tests of mechanical properties of textiles; thermal properties of fibers, yarns, fabrics, and coatings; special investigations of conductive or magnetic yarns; etc.

We wish you an inspiring reading and a lot of success while testing your textiles, building your own test equipment, and developing existing methods further.

Bielefeld, Germany   Andrea Ehrmann
Gliwice, Poland   Tomasz Blachowicz

Contents

About the Authors

Andrea Ehrmann (née Tillmanns) has studied physics in the RWTH Aachen University and finished her Ph.D. in magneto-optical examination of thin film samples. Afterward, she started working as a scientific coworker in the Niederrhein University of Applied Sciences, Faculty of Textile and Clothing Technology. In research projects as well as in teaching, she deals with intelligent/functional textiles, optical examination of textile materials, spectroscopic methods used for textiles, and transfer of physical and also mathematical methods well known from other fields onto textile fabrics.

She has been working on the topics of this book for more than 10 years in Niederrhein University of Applied Sciences. Since 2015, she is full professor for physics, measurement technology, and textile technologies in Bielefeld University of Applied Sciences where she built up a textile research laboratory and a research group concentrating on measurement processes related to the whole textile chain.

Tomasz Blachowicz has studied physics in the Pedagogical University Krakow and finished his Ph.D. in the Silesian University of Technology and his habilitation in Gdansk University with a focus on Brillouin spectroscopy of bulk crystals and non-transparent layers.

He is professor at Silesian University of Technology since March 2009. While teaching all areas of physics, including technical physics and simulation of physical phenomena, he has additionally long-lasting experience in research on optical properties of materials, experimental design, and the application of mathematical and physical methods on textile materials, e.g., transfer of the random-walking approach used for the calculation of cave systems onto textile fabrics in order to calculate their hairiness, or utilization of statistical methods to understand the relaxation process of knitted fabrics.

Chapter 1
Measurement Technology in Textile Industry and Research

We understand our world and the things which surround us using our senses, such as our eyes and ears. All our senses, however, are prone to misperceptions. Depending on the situation and our environment, times or lengths can be over- or underestimated. Other measures are misjudged due to our lack of the possibility of comparison.

Measuring, counting, and weighing are, as Plato (427–347 BC) already mentioned, the best way to avoid such misperceptions and to eliminate the domination of our senses. Thus, measuring and calculating the desired values from these results should be preferred to the pure sensory perception.

Galileo Galilei (1564–1642) recapitulated this idea of the quantitative determination of phenomena in the principle that everything which can be measured should be measured and everything which cannot be measured should be made measurable. Replacing sensual perceptions by measurement instruments should lead to mathematical descriptions of the experimentally found rules, resulting in experiments to evaluate these theoretical models. Subjective descriptions should be completely eliminated in favor of objective measures.

Nowadays, measurement technology is necessary in a variety of areas, starting from production processes in which the desired reproducibility is ensured by permanent quality control to high-precision measurements in research, often using unique and expensive equipment which is built for one special purpose.

In textile industry and research, measurement methods range from simple and inexpensive equipment to rare special devices. Several methods still include the "human factor," using subjective measurement procedures, such as tactile tests by touching fabrics with the hands. Others are highly objective and reproducible.

This book aims at giving an overview of possible measurement methods, mostly without too specialized equipment. Most important in all measurement processes, however, is not only to use reliable equipment but also to understand the used procedures well enough to be able to detect possible problems and perturbations—which is much a heavier task in textile testing than in several other material sciences.

Thus, this introduction will give a short overview of measurement technology tasks in common and special textile requirements in particular.

1.1   Measurement Procedures

Several criteria exist to describe or classify measurement procedures. Measuring a length using a scale, e.g., belongs to the direct measurement procedures, while measuring a length by a triangulation technique is identified as indirect procedure. Measurements can be analogue or digital, both realized, e.g., in respective thermometers. Measurement equipment can use a differential method, such as a diode bridge, a compensation method, as in an analytical balance, or do without these enhancements, as in a moving coil instrument.

In some cases—especially when testing several samples—using a gauge with a fixed adjustment, showing directly whether a sample is inside its specifications, is easier and faster than measuring each sample with a general measure. There are, e.g., gauges to check lengths, angles, surface straightness, etc.

Measuring values that are not simply countable always requires a scale, such as a meter, a kilogram, or a second. These scales are subject to permanent adjustments—not in order to change them but to allow for more precise definitions.

1 m, e.g., was firstly defined in 1791 as the ten-millionth of the distance between equator and North Pole. An international meter prototype was produced from platinum-iridium in 1889. In 1960, a new definition of a meter as the 1,650,763.73th part of the wavelength radiated by ^{86}Krypton during the transition from $5d^5$ to $2p^{10}$ shells was introduced. Nowadays, the meter is defined as the distance the light travels in the 299,792,458th part of a second (Agnoli and D'Agostini 2005).

Each of these definitions aims at being more exact than the predecessors, while trying not to change the previous definitions.

1.2   SI and Other Unit Systems

In 1960, the Système International d'Unités (SI) was determined, consisting of seven base units of measurement which can be used to derive units for each measurement process.

Additionally, the SI system includes prefixes which are powers of ten, mostly powers of a thousand. Typical examples are kilo, milli, or micro. Rules define how these prefixes are allowed to be used: Only one prefix per unit is allowed; multiples of kilograms use a gram as the base unit (milligram instead of micro-kilogram).

The base units and quantities are meter (length), kilogram (mass), second (time), ampere (electric current), kelvin (absolute temperature), mole (amount of substance), and candela (luminous intensity). Recently, attempts are being made to

derive these base units from one or more constants of nature, such as defining a second as 9,192,631,770 periods of the radiation of the transition between the hyperfine levels of a cesium ^{133}Cs atom in the ground state (Mills 2010).

Some derived units are, e.g., hertz (=1/second), newton (=kilogram * meter/second^2), or coulomb (=second * ampere). The SI specifies 22 of these derived units. Additionally, some units outside the SI are accepted, such as liter, ton, astronomical unit, or daily used units like minute, hour, or day. In special areas of physics, units like electron-volt or electron mass are used as well as bar or ångström, gauss, or œrsted.

Amongst these units which are "allowed" but not included in the SI, some typical textile ones can be found, too. A unit widely used in the textile area is "tex," used to measure fiber fineness not only in yarns and other textile products but also in optical cables or paper. 1 tex is defined as a mass of 1 gram per 1000 meters; yarns with higher fineness (larger tex value) thus have a larger mass per length unit.

The decitex—abbreviated dtex—is even more often used, defining the mass in grams per 10,000 meters.

Another possibility to specify the linear density of fibers is given by the unit denier—abbreviated den or D—which is defined as the mass in grams per 9000 meters. This means that 9 den = 1 tex. The idea behind this—at a first glance strange—definition is that a single silk strand has approximately a linear density of one denier. Fine fibers with maximum one denier are called microfibers. A one-denier fiber of polyester has a diameter of approximately 10 μm.

Other units for the linear density of a fiber or yarn are "number English" (Ne) and "number metric" (Nm), defining an inverse linear density. While Ne is subdivided into different definitions for cotton yarns, linen yarns, worsted yarns, and woolen yarns, the Nm is generally defined as the number of meters of a yarn or fiber having a mass of 1 g. This means that higher Nm values are correlated with finer yarns of fibers. Compared to the unit tex, 1 Nm = 1000/tex.

1.3 Environmental Conditions

Due to the influence of environmental conditions on textile test results, standard atmospheres are defined in the international standard DIN EN ISO 139 which is to be used for sample preparation and the determination of the physical textile properties. A standard atmosphere specifies values of relative humidity and temperature which must be maintained.

Textile fibers are often hygroscopic, i.e., they absorb moisture, resulting in possible changes of their physical properties like their weight, dimensions, rigidity, elongation, and other physical and chemical characteristics. Temperature can also influence textile properties. Additionally, other environmental conditions, such as the atmospheric pressure, have to be taken into account to guarantee reliable measurements. Even the measurement equipment itself can alter due to these

parameters. Thus, standard atmospheres are defined which have to be used in testing rooms (DIN EN ISO 139; Reumann 2013).

In the textile area, sample preparation and testing must be performed at a temperature of (20 ± 2) °C and a relative humidity of (65 ± 4) %; these average values are identical with test conditions for wood (Hänsel 2014). If all involved partners agree, a specific standard atmosphere of (23 ± 2) °C and a relative humidity of (50 ± 4) % may be used which is typical for plastics (DIN EN ISO 291). Samples must be conditioned in the chosen standard atmosphere for a defined time, starting from 2 h for polyester fibers up to 24 h for knitted or woven fabrics.

Additional to these temperature and humidity conditions, several other factors must be taken into account. In a variety of test procedures, vibrations can significantly influence the results. This means on the one hand that measurement instruments must be protected from vibrations due to the influence of other equipment, traffic outside the building, sound waves, or the like. On the other hand, the instruments' vibrations themselves must be minimized by respective vibration damping.

Dust, fibers parts, and other small particles can also influence results especially of optical inspections. Air currents can even distort weighing results. In all measurements, these environmental conditions must be controlled and, if necessary, compensated.

1.4   Error Calculation

Measurement errors—or observational errors—can be subdivided into blunders, systematic errors, and random errors. The latter belong to measurements and measuring processes; they are no sign of any mistake being made (Taylor 1999).

Blunders describe mistakes which can be avoided by a critical review of the measurement setup and process. They can be based on defect measurement instruments, loose connections, external perturbations, and other instrumental defects. On the other hand, they can arise from human errors, such as exchanging the samples under investigation, using the wrong measurement procedure (e.g., measuring voltage instead of current), ignoring a multiplier in the instrument display, adjusting the equipment in a wrong way, misinterpreting measurement data, etc. Such errors cannot be considered in the evaluation of the measured values; thus they have to be excluded—e.g., by testing retained samples, test measurements in other laboratories or with other instruments, calibrating the measurement equipment with working standards, etc.

Opposite to such mistakes, random and systematic errors can be considered in the statistic evaluation of measurement series—systematic errors are corrected or estimated, while random errors are minimized by multiple measurements and statistical treatments, resulting in the definition of a measurement uncertainty.

Systematic errors are characterized by their appearance: they always occur and keep their sign and their value, resulting in a constant deviation between

measurement value and true value. They can arise, e.g., from erroneous calibration of measurement instruments, interactions between devices and the surrounding or the measurement object, differences between the characteristic curve of the instrument and the nominal characteristic, etc. Systematic errors can often be determined and thus corrected; else they have to be estimated.

Typical systematic errors are zero point error (drift), nonlinearity of the characteristic curve, pitch error, or hysteresis error. Often an envelope can be defined which includes all systematic errors and ensures that the true values can be found within these tolerances. Additionally, time-dependent errors are possible, e.g. a constant drift, a deviation starting at a certain time, or a constant offset which is approached after a certain time. On long timescales, for example, textile measuring tapes which are strongly coiled can lengthen and thus give wrong results in length measurements.

Systematic errors can occur, e.g., in current or voltage measurements where the internal resistance of the instrument results in potential or power drops in the device, respectively. A temperature sensor can heat or cool the measured medium. Measuring physical quantities by electrical means can lead to limitations. Another typical example is based on the Abbe principle that the measured dimension should lie on the line between reference point and sensing point (Zhang 1989)—a principle that is taken into account in a micrometer screw but not in a caliper gauge. In the latter, tilt errors can occur if the caliper gauge is pressed too hard on the measured object.

In all measurements, disturbances (noise) can occur influencing the output signal, additionally to the influence of the measurement signal. Examples for such disturbances are the environmental temperature, fluctuations in the power supply, mechanical vibrations, or humidity. Such disturbances can be eliminated if there are significant differences between desired signal and noise, e.g. different amplitudes, frequencies, signs, or points of application, using filters, calculating the signal difference, or using control engineering approaches.

Besides such systematic errors, random variations of the measured values can occur which are often statistically distributed. They can originate from temperature deviations, interactions between different electronic components, high-frequency cross talk, thermal movements of atoms, thermal radiation, etc. Several independent factors affect the measurement values, with only a small influence of each single factor. Positive and negative influences have the same probability.

Random errors can be differentiated from systematic errors by repeating the measurement under identical conditions. Random errors lead to a distribution of values around a mean value, while a shift of the measured mean value with respect to the true value can occur due to systematic errors. This results in the demand of a measurement to find a measurement value which is as near to the true value as possible, by correcting systematic errors and investigating and taking into account random errors. On the other hand, the time and effort necessary for the elimination or minimization of errors must be weighed against the possible improvement of the measurement uncertainty.

The uncertainty of a single measurement depends on the reading accuracy—which is for analogue instruments based on our eyes, the number of scale lines, lighting conditions, a possible parallax, etc. Additionally, the uncertainty of the measurement equipment is added which is given by accuracy classes which define a maximum intrinsic error based on the maximum value of the scale used—which means that the same value is measured with less accuracy if it is measured on a too large scale. This intrinsic error can become larger for deviations of the nominal range of use—outside, no maximum intrinsic errors are guaranteed. Finally, the experimentation accuracy must be taken into account.

In order to arrange the measured values with their random errors clearly, they can be depicted in a histogram, as shown in Fig. 1.1. Here, the x-axis is subdivided into a chosen number of classes with identical widths. On the y-axis, the number of measured values for each of these classes is depicted. In this way, optical examination of the resulting graph gives a first hint whether the values are normally distributed, i.e., can be approximated by a Gaussian (red line in Fig. 1.1) for large numbers of measurements. Most error analysis methods are only valid for normally distributed results.

The most important properties of a Gaussian are as follows: The maximum is located at the mean μ; the inflection points can be found at $\mu \pm \sigma$ with the standard deviation σ (Fig. 1.2). The standard deviation describes the average deviation from the mean value.

The standard deviation can be calculated by

$$\sigma = \sqrt{\frac{\sum_{i=1}^{n}(x_i - \mu)2}{n}}$$

with the single measurement value x_i, the average μ, and the number of measurements n, if it is related to the complete population—if, e.g., statistics are applied on all coworkers in a company and these statistics are not meant to be transferred to all company workers or the like.

Fig. 1.1 Measurement results with typical Gauss distributed random error
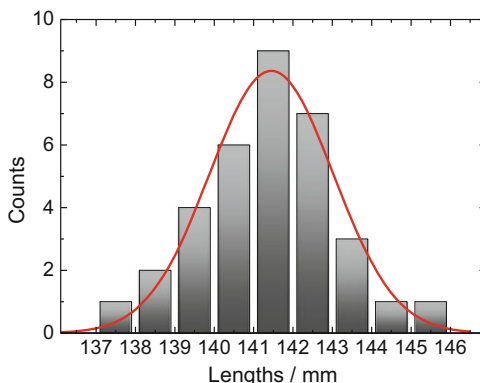
Fig. 1.2 Gauss distributed
measurement results with
mean μ and standard
deviation σ
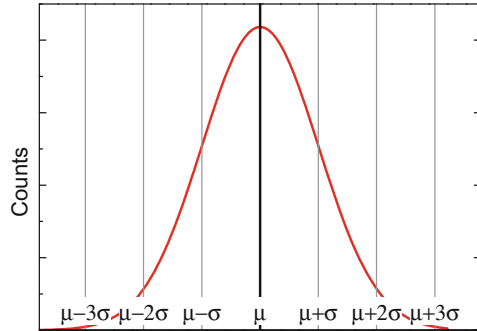
On the other hand, if statistics is based only on a small part of the population, the formula for the standard deviation changes to

$$s = \sqrt{\frac{\sum_{i=1}^{n}(x_i - \mu)2}{n-1}}$$

with a slightly changed denominator. For large numbers of measurements, the difference between both calculations vanishes.

For normally distributed measurement values, it can be shown that approximately 68.3 % of all results can be expected to be within a range of $\mu \pm \sigma$, while 95.5 % of the values are within a range of at $\mu \pm 2\sigma$ and 99.7 % in the range of at $\mu \pm 3\sigma$.

This means, on the other hand, that approximately 32 % of all measured values can be expected to be *outside* the range of $\mu \pm \sigma$—apparently this range must not be confused with the confidence interval.

The confidence interval instead can be calculated by

$$e = t\frac{\sigma}{\sqrt{n}}$$

with the number of measurements n, the standard deviation σ, and the factor t taken from a table of Student's t-distribution (Student 1908). For a typical range of two-sided critical regions of 0.95 (=95 % confidence level) and at least 10 measurements, the value of t is approximately 2. This formula includes the number of measurements which results in the confidence interval being approximately proportional to $1/\sqrt{n}$—if the confidence interval should be smaller by a factor of 2, the number of measurements has to be increased by a factor of 4.

The value t also occurs in a group of hypothesis tests, which are most often applied in the form of the One-sample t-Test or the Two-sample t-test. While the first one tests, based on the mean of a sample, whether the mean of the respective population differs from a specified value, the latter compares the mean values of

two independent samples. Both tests are only valid for Gaussian populations. Some more t-tests were developed which can be used for specific situations.

In the One-sample t-Test, a sample of the population under examination is chosen. For this sample, the mean value μ and the standard deviation s are calculated. In order to test whether μ differs from the desired mean value μ_0, the test value t is calculated as follows:

$$t = \sqrt{n}\frac{\mu - \mu_0}{s}$$

This formula is identical with the confidence interval calculation above. Now this value of t is compared with the value for t_{table} taken from the table of Student's t-distribution for $n - 1$ degrees of freedom (i.e., 9 degrees of freedom for 10 samples), taking into account the desired level of significance α:

$$|t| > t_{\text{table}}\left(1 - \frac{\alpha}{2}, n - 1\right)$$

For a desired level of significance of $\alpha = 5\%$ and $n = 10$, e.g., the value $t_{\text{table}}(0.975, 9) = 2.262$ is used. The hypothesis is rejected in this case if the calculated $|t|$ is greater than 2.262.

To depict this idea more clearly: if the difference between the measured and the desired mean values becomes larger than the confidence interval related to a desired level of significance, then the hypothesis is rejected.

The Two-Sample t-Test works quite similarly. To compare two populations A and B, sample sizes n and m are taken from these populations, respectively. For both samples, the mean values μ_A and μ_B and the standard deviations s_A and s_B are calculated. Afterward, the weighted variance s^2 is calculated:

$$s^2 = \frac{(n-1)s_A^2 + (m-1)s_B^2}{n + m - 2}$$

The test value t is now calculated as

$$t = \sqrt{\frac{nm}{n+m}}\frac{\mu_A - \mu_B}{s}$$

and this value is again compared with the table value of t:

$$|t| > t_{\text{table}}\left(1 - \frac{\alpha}{2}, n + m - 1\right)$$

These tests are of special interest in quality assurance, if it is necessary to test whether a sample has identical parameters as defined (One-sample t-Test) or as another sample (Two-sample t-Test). In the same way, it is often used in the lab to

prove whether an apparent difference between experimental results is significant
or not.

After calculating standard deviations, confidence intervals, etc., for measured
values, the influence of one error-prone input variable x on the result y is examined
now. How does a deviation Δx affect Δy?

Since Δy can be developed in a Taylor series, small values of Δx allow for using
a first-order approximation:

$$y(x \pm \Delta x) = y(x) \pm \frac{dy}{dx} \Delta x$$

This means that the deviation Δy is proportional to the known deviation of the
measured value Δx, multiplied by the partial derivative of the function $y(x)$. A few
examples shall depict this connection more clearly:

$$y(x) = x^2 \rightarrow \frac{dy}{dx} = 2x \rightarrow y(x \pm \Delta x) = x^2 \pm 2x\Delta x$$

$$y(x) = \sqrt{x} \rightarrow \frac{dy}{dx} = \frac{1}{2\sqrt{x}} \rightarrow y(x \pm \Delta x) = \sqrt{x} \pm \frac{1}{2\sqrt{x}} \Delta x$$

$$y(x) = \sin(x) \rightarrow \frac{dy}{dx} = \cos(x) \rightarrow y(x \pm \Delta x) = \sin(x) \pm \cos(x) \Delta x$$

If more than one error-prone input value x_i is used to calculate a result y, either
the maximum error or the total error (mean square error) can be calculated to get an
idea of the collective influence of all single independent errors of the input values.
The maximum error is normally used if the error limits are values taken from
measurement equipment or if the measured values are not independent; the total
error is usually a better choice if independent values with their standard deviations
are measured. The maximum error can be calculated by inserting the maximum and
minimum measured values (i.e., $\mu + \sigma$ and $\mu - \sigma$) into the calculation of $y(x_i)$ with
the most unfavorable sign combination. This method is often easier than the closed
form:

$$\Delta y_{maximum} = \left| \frac{\partial y}{\partial x_1} \right| \Delta x_1 + \left| \frac{\partial y}{\partial x_2} \right| \Delta x_2 + \left| \frac{\partial y}{\partial x_2} \right| \Delta x_2 + \dots$$

Similarly, the total error can be calculated:

$$\Delta y_{total} = \sqrt{\left(\frac{\partial y}{\partial x_1} \Delta x_1 \right)^2 + \left(\frac{\partial y}{\partial x_2} \Delta x_2 \right)^2 + \left(\frac{\partial y}{\partial x_3} \Delta x_3 \right)^2 + \dots}$$

In this way, the deviations of the calculated value y can be attributed to the
deviations of the single measured values.

Finally, it should be mentioned that even if all the abovementioned sources for random errors are minimized, there may still be large variations of the measured values—simply because textiles are anisotropic, i.e., have directional dependent properties, or because their properties change from one measurement point or sample to the next one. Unlike metals, plastics, glass, etc., textile materials along the whole textile chain (from fiber to yarn to woven or knitted fabric to garments or technical textiles) tend to be irregular with respect to several properties. This is another reason why taking enough representative samples from different positions of the sample and from different orientations is of special importance in the field of textiles—not only to take into account the random error but also to recognize the natural variations of the textile under examination.

1.5 Basic Principles of Measurements

The above-described possible measurement errors result in several requirements which have to be met during reliable measurements.

First, values are written down exactly as measured—no decimal places are omitted, and the measured values are not directly converted into the desired ones to avoid unnecessary errors.

The measurement instruments used are noted. This allows for checking accuracy classes and testing the equipment afterward in case of possible systematic errors.

Measuring once does not count. Measurements are performed several times, often ten times, depending on standards describing the measurement process and/or the measurement results. Values which scatter significantly are measured more often than values with smaller standard deviation. Each measured result is given with mean and standard deviation; results depicted in graphs contain error bars.

The number of significant digits is defined by the measurement uncertainty. Presenting values with too many significant digits gives an erroneous impression of higher precision than really achieved; cutting too many significant digits leads to unnecessary loss of precision.

Finally, measured values—and the values calculated from them—should be checked with respect to plausibility. In a lot of measurement situations, a plausibility check can easily be performed since some comparison possibilities exist, especially when measuring lengths, times, or masses. If the mass per unit area of a specific fabric, e.g., shall be measured, a simple comparison possibility is given by standard copying paper, having typical masses per unit area of 70–80 g/m^2.

Literature

Agnoli, P., D'Agostini, G.: Why does the meter beat the second? arXiv:physics/0412078v2 (2005)
DIN EN ISO 139:2011: Textiles – Standard atmospheres for conditioning and testing

DIN EN ISO 291:2008: Plastics – Standard atmospheres for conditioning and testing

Hänsel, A.: Holz und Holzwerkstoffe: Prüfung – Struktur – Eigenschaften (Grundwissen für Holzingenieure). Verlag Logos, Berlin (2014)

Mills, I.: Draft Chapter 2 for SI Brochure, following redefinitions of the base units, Consultative Committee for Units (CCU). http://www.bipm.org/utils/en/pdf/si_brochure_draft_ch2.pdf (2010)

Reumann, R.-D.: Prüfverfahren in der Textil- und Bekleidungstechnik. Springer, Berlin (2013) (Softcover reprint of the original 1st ed. 2000)

Student: The probable error of a mean. Biometrika **6**, 1–25 (1908)

Taylor, J.R.: An Introduction to Error Analysis: The Study of Uncertainties in Physical Measurement. University Science, Mill Valley (1999). ISBN 0-935702-75-X

Zhang, G.X.: A study on the Abbe Principle and Abbe errors. CIRP Ann. Manuf. Technol. **38**, 525–528 (1989)

Chapter 2
Conductive Yarns, Fabrics, and Coatings

Conductive textiles are nowadays used in a broad variety of applications in the area of smart textiles, starting from data and energy transfer lines to textile sensors to shielding of electromagnetic waves. They are necessary in textile capacitors, batteries, solar cells, and electroluminescent systems.

Conductive fabrics can be produced using inherently conductive fiber materials, conductive fiber coatings, or conductive coating or finishing methods on the whole textile fabrics. On the other hand, opposite to the large number of methods to make textiles conductive, it is quite complicated to create sustainable, washing-, and abrasion-resistant conductive textiles. This chapter thus shows some applications and typical measurement methods for conductive textiles.

2.1 Basics of Conductivity

Electrical conduction is the physical property of some materials to transfer energy by the use of cooperative movement of free electric carriers, the electrons (or holes in other conductors). Their movement is enforced by the use of an externally applied electric field taken from a battery or power supply.

Metals in general are conductive, meaning in practice they deliver energy from a source to a receiver, while some materials are semi-conductive, meaning they have worse conduction capabilities. Finally, some materials are insulators known also as dielectrics, meaning they have no free electrons available.

The widely known electrical conductors are metals like gold, silver, copper, or aluminum. Semiconducting materials, like silicon (Si), gallium arsenide (GaAs), or gallium phosphate (GaP), are used in the construction of electronic devices, especially for temperature and light sensing applications. Isolating properties have, e.g., paraffin, cellulose, paper, wood, rubber, teflon, polystyrene and polyethylene, mineral and synthetic oils, epoxy resin, asbestos, or porcelain.

In this chapter, the origin of the conducting properties will be explained. To reach this aim, we should firstly analyze the underlying effects from the atomic-scale perspective.

An electron is an elementary point-like particle without internal structure, possessing a mass at rest equal to 9.1×10^{-31} kg and the elementary amount of electricity equal to $e = 1.6 \times 10^{-19}$ C (coulomb). Electrons in metals are free and form a so-called electron gas. They are in a state of chaotic movement influenced by collisions with atoms, defects, and other charge carriers. The average velocity of such a chaotic ensemble is of the order of 10^6 m s^{-1}. The pressure of the electron gas exceeds what we sense as normal atmospheric pressure of air (1 atm) by 10^5 times. Why are the conducting materials nevertheless not explosive? The reason is that electrons are kept in a material by very intense electrical attraction forces with positively charged atomic nuclei, even if the negatively charged electrons are under the influence of repulsive forces.

However, the problem of understanding is wherefrom such huge values of electron velocities result. This can be explained from the energetic point of view, more specifically using the energy level picture.

In the atomic world, or rather quantum world, one energy level can be occupied only by two electrons. This results from the so-called Pauli Exclusion Principle. A third electron, creating a system with the first two electrons, has to take the next accessible energy level (Fig. 2.1). Hence, the energy levels are separated or quantized. In real materials, with concentrations of electrons in the order between 10^{13} m^{-3} and 10^{28} m^{-3}, the energy levels are subsequently split and form energy bands. In other words, electrons are enforced to differ in energies and consequently possess such great values of chaotic velocities.

Next, taking into account the energy bands' picture, we can more precisely divide materials into conductors, semiconductors, and isolators. Remembering that elementary energy levels are imposed by atomic orbits, the real piece of matter may possess many energy bands; however, for the electric conductivity the last two bands and the distance (in the sense of energy) between them are most important. The last band, created by energy levels most distanced from the atom cores, is called the conduction band. The one before the last band is named the valence band. The distance between the top of the valence band and the bottom of the conduction band is called the energy gap ΔE. The gap and the accessibility for empty energy levels in the conduction band constitute the division into three types of electric conductivity (Fig. 2.2).

Fig. 2.1 The idea of the Pauli Exclusion Principle and creation of quantized energy levels
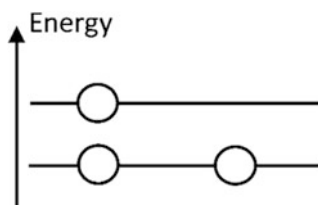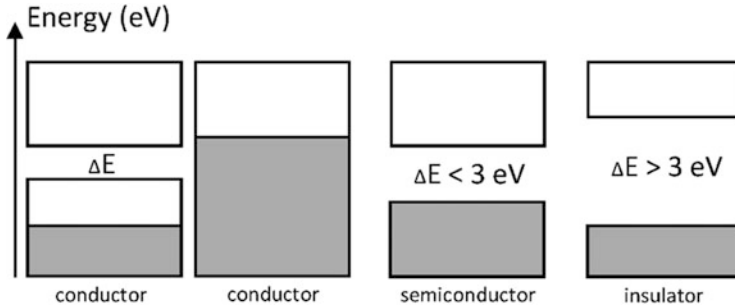
Fig. 2.2 Classification of materials into conductors, semiconductors, and insulators from the energy band structure perspective. *Gray regions* mean completely filled states; *white regions* show empty states. There are two types of conductors: those with empty states available in the valence band and relatively narrow energy gap ΔE, like in sodium (first case from the *left*), and those where there is no energy gap and the empty states are located directly above the filled ones, like in magnesium (second case from the *left*)

Here one remark about energy units commonly used in such types of analysis should be given. The unit is 1 eV (electron-volt), meaning that an elementary electric charge is accelerated by the electric potential difference of 1 V. Hence, $1\,\text{eV} = 1.6 \times 10^{-19}\,\text{J}$. The distinction between semiconductors and insulators is not sharp. An energy gap of 3 eV is sometimes used as the arbitrary criterion of recognition. An energy gap of 10 eV means definitely a complete lack of conductivity.

Before some considerations related to practical measurements of real species follow, let us summarize again the intrinsic points of the underlying effects at the atomic scale. Metals are very good conductors since there are empty energy levels accessible for energy carriers, the free electrons.

The empty levels are also accessible in semiconductors. However, while the valence band is fully occupied here, the free states in the conduction band are available above an energy barrier of approximately 1–3 eV. This barrier can be bypassed due to thermal excitations, even at room temperature of 293 K. Such a mechanism of free carriers occurring in the conduction band results in a relatively low electron concentration of the order of $10^{13}\,\text{m}^{-3}$ for GaAs and $10^{16}\,\text{m}^{-3}$ for Si. The corresponding energy gaps are equal to 1.4 eV and 1.1 eV, respectively. The concentration of free carriers in metals is significantly greater and reaches $10^{28}\,\text{m}^{-3}$ for most metals.

Keeping in mind the above picture of electron gas properties, the question arises what will happen if a metal fiber is connected to a battery or other power supply with a constant voltage. After that, electrons will start a correlated movement directed to the positive terminal of the power supply. The movement is nevertheless disturbed. The dominating mechanism of the resistance relies on scattering of electrons by thermal vibrations of material atoms or ions around their positions of equilibrium. The average time from collision to collision, called the relaxation time, is of the order of 10^{-14} s. Thermal vibrations are natural and imaginations about keeping the static positions of atoms incorrect. The constant speed of the correlative

movement is called the drift velocity v_D. Surprisingly, the value of the drift is quite low, of the order of 1 m s^{-1}. The drift velocity divided by the intensity of the imposed electric field, v_D/E, is called the electric mobility and usually marked by the symbol μ.

In a typical situation, the electrons flowing along a conductor can be expressed by the linear relation between the current density $\vec{j}$ and the externally applied electric field intensity $\vec{E}$, namely,

$$\vec{j} = \sigma \cdot \vec{E},$$

where the proportionality constant σ is named electric conductivity. The current density is understood as the amount of electric charge (in coulombs) flow per second per area unit [C/(s m^2)] or expressed in amperes per area unit (A/m^2). The electric field intensity is expressed in volts per meter (V/m). The common unit of the conductivity is (Ω m)$^{-1}$; however, the SI unit is siemens per meter (S/m). The conductivity depends linearly on the abovementioned mobility μ by

$$\sigma = en\mu,$$

where e is the elementary charge and n the carrier concentration. The inverse of the conductivity, $\rho = 1/\sigma$, is named resistivity and is expressed in (Ω m) units. The resistivity is the proportionality constant in the relation between the electric resistance R of the linear conductor and its length l, having the cross section S, namely,

$$R = \rho \frac{l}{S}.$$

The unit of the resistance is ohm (Ω). The inverse of the resistance is the conductance, $G = 1/R$, and its unit is Siemens (S).

Finally, if to apply a given voltage U(V) between the terminals of a constant resistance $R(\Omega)$ in order to enforce a current I(A), the following linear relation holds:

$$I = \frac{U}{R} = G \cdot U$$

which is called Ohm's law. It states that the current intensity is proportional to the applied voltage and inversely proportional to the resistivity or proportional to the conductance (Fig. 2.3).

Table 2.1 presents an overview of typical resistance values which can be found in pure and coated textile fabrics. While metallic coatings, e.g., with nickel, or intrinsically conductive materials, such as carbon fibers, can result in quite low resistance values, depending on their geometries, typical textiles fibers have rather high resistances.

In many materials, the resistivity depends strongly on the fabric humidity and may change by several orders of magnitude. For cellulosic threads, such as viscose
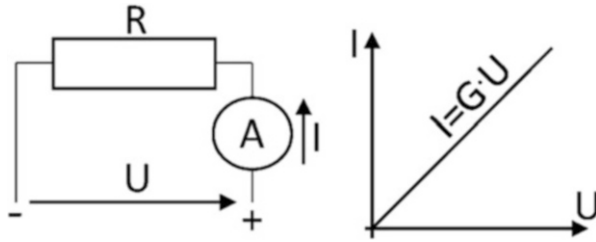
Fig. 2.3 Ohm's law: linear dependence between the current intensity I and the applied voltage U. The current intensity is measured by the ammeter. The convention of the current flow direction assumes the flow from a positive voltage terminal to a negative voltage terminal

Table 2.1 Results of resistance measurements of selective textile materials

Sample	Resistance/Ω	References
Acetate yarn	1.4×10^{12}	Hersh and Montgomery (1952)
Carbon-epoxy composites	<1	Berry (2014)
Cotton yarn polypyrrole coated	10^5–10^7	Yildiz et al. (2013)
Cotton fiber polyaniline coated	3.5×10^2	Onar et al. (2009)
Cotton yarn	10^4	Kaynak et al. (2008)
Nickel-coated polyester fabric	<1	Tokarska et al. (2013)
Nylon monofilament	10^{13}–10^{14}	Hersh and Montgomery (1952)
Kapok fiber	10^1–10^7	Mani et al. (2012)
Viscose filament	10^{11}–10^{12}	Hersh and Montgomery (1952)
Viscose yarn	10^{10}	Hersh and Montgomery (1952)
Wool fiber	10^{13}	Hersh and Montgomery (1952)

or cotton, this behavior was attributed to conduction being dominated by the adsorbed water, while the cellulose hydroxyl groups only participate significantly in the conduction process for very low moisture regain (Christie and Woodhead 2002). For wool, silk, and similar natural fibers, the absorbed water was described to exist in two distinct phases, resulting in a similarly strong increase of the conductance with increasing moisture regain (Christie et al. 2002).

Knowledge about the conductive properties of textiles is important due to their resulting electromagnetic shielding or electrostatic discharge (ESD) properties, but there are several more applications especially in the area of smart textiles. The next section will give an overview of possible applications of conductive textiles.

2.2 Conductive Materials for Textile Applications

There are different possibilities to make textiles conductive. On the one hand, electrically conductive fibers or yarns can be used to produce conductive fabrics; on the other hand, conductive coatings can be applied on nonconductive fabrics.

Conductive coatings often consist of conductive polymers, such as PEDOT:PSS (poly(3,4-ethylenedioxythiophene) polystyrene sulfonate), PAni (Polyaniline), polythiophene, polypyrrole, etc. PEDOT:PSS consists of two ionomers: PEDOT is a conjugated polymer carrying positive charges which is based on polythiophene, while PSS is a sulfonated polystyrene with partly deprotonated (negatively charged) sulfonyl groups. Together, both charged components build a macromolecular salt (Gronendaal et al. 2000). PEDOT:PSS is more or less transparent and thus often used in applications where this property is necessary, such as touch screens, organic light-emitting diodes (OLEDs), etc. The conductivity of PEDOT:PSS can be significantly increased by embedding silver particles, carbon nanotubes, etc. (Stapleton et al. 2015), doping with other organic materials (Kim et al. 2002; Xia and Ouyang 2010), or post-treating the material in different ways (Ouyang et al. 2005; Saghaei et al. 2015).

PAni is a radical-cation salt of a conjugated polymer with an acid and oxidatively coupled aniline units. Its different oxidation states result in different colors. It is often used in electromagnetic shielding, antistatic applications, as a hole injection layer, or for printed circuit boards (Fehse et al. 2007).

Both materials are often used as textile coatings due to their flexibility, translucence, and high conductivity.

Conductive yarns can consist of intrinsically conductive materials, such as metal wires/filaments (Fig. 2.4) or fibers, or can be created by coating nonconductive fibers or filaments with thin conductive layers, e.g., from silver. While metal filament yarns and metal fiber yarns tend to breaking due to wear and tear, silver coatings can be oxidized and abraded during washing and usage. Nevertheless, both variants may be useful for special applications. For other purposes, using metal wires or strands may be more efficient. None of the aforementioned materials is ideally suited for all situations.

Fig. 2.4 Warp knitted fabric with stainless steel wires included in defined positions as data transmission lines
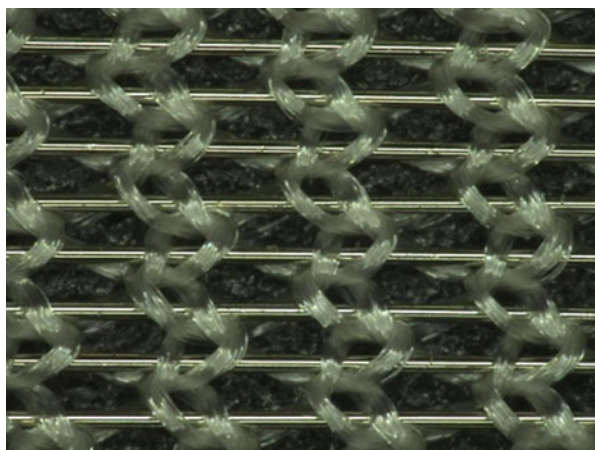
2.3   Applications of Conductive Textiles

Conductive fabrics are essential for a variety of applications. Especially in the area of smart/intelligent textiles, they are indispensable.

Textile electrocardiogram (ECG) electrodes, e.g., are necessarily conductive. Such textile ECG electrodes can be knitted, woven, or embroidered from conductive yarns and/or coated with conductive materials. Especially knitted electrodes can easily be realized by seamless knitting technologies, allowing for direct integration into a knitted shirt (Pacelli et al. 2006; Linz et al. 2006). Since very small voltages (peak–peak difference in the order of 1 mV) have to be measured, a good skin contact as well as sufficiently constant resistance of the electrodes is necessary, the latter being hard to realize in knitted electrodes. Embroidered ECG electrodes are also often utilized (Pola and Vanhala 2007; Cho et al. 2011) as well as woven ones (Song et al. 2010; Aumann et al. 2014). An additional coating may be helpful to increase the dimension and the stability of the contact between electrode and skin (Rattfält et al. 2007; Aumann et al. 2014).

While the dependence of the electrical resistance of knitted fabrics on pressure and elongation is disadvantageous for textile ECG electrodes, it can directly be used in knitted elongation or pressure sensors (Fig. 2.5). In these applications, constant measurements are necessary to detect deviations of the conductivity due to stress or pressure on the knitted sensors (Li et al. 2009; Ehrmann et al. 2014; Wang et al. 2014). Similarly, using conductive yarns or fabrics to build capacitors or coils allows for creating capacitive or inductive elongation or pressure sensors.

In textile heating elements, however, the conductivity should usually be constant again. Since such fabrics should have a not too low resistivity to allow for heating the conductive layer by applying a voltage, and the fabric should be uniformly warm, conductive coating is often applied for this purpose (Bhat et al. 2006; Cucchi et al. 2009). On the other hand, coating elastic (knitted) fabrics with conductive polymers can be used to tailor the behavior of electrochromic textiles (Ding et al. 2010).
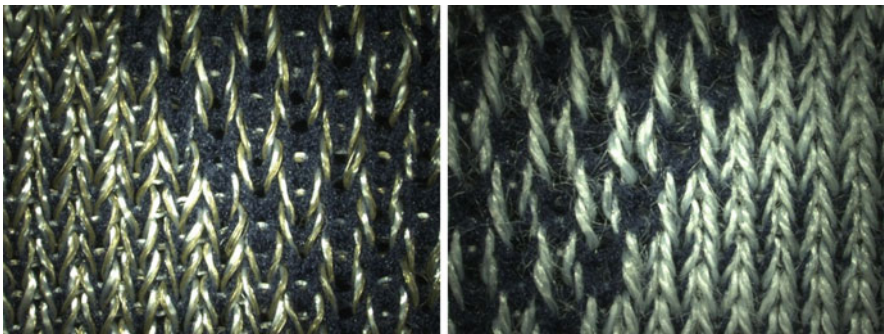
Fig. 2.5   Knitted fabric with partly conductive silver-coated yarns (*left panel*) or stainless steel fiber yarn (*right panel*)

Fig. 2.6 Conduction lines in knitted fabrics, using copper strand (*left panel*) or silver-coated polyamide filaments (*right panel*)

Besides these and other sensors, conductive textile materials are necessary in diverse actuators and other electronic components, such as electroluminescent devices coated on textile-based materials, textile-based batteries, or dye-sensitized solar cells (Normann et al. 2016; Herrmann et al. 2016).

Additionally, conductive connections are necessary to transport data and energy between different parts of smart textiles (Fig. 2.6). Here, conductive yarns, wires, or coatings can be used (Obermann et al. 2016).

In all these applications, it is necessary to test the conductivity of the respective fibers, yarns, or fabrics. Differences between measurements on common "hard" materials and on conductive fabrics are depicted in the next subchapter.

## 2.4 Measuring Conductive Properties of Yarns and Textiles

In many situations, it is necessary to measure the electric resistance of conductive yarns of fabrics, either constantly or for a short moment (Fig. 2.7). Such measurements can in principle be performed using a simple multimeter with the respective measurement ranges.

Opposite to "hard" materials, such as copper wires or metal plates, the connection between the multimeter tips and a conductive yarn or fabric cannot simply be established by pressing the tips on the textile. Two aspects have to be taken into account here: Firstly, textiles are soft and flexible and thus prone to avoiding contact with the tips. Secondly, sometimes the conductive part of the textile cannot be reached with the tips, making additional preparations necessary.

In several conductive textiles, a good contact to the measurement equipment can be made using conductive clamps which hold a textile or yarn with a defined pressure (Fig. 2.8). Alternatively, press buttons (the silvery ones; colored press
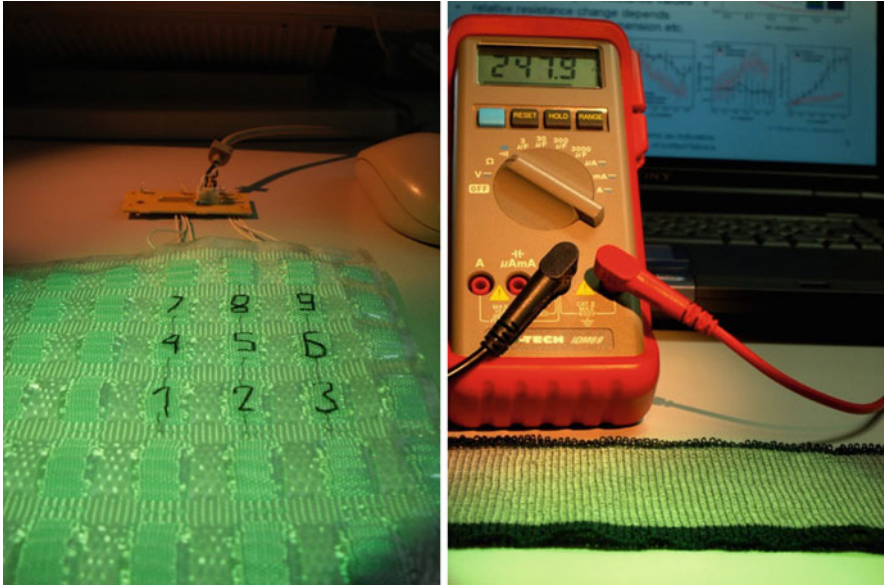
Fig. 2.7 Measurement of contact versus noncontact in textile keyboard (*left panel*); constant resistance measurement during elongation test of conductive knitted fabric (*right panel*)
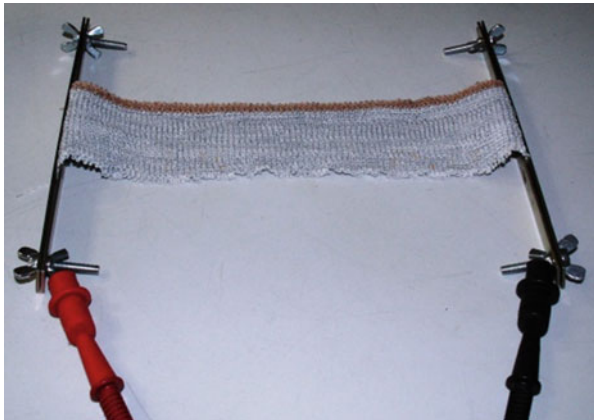
Fig. 2.8 Measuring the resistance of a knitted fabric using clamps as contacts

buttons are not conductive) can be sewn onto the respective positions on the textile. This procedure is especially well suited for measurements which have to be performed often in the same way. In both cases, it is essential to ensure that the conductive parts of the textile under examination are in electrical contact with the clamps or press buttons, respectively. This necessitates contacting exactly the correct positions in case of wires only sporadically leaving the inner part of a fabric
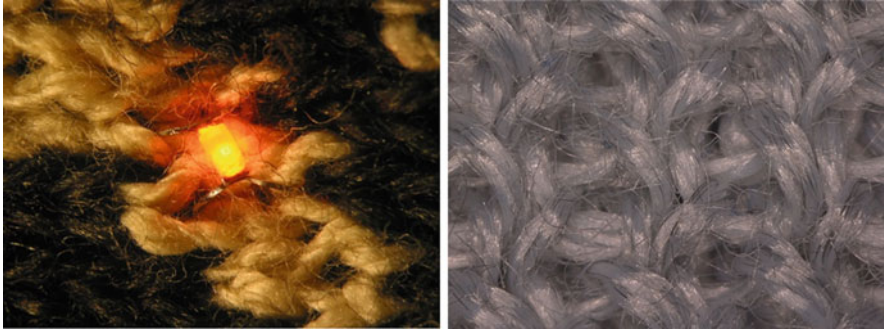
Fig. 2.9 Conductive wire exiting the inner part of the knitted fabric only at defined positions (*left panel*); conductive yarn with 20 % stainless steel and 80 % polyester (*right panel*)
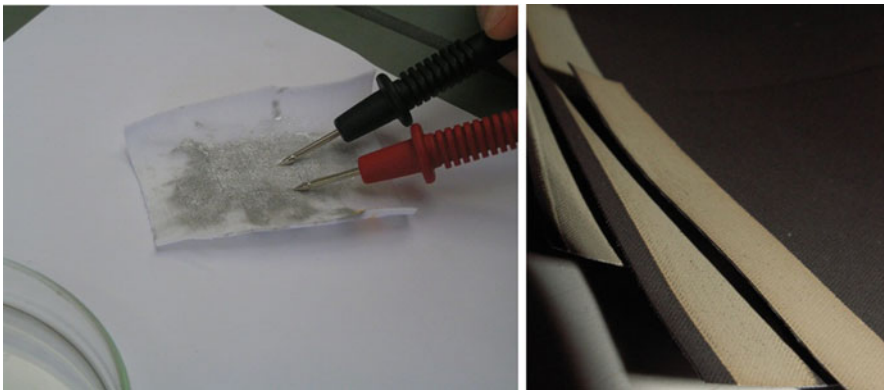

Fig. 2.10 Silver coating on cotton fabric (*left panel*); thick silver connection lines on thin graphite coatings on woven fabrics (*right panel*)

(Fig. 2.9, left panel) or large enough contact areas in case of partly conductive yarns, respectively (Fig. 2.9, right panel).

An even more challenging problem can occur if nonconductive fabrics are coated with a conductive material. For thin conductive layers, it may be impossible to contact them directly with clamps, etc., because they can be completely sunk into the woven or knitted fabric (Fig. 2.10, left panel). In these cases, sewing a press button through the fabric may help; however, a more reliable method consists in adding a second—thicker—coated layer which will penetrate into the fabric until the first conductive coating layer is reached. For such an additional connection line, a silver coating should be used since silver is known to create good, reliable contacts (Fig. 2.10, right panel).

Besides measurements with a usual multimeter, the conductivity of textiles is often examined using four-point probes. Such a four-point probe consists of four linearly arranged electrodes (Fig. 2.11), the outer ones injecting a current into the

Fig. 2.11 Four-point probe
measurement principle
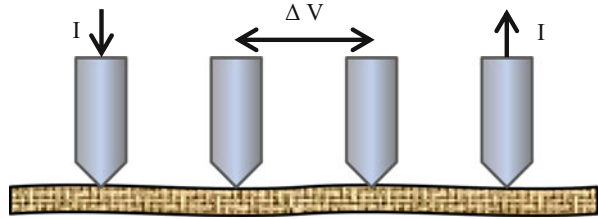
material under examination, while the inner ones measuring the resulting voltage (Schuetze et al. 2004). In this way, the contact resistance between the measurement tips and the investigated material does not influence the result (Valdes 1954; Jones 1993). The size and geometry of the sample under examination, however, will still affect the measured resistance (Schroder 1990). This can easily be understood by a simple thought experiment: If the four-point probe is applied in the middle of a conductive sheet, the current can flow through the whole sample. If this sample is now cut directly beside the four-point probe, then only half of the sheet material contributes to conducting the current, and thus the resistance will be twice as large (Schuetze et al. 2004).

It should be mentioned that measuring with four-point probe equipment on textiles is less easy and reliable than examinations of rigid surfaces. As indicated in Fig. 2.11, the textile may vary in height, even if the fabric is laid down on a flat, even surface. This means that the resistance between the tips and the textile may vary—which results in changes of the measured resistance due to the influence of the contact resistance, which should actually be avoided using this method.

Practically, the easiest way to estimate this influence is to modify the pressure of the four-point probe on the textile—if the resistance does not change, the measurement is reliable. In most cases, however, it is necessary to stabilize the contact between the four probes and the fabric. This can, e.g., be done by changing to large-area probes or by using conductive (silvery) press buttons or the like as contacts between probes and textile. In both cases, it must be kept in mind that increasing the contact areas results in undesired alterations of the measured sheet resistance. In principle, the contact areas should be made as large as necessary to ensure a reliable contact, but not larger.

Besides the textiles which are highly conductive due to their intrinsic properties or a coating, several textiles show quite high resistances which cannot be measured with usual multimeters or standard four-point probes, but are nevertheless important to be known due to their influence on the antistatic properties of textiles and clothing. Such high resistances can be measured by a tera ohm meter, also known as high resistance meter or low conductance meter.

While usual multimeters often range from $0.1\,\Omega$ to the order of $20\,M\Omega$, tera ohm meters can be used to measure resistances in the order of magnitude of $1\,k\Omega$ to $1\,T\Omega$ (tera ohm) or even up to $1000\,T\Omega$. For the highest resistances, the measurement method is changed, compared to usual multimeters. In the latter, a preset current is led through the resistor to be measured, resulting in a voltage proportional to the

resistance. For higher resistances, smaller and smaller currents must be used to measure the same voltages. For very high resistances, the method is inversed: A defined voltage drop is used to generate a current through the resistor, the latter being proportional to the conductivity, i.e., the inverse of the resistance. This method can be faster and more accurate in case of high resistances, especially if the voltage is increased.

Tera ohm meters can be used in two-point or four-point versions, as well as equipment for lower resistances.

Besides these DC (direct current) measurements, AC (alternating current) investigations of textile materials may also be of interest. Especially in the area of smart textiles, textile conduction lines are needed to transport not only energy but also data—which can often not be regarded as direct current, but have signal frequencies of 10 Hz (breathing cycle), 100 Hz (ECG signals), or higher. For such AC signals, the ohmic resistance is only one parameter which needs investigation.

Measurements of the signal quality cannot be performed by a multimeter but necessitate an oscilloscope—multimeters could only give average values of the amplitude of a sinusoidal voltage, etc., but cannot be used to investigate the signal shape. Especially in case of real—usually non-sinusoidal—data signals, multimeters are useless.

For a general measurement of the data transmission quality of conductive yarns, coated textiles, etc., the measurement setup is similar to the four-point probe depicted in Fig. 2.11. Figure 2.12 shows the corresponding situation for an AC measurement: Using a function generator, a current I_{fg} is led through the conductive yarn or textile. Between these contact points, the resulting AC voltage V_{osc} is measured using an oscilloscope. Connections between the measurement equipment and the conductive textile can be established by usual lab cables with crocodile clips fixed to the fabric or yarn.

In this way, the signal amplitudes and shapes can be tested. Former experiments have shown, e.g., that carbon fibers can be used as data lines for transmission of signals up to approximately 1 MHz, which is sufficient for typical textile applications (Fig. 2.13). On the other hand, graphite-coated transmission lines showed a significant decrease of the signal amplitude, and the signal nearly vanished during transmission through silver-coated polyamide yarns (Bilousova 2014).

Fig. 2.12 Measurement of AC voltage V_{osc} using an oscilloscope due to function generator current I_{fg} through a conductive yarn
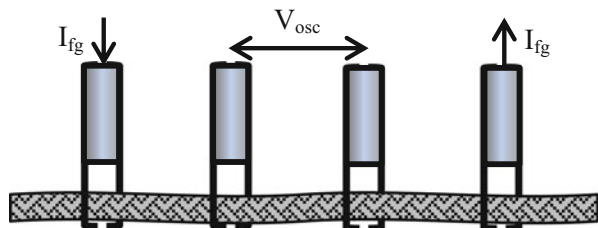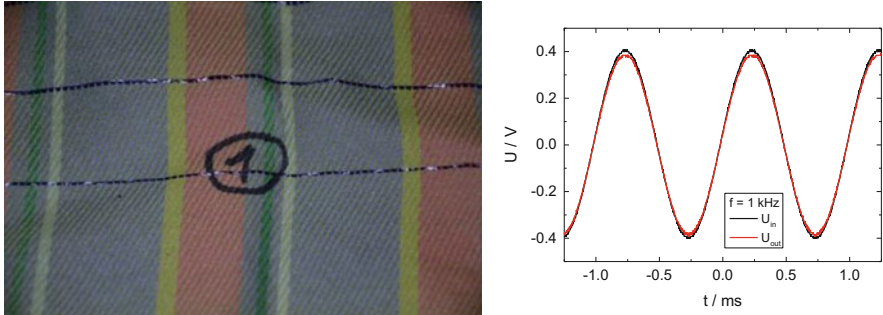
Fig. 2.13 Conductive carbon yarns as data lines in a nonconductive woven fabric (*left panel*); data transmission U_{out} of a sinusoidal signal U_{in} through carbon filament yarn with only slightly reduced amplitude (*right panel*)


Fig. 2.14 Wrap yarn composed of textile core and wound metal braid after weaving with damages due to the machine takedown. Wire diameters are approximately 20 µm

2.5 External Influences on Conductive Properties of Yarns and Textiles

The conductive properties of yarns, textiles, and textile coating may change due to abrasion, wear and tear, washing, etc. Abrasion can already occur during weaving, knitting, etc. Figure 2.14 shows a wrap yarn with a metal braid on the outer side, wound around a textile core, after weaving. Apparently the rough surface of the machine takedown has damaged the wire surfaces before the resulting conductive fabric was used for the first time.

Damages may also occur due to normal use of conductive textiles and especially after washing. As an example, Fig. 2.15 depicts a graphite-coated ECG electrode, based on a stainless steel woven fabric with relatively low conductivity. It is clearly visible that the coating is broken more and more due to washing, especially near the edges. This effect can partly be reduced by sewing the electrode edges onto a
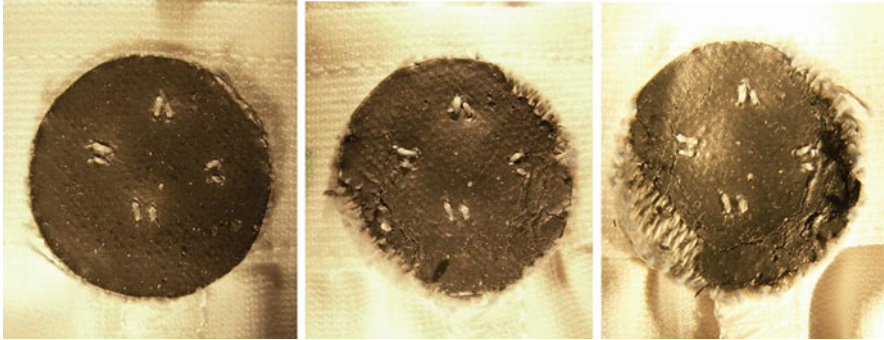
Fig. 2.15 Graphite-coated ECG electrode (diameter 30 mm) on stainless steel woven fabric before washing (*left panel*), after 5 washing cycles (*middle panel*), and after 10 washing cycles (*right panel*)
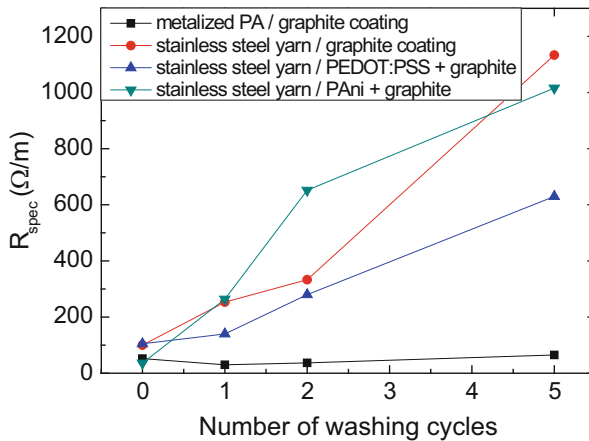
Fig. 2.16 Influence of washing on the resistivity of different electrode materials

relatively rigid textile; however, in this case the stitches through the conductive coating serve as nucleation points for cracks in the conductive layer.

In other coatings, washing supports oxidizing of a silver layer or abrades fine metal coatings on fibers. With respect to stainless steel fiber yarns, washing results in broken fiber ends and thus also reduced conductivity.

These optical changes due to washing are naturally connected with significant changes in the conductivity. Figure 2.16 shows the change of the resistance of different electrode materials, measured as linear resistance (ohm per meter) in strips of identical dimensions, due to washing.

While all electrode materials start with linear resistances of approximately $100\,\Omega/m$, this value may increase strongly during the first five washing cycles. For all electrodes based on stainless steel yarn woven fabrics, values of up to 1 kΩ/m are measured after five washing cycles. Only for the electrode material based on metalized polyamide, the resistance stays approximately identical.

Fig. 2.17 ECG signals, detected with graphite-coated woven electrodes produced from metalized polyamide yarn, after different numbers of washing cycles with color detergent at 40 °C
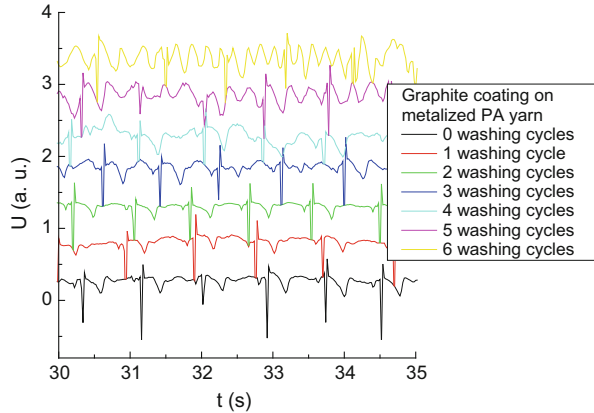
This is why this material was used for the next test in which ECG curves were measured under identical conditions after different numbers of washing cycles of the complete shirt with textile ECG electrodes included. Opposite to Fig. 2.15, the ECG electrodes based on metalized polyamide looked nearly unaltered during six washing cycles.

Figure 2.17 depicts the results of this experiment. While the ECG curve is clearly visible before washing and after 1 or 2 washing cycles, it is more and more superimposed by undesired noise if the electrodes have been washed 5 or 6 times. Apparently a pure measurement of the resistance does not always give all information necessary for a specific experiment, while it can at least help to exclude obviously unsuitable materials.

In a similar way, abrasion can significantly change the resistance of conductive coatings, fabrics, and yarns. Measuring the resistance or conductivity after different treatments is thus essential for the evaluation of conductive textiles.

Literature

Aumann, S., Trummer, S., Brücken, A., Ehrmann, A., Büsgen, A.: Conceptual design of a sensory shirt for fire-fighters. Text. Res. J. **84**, 1661–1665 (2014)

Berry, B.: Investigation of electrical and impact properties of carbon fiber textile composites. Dissertation thesis, University of Iowa (2014)

Bhat, N.V., Seshadri, D.T., Nate, M.M., Gore, A.V.: Development of conductive cotton fabrics for heating devices. Appl. Polym. Sci. **102**, 4690–4695 (2006)

Bilousova, K., Dering, E., Zuev, A., Ehrmann, A., Büsgen, A.: Examination of the suitability of carbon fiber yarns for data transmission. Tech Text **57**, E168–169 (2014)

Cho, G., Jeong, K., Paik, M.J., Kwun, Y., Sung, M.: Performance evaluation of textile-based electrodes and motion sensors for smart clothing. IEEE Sens. J. **11**, 3183–3193 (2011)

Christie, J.H., Woodhead, I.M.: A new model of DC conductivity of hygroscopic solids, Part I: Cellulosic materials. Text. Res. J. **72**, 273–278 (2002)

Christie, J.H., Woodhead, I.M., Krenek, S., Sedcole, J.R.: A new model of DC conductivity of hygroscopic solids, Part II: Wool and silk. Text. Res. J. **72**, 303–308 (2002)

Cucchi, I., Boschi, A., Arosio, C., Bertini, F., Freddi, G., Catellani, M.: Bio-based conductive composites: preparation and properties of polypyrrole (PPy)-coated silk fabrics. Synth. Met. **159**, 246–253 (2009)

Ding, Y., Invernale, M.A., Sotzing, G.A.: Conductivity trends of PEDOT-PSS impregnated fabric and the effect of conductivity on electrochromic textile. ACS Appl. Mater. Interfaces **2**, 1588–1593 (2010)

Ehrmann, A., Heimlich, F., Brücken, A., Weber, M.O., Haug, R.: Suitability of knitted fabrics as elongation sensors subject to structure, stitch dimension and elongation direction. Text. Res. J. **84**, 2006–2012 (2014)

Fehse, K., Schwartz, G., Walzer, K., Leo, K.: Combination of a polyaniline anode and doped charge transport layers for high-efficiency organic light emitting diodes. J. Appl. Phys. **101**, 124509 (2007)

Gronendaal, L., Jonas, F., Freitag, D., Pielartzik, H., Reynolds, J.R.: Poly (3,4-ethylenedioxythiophene) and its derivatives: past, present, and future. Adv. Mater. **12**, 481–494 (2000)

Herrmann, A., Fiedler, J., Ehrmann, A., Grethe, T., Schwarz-Pfeiffer, A., Blachowicz, T.: Examination of the sintering process dependent micro- and nanostructures of TiO_2 on textile substrates. In: Proceedings of SPIE 9898, Photonics for Solar Energy Systems VI, 98980S (2016)

Hersh, S.P., Montgomery, D.J.: Electrical resistance measurements on fibers and fiber assemblies. Text. Res. J. **22**, 805–818 (1952)

Jones, B.: Resistance measurements on play-doh TM. Phys. Teach. **31**, 48–49 (1993)

Kaynak, A., Najar, S.S., Foitzik, R.C.: Conducting nylon, cotton and wool yarns by continuous vapor polymerization of pyrrole. Synth. Met. **158**, 1–5 (2008)

Kim, J.Y., Jung, J.H., Lee, D.E., Joo, J.: Enhancement of electrical conductivity of poly (3,4-ethylenedioxythiophene)/poly(4-styrenesulfonate) by a change of solvents. Synth. Met. **126**, 311–316 (2002)

Li, L., Au, W.M., Li, Y., Wan, K.M., Chung, W.Y., Wong, K.S.: A novel design method for intelligent clothing embedded sensor system based on knitting technology and garment design. Text. Res. J. **79**, 1670–1679 (2009)

Linz, T., Kallmayer, C., Aschenbrenner, R., Reichl, H.: Fully integrated EKG shirt based on embroidered electrical interconnections with conductive yarn and miniaturized flexible electronics. In: Proceedings of International Workshop on Wearable and Implantable Body Sensor Networks, pp. 4–26 (2006)

Mani, G.K., Rayappan, J.B.B., Bisoyi, D.K.: Synthesis and characterization of kapok fibers and its composites. J. Appl. Sci. **12**, 1661–1665 (2012)

Normann, M., Kyosev, Y., Ehrmann, A., Schwarz-Pfeiffer, A.: Multilayer textile-based woven batteries. In: Kyosev, Y. (ed.) Recent Developments in Braiding and Narrow Weaving, pp. 129–136. Springer, Berlin (2016)

Obermann, M., Ellouz, M., Aumann, S., Martens, Y., Bartelt, P., Klöcker, M., Kordisch, T., Ehrmann, A., Weber, M.O.: Non-destructive X-ray examination of weft knitted wire structures. In: IOP Conference Series: Materials Science and Engineering vol. 141, p. 012007 (2016)

Onar, N., Aksit, A.C., Ebeoglugin, M.F., Birlik, I., Celik, E., Ozdemir, I.: Structural, electrical, and electromagnetic properties of cotton fabrics coated with Polyaniline and Polypyrrole. J. Appl. Polym. Sci. **114**, 2003–2010 (2009)

Ouyang, J., Chu, C.-W., Chen, F.-C., Xu, Q., Yang, Y.: High-conductivity poly(3,4-ethylenedioxythiophene):Poly(styrene sulfonate) film and its application in polymer optoelectronic devices. Adv. Funct. Mater. **15**, 203–208 (2005)

Pacelli, M., Loriga, G., Taccini, N., Paradiso, R.: Sensing fabrics for monitoring physiological and biomechanical variables: E-textile solutions. In: Proceedings of the 3rd IEEE-EMBS international summer school and symposium on medical devices and biosensors, Boston (2006)

Pola, T., Vanhala, J.: Textile electrodes in ECG measurement. In: 3rd International conference on intelligent sensors, sensor networks and information, pp. 635–639 (2007)

Rattfält, L., Lindén, M., Hult, P., Berglin, L., Ask, P.: Electrical characteristics of conductive yarns and textile electrodes for medical applications. Med. Biol. Eng. Comput. **45**, 1251–1257 (2007)

Saghaei, J., Fallahzadeh, A., Saghaei, T.: ITO-free organic solar cells using highly conductive phenol-treated PEDOT:PSS anodes. Org Electron **24**, 188–194 (2015)

Schroder, D.K.: Semiconductor Material and Device Characterization. Wiley, New York (1990)

Schuetze, A.P., Lewis, W., Brown, C., Geerts, W.J.: A laboratory on the four-point probe technique. Am. J. Phys. **72**, 149–153 (2004)

Song, H.-Y., Lee, J.-H., Kang, D., Cho, H., Cho, H.-S., Lee, J.-W., Lee, Y.-J.: Textile electrodes of jacquard woven fabrics for biosignal measurement. J. Text. Inst. **101**, 758–770 (2010)

Stapleton, A.J., Yambem, S.D., Johns, A.H., Afre, R.A., Ellis, A.V., Shapter, J.G., Andersson, G. G., Quinton, J.S., Burn, P.L., Meredith, P., Lewis, D.A.: Planar silver nanowire, carbon nanotube and PEDOT:PSS nanocomposite transparent electrodes. Sci. Technol. Adv. Mater. **16**, 025002 (2015)

Tokarska, M., Frydrysiak, M., Zięba, J.: Electrical properties of flat textile materials as inhomogeneous and anisotropic structure. J. Mater. Sci.: Mater. Electron. **24**, 5061–5068 (2013)

Valdes, L.B.: Resistivity measurements on germanium for transistors. Proc. IRE **42**, 420–427 (1954)

Wang, J., Long, H., Soltanian, S., Servati, P., Ko, F.: Electro-mechanical properties of knitted wearable sensors: Part 2 – Parametric study and experimental verification. Text. Res. J. **84**, 200–213 (2014)

Xia, Y., Ouyang, J.: Significant conductivity enhancement of conductive poly (3,4-ethylenedioxythiophene): Poly(styrenesulfonate) films through a treatment with organic carboxylic acids and inorganic acids. ACS Appl. Mater. Interfaces **2**, 474–483 (2010)

Yildiz, Z., Usta, I., Gungor, A.: Investigation of the electrical properties and electromagnetic shielding effectiveness of polypyrrole coated cotton yarns. Fibres Text. East. Eur. **21**, 32–37 (2013)

Chapter 3
Magnetic Yarns, Fabrics, and Coatings

A less usual but also quite interesting form of functionalizing fibers, yarns, or fabrics, compared with conductivity, is magnetism. Magnetism can occur in different forms, intrinsically or as a finishing, in thicker or thinner layer, more or less strong, durable or changeable ... While conductivity is clearly defined by an electrical resistance or a value of the conductivity and can be measured with a few simple devices, magnetism can occur in more different forms, and measurements are normally not easy. However, magnetic textiles can be used for a broad variety of applications which are often not as evident as applications of conductive textiles.

This chapter first gives an overview of different forms of magnetism, before depicting examples of possible applications for magnetic textiles. Simulations as well as—direct and indirect—measurement methods will be shown.

3.1 Different Forms of Magnetism

Most materials, including textiles, are diamagnetic, meaning in practice they are nonmagnetic. However, to be precise, some materials are paramagnetic and some ferromagnetic, i.e., they exhibit weak magnetism or significant magnetism, respectively. Widely known ferromagnetic materials are the elements iron (Fe), nickel (Ni), and cobalt (Co).

Starting from elementary substances, noble gases like Ar, Kr, and Xe, semiconducting Ge and Si, and metals like Cu, Ag, and Au are diamagnetic. Oxygen (O_2) and air, however, are paramagnetic. Chemical compounds such as CaO, $FeCl_2$, $NiSO_4$, and $CoCl_2$ exhibit larger paramagnetism than gaseous air. The strongest ferromagnetic materials—besides the abovementioned Fe, Ni, and Co—are alloys of nickel and iron such as $Ni_{80}Fe_{20}$ or $Ni_{78}Fe_{22}$ (permalloy) or alloys of nickel, iron, and molybdenum ($Ni_{75}Fe_{20}Mo_5$, supermalloy). These materials can be sputtered onto different substrates creating thin layers used in covering tapes or shields.

In order to better understand why some specific magnetic properties are so intense or not intense at all, we have to look for an explanation at the atomic scale. Atomic means that the useful unit to measure a distance is 10^{-10} m, a unit which is named ångström (or angstrom), symbolically expressed as 1 Å. Typical atom diameters are equal to about 1 Å, while distances between atoms in solid states vary between 3 Å and 5 Å in many situations. Nevertheless, the macroscopic properties tested in laboratories result from the superposition of the elementary sources of magnetism, the atoms.

The common rule for the occurrence of diamagnetism is that the number of negatively charged electrons, orbiting along the heavy atomic nucleus of the positively charged center, is even. Thus, each electron movement can be treated as an electric current. If there are even numbers of elementary currents, being a principal source of magnetic fields, the total effect is compensated. Importantly, this compensation happens at the atomic level.

For paramagnetic atoms, the number of electrons per atom can be odd and the atoms can be treated as very small magnets possessing north and south poles, so-called magnetic moments. The macroscopic effect is, however, weak, since atoms of paramagnetic substances are independently oriented and disturbed by ambient temperature.

The most surprising situation takes place in ferromagnetic matter. Ferromagnetic atoms are magnetic, but they are additionally coupled to each other due to specific exchange interactions. This coupling is so strong that uniformly magnetized regions, so-called domains, have sizes of up to 1 mm and can be easily observed using optical methods.

In order to identify the type of magnetism in materials at the macro scale, a specimen under investigation should be placed between the poles of a magnetic field. Diamagnetic materials can be ejected from the field region or kept at rest depending on the field intensity. Paramagnetic materials are weakly enforced to be drawn to the field region. Ferromagnetic materials are strongly attracted by the magnetic poles and the magnetic domains are oriented in parallel to the applied field.

Another important factor which can be employed for testing purposes is the dependence of magnetic properties on temperature. Diamagnets are insensitive. Paramagnets are sensitive and the rule is that the higher the temperature of the sample, the lower its sensitivity to magnetization. The behavior of ferromagnets is similar to paramagnets; however, above a certain value of temperature which is called the Curie temperature, being a specific property of a given material, ferromagnetism vanishes and the sample behaves like paramagnetic. For example, the Curie temperature of permalloy equals several hundreds of Kelvins.

To express magnetic properties more quantitatively, the following expression introduces standard magnetic material parameter, the volume susceptibility κ, being the proportionality coefficient between the magnetization M, and the externally applied magnetic field intensity H, namely,

Table 3.1 Values of volume magnetic susceptibilities for several representative substances

Symbol	κ	Substance
He	-9.90×10^{-10}	Gas, diamagnetic
Si	-0.32×10^{-5}	Solid semiconductor, diamagnetic
Au	-3.43×10^{-5}	Metal, diamagnetic
Cu	-0.96×10^{-5}	Metal, diamagnetic
Water	-0.90×10^{-5}	Liquid, diamagnetic
Air	0.04×10^{-5}	Gas, paramagnetic
FeCl$_2$	350.00×10^{-5}	Solid state, paramagnetic
Permalloy	8.00×10^{3}	Solid state, ferromagnetic
Fe	2.00×10^{5}	Metal, ferromagnetic

$$M = \kappa \cdot H.$$

The meaning of the equation above is as follows: The field is a cause and the magnetization is a response. Magnetization expresses the total value of magnetic moments per sample volume.

In order to have idea as to the values of susceptibilities, Table 3.1 provides some values of different substances. It also worth mentioning that the susceptibility of diamagnetic materials is a constant of negative value, which reveals the fact that the diamagnetic specimen can be removed from the regions of an external field. The susceptibilities of paramagnetic and ferromagnetic materials are always positive. Magnetic properties of many materials show a strong directionality (anisotropy); thus magnetization and magnetic field intensity are vector quantities in general.

Figure 3.1 shows different types of magnetism from an atomic perspective, with the single magnetic moments' behavior without an external magnetic field in the left panels and the performance inside an external magnetic field in the right panels.

In the diamagnetic case, only a small net magnetic moment opposite to the external magnetic field is created. In a paramagnetic material, an external magnetic field aligns the atomic magnetic moments which are oriented more and more parallel to the field, the stronger it gets.

In ferromagnetic materials, finally, magnetic domains exist already before applying an external magnetic field and are oriented parallel if brought into such a field. When setting the external field to zero again, this parallel orientation of the single domains is approximately retained. This means that ferromagnets—opposite to materials with other forms of magnetism—show a permanent magnetic orientation even outside any magnetic field, resulting in a so-called hysteresis loop if the magnetization is measured. They can thus be used in a variety of applications some of which are described in the next subchapter.

Figure 3.2 shows a hysteresis loop with typical terms: The coercive field is the external magnetic field at which the magnetization of a sample is set to zero; for pure ferromagnets both coercive fields should be symmetric. The remanence is the residual magnetization in a sample after switching the external magnetic field off.
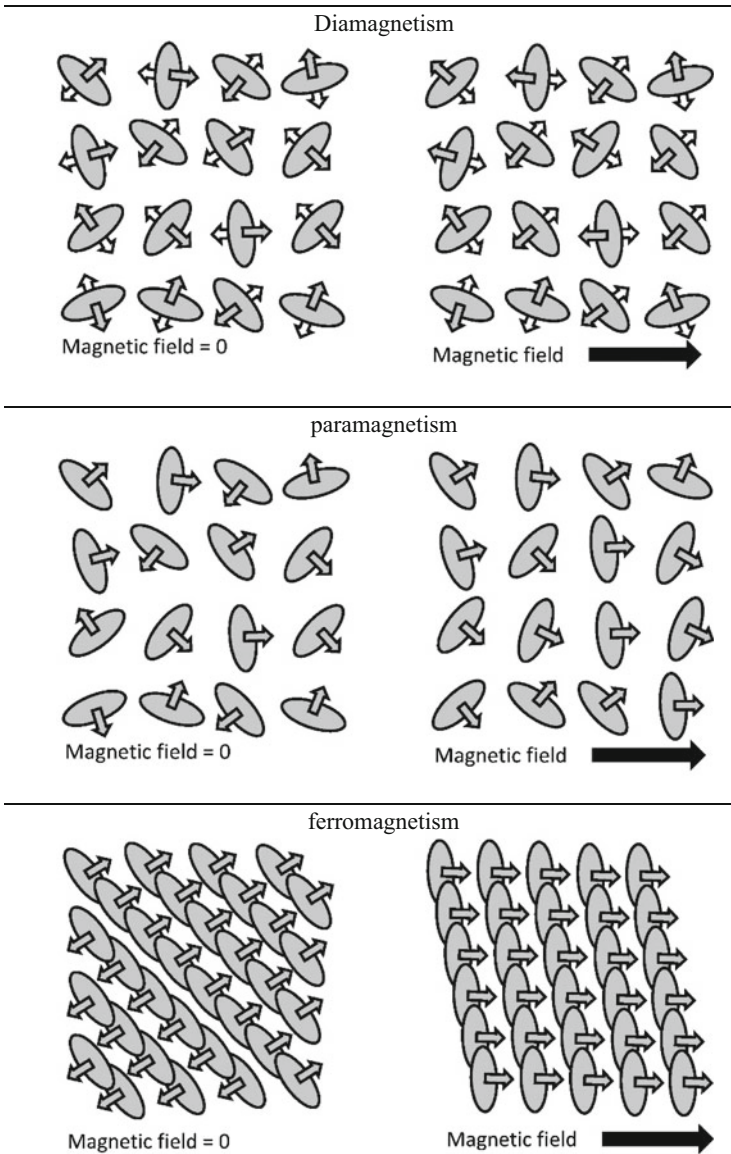
Fig. 3.1 Types of magnetism from the atomic perspective. *Single arrows* represent elementary sources of magnetism (magnetic moments). Different magnetic materials react differently to the influence of an externally applied magnetic field

The saturation magnetization, finally, is the maximally reached magnetization for large external magnetic fields (here ± 1).

Another form of magnetism is, e.g., antiferromagnetism. Here, neighboring magnetic moments are oriented antiparallel so that no net magnetization occurs.

Fig. 3.2 Hysteresis loop of a ferromagnetic material with definitions of coercive fields and remanence
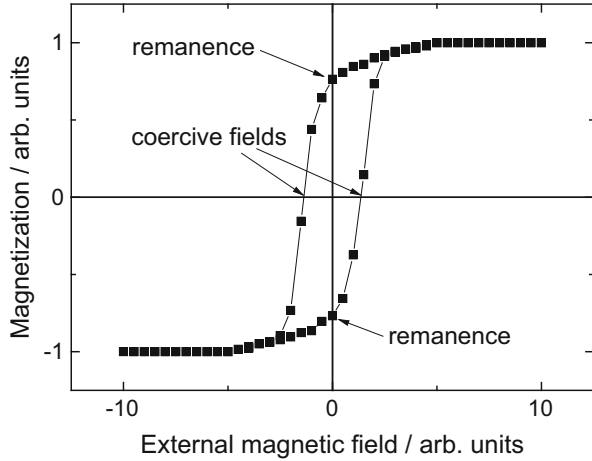
They can especially be used in special combinations with ferromagnetic materials, e.g., in hard desk read/write heads. For higher temperatures, they behave like paramagnets.

Ferrimagnetic materials are built similar to antiferromagnetic ones, with two (or more) different sub-lattices with differently "strong" magnetic moments. Thus, there is a net magnetization measurable in ferrimagnetic materials.

Superparamagnetism, finally, occurs often in very small particles and is thus of technological interest especially in nanotechnology, e.g., in nanoscale finishings or coatings including separate nanoscale particles. Superparamagnetic materials show "closed hysteresis loops," similar to ferromagnets (Fig. 3.2), but without an open area between forward and backward field sweeps. Some possible applications of magnetic materials are given in the next chapter.

3.2 Applications of Magnetic Textiles

While possible utilizations of conductive textiles and coatings are obvious, magnetic textiles seem to be quite special at a first glance. Thus, an overview of possible applications is given in this subchapter.

The first applications coming to one's mind thinking about magnetic textiles are probably related to the magnetic adhesion of such textiles. Magnetic textiles could be used as "foldable whiteboards"—they could be drawn out of the pocket, hanged, and notes could be placed on them with magnets during a meeting or the like (Etre et al. 2014; Sedlatzek 2011).

Depending on the weight of a textile, it could be possible to coat defined areas with a magnetic material in order to allow for transporting it by an electromagnet—in this way, the textile could be "grabbed" not only at the edges but also centrally without the necessity of using needles or similar equipment (which would include

the danger of damaging the surface) to handle it. If the magnetization is high enough in the absence of an external magnetic field, it would even be possible to stick a magnetized textile to a magnetizable object, such as a metallic door frame.

Similarly, magnetic coatings could deal as closure devices in clothing (Bayhan 2014).

These ideas, however, only deal with the mechanical impact of magnetization, i.e., with magnetic forces. Several other applications are possible and have been examined by different research groups in recent times.

A typical application is the shielding against static magnetic fields which can occur around magnetic resonance tomography (MRT) devices, oscilloscopes, laboratory magnets, transformers, motors, etc. Opposite to high-frequency electromagnetic fields which can be screened by conductive materials, low-frequency or static magnetic fields can only be shielded by magnetic materials. Especially leakage magnetic fields around a transformer (in a building) should be shielded if they are higher than the threshold magnetic field value defined by the international Agency for Research on Cancer (IARC) (Sirav et al. 2014). Several recent patents also deal with this issue (Ge et al. 2014; Tang and Tang 2014; Tsuda 2014; Meng and Qi 2012).

It is important to know that the shielding properties are highest around the coercive field of a magnetic material. This means that large magnetic fields should be screened by materials with high coercive fields, e.g., special stainless steel, while shielding against small magnetic fields is ideally performed using materials with low coercive fields, e.g., permalloy. Especially for such relatively small magnetic fields, the possibility to shield them by textiles has been proven by different research groups (Weber et al. 2013; Grabowska et al. 2011; Rau et al. 2011; Brzezinski et al. 2009).

Interestingly, magnetic nanofibers or nanoparticles can also be used as microwave absorbers (Hosseini and Sadeghi 2014; Akman et al. 2013; Aksit et al. 2009).

Another idea is using a magnetic water mark as an option of protection against imitations (Fiedler 2010; Benesovsky 2008). Using a ferrofluid sheet, it is principally possible to make magnetic signs visible. However, thin magnetic coatings on textiles are hard to detect using such an easy detector; thus, for an industrial application either the magnetic field strength or the detector sensitivity has to be increased (Costandache and Baltag 2009).

Similarly, magnetic ink on textiles could be used for technical production error detection systems in order to overcome the sometimes not optimal efficiency of artificial eyes (You 2014).

Magnetic coatings can also modify the hydrophobicity (water repellency) of textile surfaces by changing the surface structure in the presence of an external magnetic field. The challenge in this aim is to increase the effect from recent changes of the contact angle about 10° and changes of the roll-off angle about 20° (Ho et al. 2013) to technologically more significant modifications—possibly using a combination of optical, magnetic, mechanical, chemical, and thermal conditions (Verplanck et al. 2007).

Alternatively, it is possible to enhance the hydrophobicity of a textile by coating with hydrophobic magnetic nanoparticles in a magnetic field (Fang et al. 2010).

One of the applications of magnetic particles attracting much interest of diverse research groups is the textile wastewater treatment. Mesoporous nanocomposites containing magnetic particles can, e.g., be used as adsorbent in the removal of textile wastewater (Wang et al. 2015). Biosynthesized iron oxide nanoparticles can be used to decolorize textile dyes by ultrasonication (Karthikeyeni et al. 2015). Similarly, magnetic catalysts can be separated from the solution in textile waste-waters (Narian et al. 2015; Bhukal et al. 2015). Comparable ideas can be found in several approaches of wastewater treatment.

Other applications are more related to biology or medicine. Composites containing magnetic nanoparticles can, e.g., be used in adsorption–desorption cycles of rhodamine B (Mittal and Mishra 2014). Superparamagnetic iron oxide nanoparticles in textile fibers can be used to prepare tissue-engineered vascular grafts which can be imaged in magnetic resonance tomography (MRT) (Mertens et al. 2015). Similarly, magnetic iron particles can be used in other implants (Hansen et al. 2013; Slabu et al. 2012; Kramer et al. 2010) for visualization in MRT.

Magnetic conductors are often used as antenna substrates, allowing for enhancing the transmission of coplanar waveguide and other antennas (Kamardin et al. 2015; Yan et al. 2014). Such textile antennas with artificial magnetic conductors (AMC) can, e.g., be integrated in wearable medical body area network devices (Jiang et al. 2014) or telemedicine applications (Raad et al. 2013) and are thus intensively investigated by diverse research groups (Virili et al. 2014; Mantash et al. 2012; Bai and Langley 2009).

The application of magnetic fibers, yarns, and fabrics for textile antennas and other smart textiles in forms of coils, sensors, and actuators has drawn a lot of attention onto this area, leading to several research groups investigating and optimizing magnetic properties of textiles (Grosu et al. 2015; Rubacha and Zieba 2007; Farshad et al. 2007; Rubacha and Zieba 2006).

Special applications of magnetic textiles include magneto-chromatic microactuators fixed in a polymeric microstructure, allowing for changing the color of a textile in different positions by changing the external magnetic field, which makes this technique capable of creating pixels in color-changing patterns (Kim et al. 2012), or magneto-rheological fluids in a spacer fabric to change the stiffness of a composite according to an external magnetic field (Mistik et al. 2012).

Finally, magnetic actuators can be used in shape memory polymers which change their shape according to external triggers, such as thermal, chemical, or also magnetic influences (Meng and Li 2013; Leng et al. 2009). Especially nickel–manganese–gadolinium polymer composites are often used in textile applications (Kauffmann-Weiss et al. 2012; Leng et al. 2011; Dunand and Mullner 2011).

All these possible applications, however, require magnetic materials being integrated into textiles. The next subchapter describes some methods to reach this aim.

3.3   Making Textiles Magnetic

Several possibilities exist to create (ferro)magnetic textiles, similar to the methods to produce conductive textiles.

First, textiles can be woven, knitted, or braided from magnetic yarns. Several stainless steel yarns—mostly used due to their conductive properties—are also magnetic, even if the specified alloy is actually nonmagnetic. Magnetic properties can occur due to the production process of the fine magnetic fibers which are drawn from thicker fibers. In this process, modifications of the grain structure inside the alloy may occur, resulting in ferromagnetic properties instead of the original paramagnetic ones. Whether a stainless steel yarn is magnetic or not can simply be tested using a permanent magnet and watching whether it attracts the yarn or not.

If a fabric is basically produced from nonmagnetic materials, magnetic properties can be added by adding magnetic yarns or wires. Figure 3.3 shows two polyester warp knitted fabrics with additional stainless steel wires of different diameters which are included in weft direction. The resulting magnetic fabrics can, e.g., be used for shielding of static magnetic fields.

Another possibility to create magnetic textiles is based on magnetic coatings. On the one hand, simple iron powder can be integrated in a coating compound. However, problems may occur due to oxidizing of the powder which has to be avoided adding special anti-oxidizing agents.

On the other hand, commercially available iron pigments can be used which are constructed as core–shell particles, with a magnetic core and a shell preventing it from oxidization. It should be mentioned that such particles do not form a conductive coating due to the nonconductive shells. Figure 3.4 shows examples of such core–shell flakes coated on different polyester fabrics, resulting in more or less closed magnetic layers.

A recent method to make textiles magnetic is based on 3D printing. Since ferromagnetic filaments exist for Fused Deposition Modeling (FDM) printers, it is
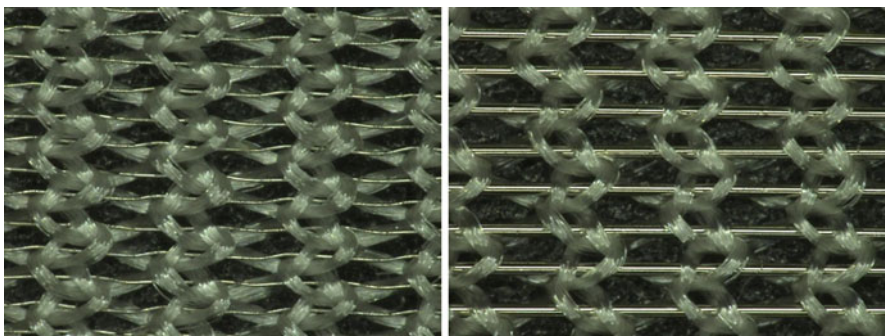
Fig. 3.3 Stainless steel wires of diameter 18 μm (*left panel*) and 100 μm (*right panel*), respectively, in warp knitted polyester fabrics
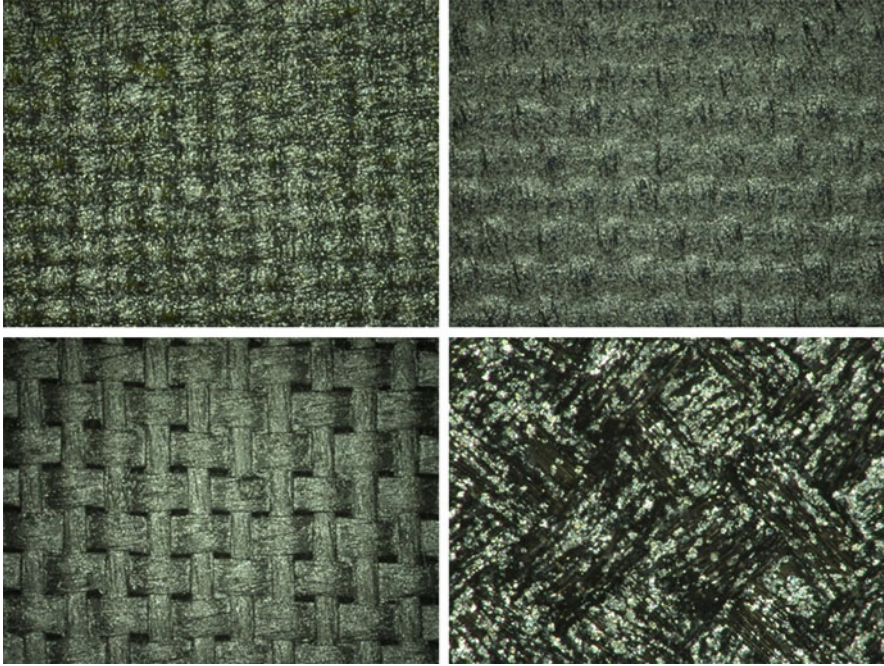
Fig. 3.4 Coatings with Ferricon® flakes (produced by Eckart GmbH, Germany) on different polyester fabrics

now possible to add magnetic properties in the desired strength—modified by the printed layer thickness—on exactly defined positions of a sample.

Figure 3.5 shows that one 3D printed layer of approximately 0.2 mm thickness is already sufficient to allow for lifting the fabric with a usual magnet. The layer thickness can be modified to about 0.1 mm, depending on the 3D printer used—which is not a significantly higher value than usual in common coating processes. Additionally, depending on the distance between printing nozzle and textile fabric, the printed layer can even be thinner.

One disadvantage of the utilization of 3D printing for textile coating processes, however, is the low production speed, making this technique especially useful for printing special shapes which may be difficult in common screen printing or coating.

Additionally, 3D printing can become interesting if closed layers are necessary. Figure 3.6 shows the surface structure of one- (left panel) and two-layer (right panel) magnetic 3D printing on a polyester woven fabric. While the surface is significantly smoother after two printed layers, the first layer is already completely closed, opposite to the common coatings depicted in Fig. 3.4.

Fig. 3.5 One magnetic layer 3D printed on a polyester woven fabric
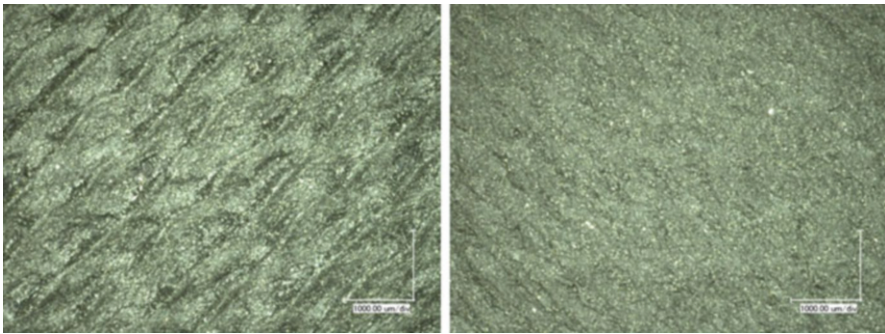
Fig. 3.6 3D printed Magnetic Iron PLA (Proto-pasta, USA) on polyester woven fabrics, one layer (*left panel*) and two layers (*right panel*), respectively

3.4 Measuring Textile Magnetism

Measuring the magnetic properties of a sample is often done using a Superconducting QUantum Interference Device (SQUID) or a Vibrating Sample Magnetometer (VSM). These instruments, however, are expensive and only available in a few universities or research institutes. Additionally, they show another problem related to the magnetism of textile fabrics: usually only small samples (e.g., 10 mm × 10 mm) can be examined. Thus, these devices are in most cases not the first choice to determine the magnetic properties of textile materials.

Instead, it is often helpful to directly measure the properties which are desired in a certain application.

The magnetic force, e.g., can simply be compared between different samples in the following way: similar to a detachment force sensor which is used to measure the layer thickness of a non-magnetizable layer on a ferromagnetic base material, it is possible to measure the detachment force of a specific magnet from a magnetic material with a simple dynamometer or luggage scale (Fig. 3.7). This force depends

Fig. 3.7 Measurement of magnetic force between a magnetic textile which is fixed (*black arrows*) on a base (table, etc.) and a magnet (*gray rectangle*)
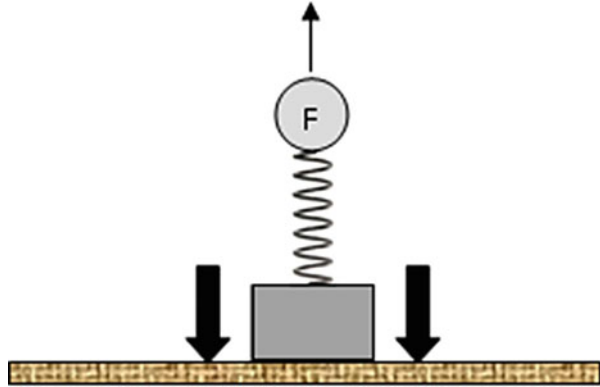
on the properties of the magnet used for this experiment (remanence, geometry), on the distance between test magnet and magnetic textile (it can significantly be reduced by putting a sheet of paper or even higher items between both test partners), and on the magnetic properties of the magnetic textile which are to be tested. If the first parameters are kept constant, the latter can be examined. It should be mentioned that only a relative measurement is possible as long as no other instrument is available to calibrate this self-constructed device.

Another typical application of magnetic textiles is related to their shielding properties against constant magnetic fields. These properties can be measured, e.g., using a Hall probe which can detect the external magnetic field and determine this magnetic field with and without the Hall probe wrapped in a defined number of layers of the magnetic textile under investigation. The magnetic field lines are drawn into the cylinder material, leading to a reduction of the magnetic field inside the cylinders and a respective deformation of the field lines depending on the permeability of the wires (Weber et al. 2013).

Since the shielding factor depends strongly on the value of the external magnetic field, i.e., can nearly vanish for large fields and be quite high for smaller fields, it should be measured like a hysteresis loop: starting from high positive fields, the field is reduced to zero and further swept to large negative values, before the reverse direction is examined. This process is performed with and without the Hall probe being shielded by the magnetic textile.

The shielding properties can be given by the shielding factor

$$S = B_{\text{without}}/B_{\text{with}}$$

giving the relation between the measured magnetic fields with and without the shielding textile. Figure 3.8 shows respective measurements of a pure polyester (PES) warp knitted fabric (green curve) and a warp knitted fabric with nickel (Ni) wires included. While pure PES has no shielding effect, the warp knitted fabric with nickel wires shows strong shielding with a maximum around 0.5 mT. This means that this textile fabric is ideally suited to shield relatively small magnetic

Fig. 3.8 Shielding factors
of a pure PES fabric and a
PES fabric with Ni wires
included as a function of the
externally applied magnetic
field B
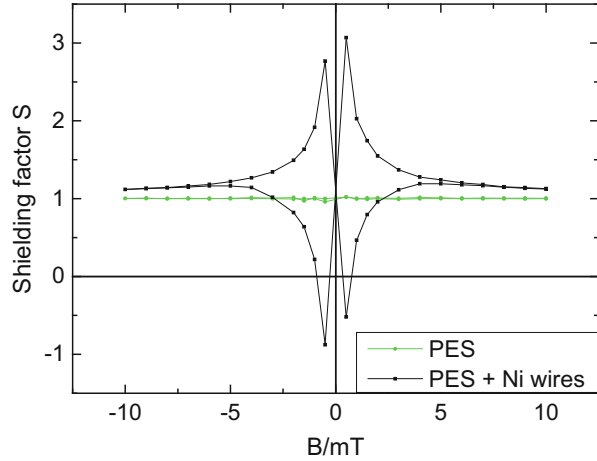
fields of approximately this value. For larger fields, the shielding efficiency is
significantly reduced.

In a similar way, other magnetic textiles should be tested with respect to their
planned application: the possibly changed hydrophobicity of a magnetic textile can
be measured using the contact angle method (see Chap. 5) or similar procedure;
magnetic filters can be tested according to their filtering effect; magnetic water-
marks can be inspected using commercially available ferrofluid sheets; etc.

In all cases, typical permanence tests (such as abrasion resistance, washing
permanence, etc.) which are described in the next chapters can be helpful to
understand the behavior of magnetic textiles during use.

3.5   Simulation of Magnetism in Textiles

Since measuring the magnetic properties of textiles directly is often complicated
due to a lack of measurement instruments, simulations of these properties can help
understanding some basic concepts which are of special importance for textile
coatings and magnetic fibers or wires. All these possibilities to make a textile
magnetic have in common that only thin layers or long, thin objects are involved.
These shapes, however, strongly influence the possible orientation of the magneti-
zation and may thus hamper the utilization of textiles in applications where the
magnetization perpendicular to the textile fabric is important.

Figure 3.9 depicts the differences between in-plane and out-of-plane magnetiza-
tion using the example of very fine iron wires with an aspect ratio (diameter:length)
of 1:7. The in-plane simulation shows an approximately square hysteresis loop,
with large remanences and coercive fields around 400 mT. For the out-of-plane
case, however, the simulation depicts a completely closed loop, with no remanence
and no coercive field. This means that magnetizing a fiber in out-of-plane direction,

Fig. 3.9 In-plane and out-of-plane magnetization of a thin magnetic iron fiber. From Ehrmann (2014), modified
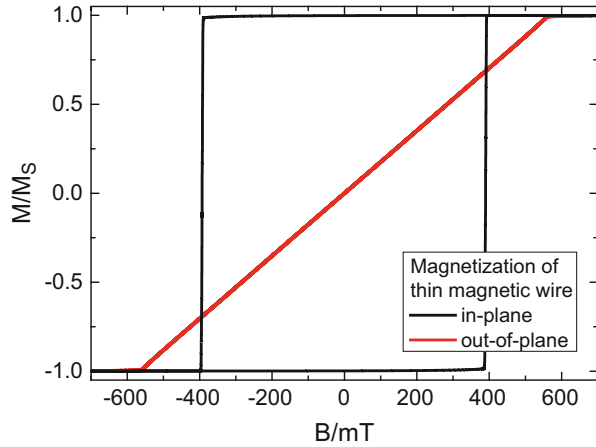
i.e., perpendicular to the fiber axis, does not lead to any remanent magnetization which could be "stored" in the magnetic fiber. In other words, it is not possible to create a magnet in this way which would stick to a refrigerator's door since the magnetization in the fiber is strongly oriented along the fiber axis.

Very similar results were found in diverse simulations of coated fibers or fiber bundles (Ehrmann and Blachowicz 2015) and of thin coatings. In all these cases which are typical for the aforementioned ways to make textiles magnetic, it is only possible to create textiles which are magnetizable—but not magnetic—out of plane (i.e., attracted by an external magnetic field) and which can be permanently magnetic along the fiber/layer orientation. This finding must be taken into account when magnetic textiles are designed for special applications.

Simulations like these can be performed, e.g., using the noncommercial software packages Magpar (Scholz et al. 2003) or OOMMF (Donahue and Porter 1999). Alternatively, several other commercial or free programs allow easy modeling of simple geometries which is often sufficient for getting a first impression of the possible magnetic properties of magnetic fibers or coatings.

Literature

Akman, O., Kavas, H., Baykal, A., Toprak, M.S., Coruh, A., Aktas, B.: Magnetic metal nanoparticles coated polyacrylonitrile textiles as microwave absorber. J. Magn. Magn. Mat. **327**, 151–158 (2013)

Aksit, A.C., Onar, N., Ebeoglugil, M.F., Birlik, I., Celik, E., Ozdemir, I.: Electromagnetic and electrical properties of coated cotton fabric with barium ferrite doped polyaniline film. J. Appl. Polym. Sci. **113**, 358–366 (2009)

Bai, Q., Langley, R.: Crumpled integrated AMC antenna. Electron. Lett. **45**, 662–663 (2009)

Bayhan, S.: Band-shaped closure device for cape or bib, has mutually attracting magnetic units, where magnetic units are arranged watertight on band-shaped water-proof carrier, and filler is arranged to carrier between enclosed magnetic units, Patent CH706946-A2 (2014)

Benesovsky, P.: New System for Brand Protection of Textiles Based on Magnetically Detectable Prints, 4th ITC & CD (2008)

Bhukal, S., Sharma, R., Mor, S., Singhal, S.: Mg-Co-Zn magnetic nanoferrites: characterization and their use for remediation of textile wastewater. Superlattices Microstruct. **77**, 134–151 (2015)

Brzezinski, S., Rybicki, T., Karbownik, I., Malinowska, G., Rybicki, E., Szugajew, L., Lao, M., Sledzinska, K.: Textile multi-layer systems for protection against electromagnetic radiation. Fibres Text. East. Eur. **17**, 66–71 (2009)

Costandache, D., Baltag, O.: Detection of ferromagnetic inclusions. Sens. Lett. **7**, 420–422 (2009)

Donahue, M.J., Porter, D.G.: OOMMF User's Guide, Version 1.0, *Interagency Report NISTIR 6376*, National Institute of Standards and Technology, Gaithersburg, MD (1999)

Dunand, D.C., Mullner, P.: Size effects on magnetic actuation in Ni-Mn-Ga shape-memory alloys. Adv. Mater. **23**, 216–232 (2011)

Ehrmann, A.: Examination and Simulation of New Magnetic Materials for the Possible Application in Memory Cells. Logos Verlag Berlin, Berlin (2014)

Ehrmann, A., Blachowicz, T.: Micromagnetic simulation of fibers and coatings on textiles. J. Inst. Eng. (India) Ser. E **96**, 145–150 (2015)

Etre, K., Stein, R., Dunn, E., Commander, J.: Short communication: rare attraction: evaluating magnetic primers for mounting textiles on rigid backboards with rare earth magnets. J. Am. Inst. Conserv. **53**, 211–218 (2014)

Fang, J., Wang, H.X., Xue, Y.H., Wag, X.A., Lin, T.: Magnet-induced temporary superhydrophobic coatings from one-pot synthesized hydrophobic magnetic nanoparticles. ACS Appl. Mater. Interfaces **2**, 1449–1455 (2010)

Farshad, M., Clemens, F., Le Roux, M.: Magnetoactive polymer composite fibers and fabrics – processing and mechanical characterization. J. Thermoplast. Compos. Mater. **20**, 65–74 (2007)

Fiedler, M.: Authenticity marking set for identifying authenticity of products, has multiple authenticity marking materials which are different from each other and are provided in form of paint or ink on carrier material, Patents DE102008056167-A1; WO2010052270-A1; EP2352880-A1 (2010)

Ge, M., Song, X., Zhou, B.: Low-frequency magnetic fabric shielding efficiency test device, has cylinder fixed with clamp, test station formed with circular-hole, and electric current source fixed with magnetic flux unit that is formed with deep groove, Patent CN203732646-U (2014)

Grabowska, K.E., Marciniak, K., Ciesielska-Wrobel, I.L.: The analysis of attenuation of electromagnetic field by woven structures based on hybrid fancy yarns. Text. Res. J. **81**, 1578–1593 (2011)

Grosu, M.C., Lupu, I.G., Cramariuc, O.: Magnetic cotton yarns – optimization of magnetic properties. J. Text. Inst. (online first) (2015)

Hansen, N.L., Barabasch, A., Distelmaier, M., Ciritsis, A., Kuehnert, N., Otto, J., Conze, J., Klinge, U., Hilgers, R.D., Kuhl, C.K., Kramer, N.A.: First in-magnetic resonance visualization of surgical mesh implants for inguinal hernia treatment. Invest. Radiol. **48**, 770–778 (2013)

Ho, T., Ghochaghi, N., Tepper, G.: Development of magnetic fabrics with tunable hydrophobicity. J. Appl. Polym. Sci. **130**, 2352–2358 (2013)

Hosseini, S.H., Sadeghi, M.: Investigation of microwave absorbing properties for magnetic nanofiber of polystyrene polyvinylpyrrolidone. Curr. Appl. Phys. **14**, 928–931 (2014)

Jiang, Z.H., Brocker, D.E., Sieber, P.E., Werner, D.H.: A compact, low-profile metasurface-enabled antenna for wearable medical body-area network devices. IEEE Trans. Antennas Propag. **62**, 4021–4030 (2014)

Kamardin, K., Rahim, M.K.A., Samsuri, N.A., Jalil, M.E., Majid, H.A.: Transmission enhancement using textile artificial magnetic conductor with coplanar waveguide monopole antenna. Microw. Opt. Technol. Lett. **57**, 197–200 (2015)

Karthikeyeni, S., Vijayakumar, T.S., Vasanth, S., Ganesh, A., Vignesh, V., Akalya, J., Thirumurugan, R., Subramanian, P.: Decolourisation of direct orange S dye by ultra sonication using iron oxide nanoparticles. J. Exp. Nanosci. **10**, 199–208 (2015)

Kauffmann-Weiss, S., Scheerbaum, N., Liu, J., Klauss, H., Schultz, L., Mäder, E., Häßler, R., Heinrich, G., Gutfleisch, O.: Reversible magnetic field induced strain in Ni_2MnGa-polymer-composites. Adv. Eng. Mater. **14**, 20–27 (2012)

Kim, J., Choi, S.E., Lee, H., Kwon, S.: Magnetochromatic microactuators for a micropixellated color-changing surface. Adv. Mater. **25**, 1415–1419 (2012)

Kramer, N.A., Donker, H.C.W., Otto, J., Hodenius, M., Senegas, J., Slabu, I., Klinge, U., Baumann, M., Müllen, A., Obolenski, B., Günther, R.W., Krombach, G.A.: A concept for magnetic resonance visualization of surgical textile implants. Invest. Radiol. **45**, 477–483 (2010)

Leng, J.S., Lu, H.B., Liu, Y.J., Huang, W.M., Du, S.Y.: Shape-memory polymers-a class of novel smart materials. MRS Bull. **34**, 848–855 (2009)

Leng, J.S., Lan, X., Liu, Y.J., Du, S.Y.: Shape-memory polymers and their composites: stimulus methods and applications. Prog. Mater. Sci. **56**, 1077–1135 (2011)

Mantash, M., Tarot, A.C., Collardey, S., Mahdjoubi, K.: Investigation of flexible textile antennas and AMC reflectors. Int. J. Antennas Propag. **2012**, 236505 (2012)

Meng, H., Li, G.Q.: A review of stimuli-responsive shape memory polymer composites. Polymer **54**, 2199–2221 (2013)

Meng, M., Qi, L.: Electromagnetic-wave shielding fabric comprises a conductive fiber, namely stainless steel fiber, silver fiber, aluminum fiber, copper fiber, nickel fiber or a copper-plated fiber, and a absorbing fiber e.g. magnetic powder and metal powder, Patent CN102618994-A (2012)

Mertens, M.E., Koch, S., Schuster, P., Wehner, J., Wu, Z.J., Gremse, F., Schulz, V., Rongen, L., Wolf, F., Frese, J., Gesche, V.N., van Zandvoort, M., Mela, P., Jockenhoevel, S., Kiessling, F., Lammers, T.: USPIO-labeled textile materials for non-invasive MR imaging of tissue-engineered vascular grafts. Biomaterials **39**, 155–163 (2015)

Mistik, S.I., Shah, T., Hadimani, R.L., Siores, E.: Compression and thermal conductivity characteristics of magnetorheological fluid-spacer fabric smart structures. J. Intell. Mater. Syst. Struct. **23**, 1277–1283 (2012)

Mittal, H., Mishra, S.B.: Gum ghatti and Fe_3O_4 magnetic nanoparticles based nanocomposites for the effective adsorption of rhodamine B. Carbohydr. Polym. **101**, 1255–1264 (2014)

Narian, E., Arami, M., Bahrami, H., Pajootan, E.: Modification of nickel ferrite with cationic surfactant: dye removal from textile wastewater using magnetic separation. J. Environ. Eng. **141**, U50–U59 (2015)

Raad, H.R., Abbosh, A.I., Al-Rizzo, H.M., Rucker, D.G.: Flexible and compact AMC based antenna for telemedicine applications. IEEE Trans. Antennas Propag. **61**, 524–531 (2013)

Rau, M., Iftemie, A., Baltag, O., Costandache, D.: The study of the electromagnetic shielding properties of a textile material with amorphous microwire. Adv. Electr. Comput. Eng. **11**, 17–22 (2011)

Rubacha, M., Zieba, J.: Magnetic textile elements. Fibres Text. East. Eur. **14**, 49–53 (2006)

Rubacha, M., Zieba, J.: Magnetic cellulose fibres and their application in textronics. Fibres Text. East. Eur. **15**, 101–104 (2007)

Scholz, W., Fidler, J., Schrefl, T., Suess, D., Dittrich, R., Forster, H., Tsiantos, V.: Scalable parallel micromagnetic solvers for magnetic nanostructures. Comput. Mat. Sci. **28**, 366 (2003)

Sedlatzek, F.: Magnetic wallpaper useful as hand-decorative attachments e.g. boards in exhibition booths and shop windows, comprises carrier material, and magnetic surface layer that contains PVC plastisol and magnetic particles, Patent DE102010020922-A1 (2011)

Sirav, B., Sezgin, G., Seyhan, N.: Extremely low-frequency magnetic fields of transformers and possible biological and health effects. Electromagn. Biol. Med. **33**, 302–306 (2014)

Slabu, I., Güntherodt, G., Schmitz-Rode, T., Krämer, N., Donker, H., Otto, J., Kuhl, C., Klinge, U., Baumann, M.: Investigation of magnetic nanoparticles incorporated within textile hernia implants. Biomed. Eng. **57**, 750 (2012)

Tang, X., Tang, Y.: Electromagnetic wave absorbing radiation proof magnetic healthcare composite material inorganic substance includes maghemite, copper oxide, zinc oxide, manganese

dioxide, chromium oxide, nickel oxide, cobalt oxide and magnesium oxide, Patent CN104045867-A (2014)

Tsuda, O.: Magnetic shielding paper used in e.g. electronic device, consists of metal material having magnetic shielding performance, Patent JP2014090142-A (2014)

Verplanck, N., Coffinier, Y., Thomy, V., Boukherroub, R.: Wettability switching techniques on superhydrophobic surfaces. Nanoscale Res. Lett. **2**, 577–596 (2007)

Virili, M., Rogier, H., Alimenti, F., Mezzanotte, P., Roselli, L.: Wearable textile antenna magnetically coupled to flexible active electronic circuits. IEEE Antennas Wirel. Propag. Lett. **13**, 209–212 (2014)

Wang, Y.G., Yao, M.C., Chan, Y.T., Zuo, Y.H., Zhang, X.D., Cui, L.F.: General synthesis of magnetic mesoporous FeNi/graphitic carbon nanocomposites and their application for dye adsorption. J. Alloys Compd. **627**, 7–12 (2015)

Weber, M.O., Akter, F., Ehrmann, A.: Shielding of static magnetic fields by textiles. Ind. Text. **64**, 184–187 (2013)

Yan, S., Soh, P.J., Vandenbosch, G.A.E.: Low-profile dual-band textile antenna with artificial magnetic conductor plane. IEEE Trans. Antennas Propag. **62**, 6487–6490 (2014)

You, F.: Production error detect system used in textile manufacturing industry, has magnetic ink detect and identify sub-system that is provided with control center connected with magnetic detector and alarm device and photoelectric sensor, Patent CN203444492-U (2014)

Chapter 4
Dielectric Yarns, Fabrics and Coatings

Dielectric textiles and coatings are not often mentioned. Opposite to conductive or magnetic properties, the term "dielectric" is not even well known. Dielectric properties, however, are important for several smart textiles, especially for textile capacitors which may help storing energy in textiles. This chapter will thus give a short overview of dielectricity, dielectric properties of different textiles, and some ideas when to use dielectric textiles and how to measure them.

4.1 What Is Dielectricity?

The rules and expressions given in Chap. 2 were useful for descriptions of electric charge transport phenomena. For dielectricity, however, insulators are necessary. Dielectric properties describe how different nonconductive textiles are influenced by an electric field. Since isolators have well-positioned atoms or molecules, they can react on static or oscillating electric field by deformations of electric charge distributions localized around these atoms or molecules. This effect is called polarization, and it may be static or oscillating in nature.

The response on static or oscillating electric fields is a material-dependent property. In the dynamic case, the atoms or ions oscillate with the same frequency as the external electric field. Hence, the material characteristics result from the fundamental, underlying effect of polarization.

Polarization is an atomic-scale phenomenon. Basically, it relies on a spatial deviation of the electric charges from the equilibrium positions of minimum energy. In other words, polarization is a relative shift of positive and negative electric charges in opposite directions. There are the three distinct mechanisms of polarization: orientation polarization (reorientation of molecules), ionic polarization, and electron polarization. Importantly, for the dynamic case, the frequency regions adequate for the three mechanisms are as follows:
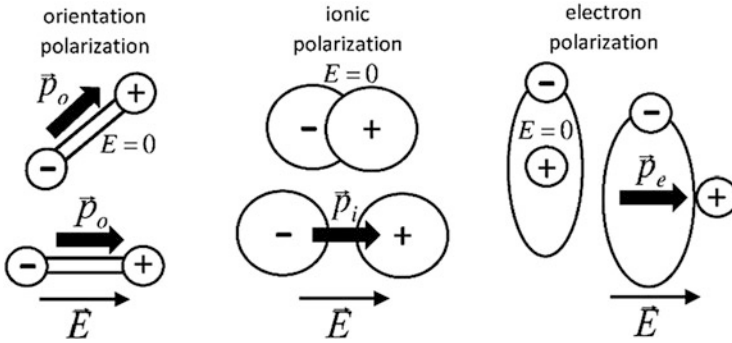
Fig. 4.1 The three mechanisms of polarization of insulating materials from the atomic-scale perspective. The deformation of electric charges results from the application of an external electric field E

- All three types of polarization: 10^8–10^{11} Hz, VHF radio waves, and microwaves.
- Ionic and electron polarization: 10^{13} Hz and infrared waves (IR).
- Electron polarization: 10^{15} Hz, visible (VIS), and ultraviolet (UV) ranges.

As we can recognize, the slowest effects result from reorientations of molecules which are polarized even if no external field is applied. Ionic polarization effects are faster, while chemical molecules do not exhibit polarization under zero electric field. The fastest effects are those based on deformation of electron clouds in atoms, while similarly to the ionic mechanism, there is no electron polarization if no field is accessible. The underlying mechanisms of polarization are explained graphically in Fig. 4.1.

Now some explanations about practical measurement will be provided. The local separation of electric charges can be expressed by the elementary dipole moment $\vec{p}$. The unit of this vector is C m (coulomb meter). The dipole moment $\vec{p}$ is a response on the electric field intensity and is thus proportional to it,

$$\vec{p} = \alpha \cdot \vec{E},$$

where α is the so-called polarizability expressed in F m^2 (farad square meter). For example, the value of the electron polarizability of carbon equals 2×10^{-40} F m^2, the ionic polarizability is of the same order for most molecules, and the orientation polarizability is about 10 times greater.

A real macroscopic sample can be characterized then by a product of the concentration n and the elementary dipole moment, namely,

$$\vec{P} = n \cdot \vec{p},$$

where $\vec{P}$ is the polarization of material, a measurable quantity, expressed in C m^{-2} units. The polarization $\vec{P}$ can obviously be treated, similarly to $\vec{p}$, as a response to

the externally applied electric field, and in many practical situations, when the field intensities are not too high, polarization is again proportional to the field. This fact can be expressed as follows:

$$\vec{P} = n \cdot \alpha \cdot \vec{E} = \kappa \cdot \varepsilon_0 \cdot \vec{E},$$

where κ is the electric susceptibility and ε_0 is the electric permeability of vacuum which equals 8.85×10^{-12} F/m.

Importantly, the electric field $\vec{D}$ inside a dielectric material, in the presence of an externally applied electric field, is the sum of this field and the internally induced field represented by the medium polarization $\vec{P}$, namely,

$$\vec{D} = \varepsilon_0 \vec{E} + \vec{P}.$$

Hence, $\vec{D} = \varepsilon_0 \vec{E} + \vec{P} = \varepsilon_0 \vec{E} + \kappa \cdot \varepsilon_0 \cdot \vec{E} = (1 + \kappa) \cdot \varepsilon_0 \cdot \vec{E} = \varepsilon \cdot \varepsilon_0 \cdot \vec{E}$, where $\varepsilon = 1 + \kappa$ is the relative electric permittivity of a material.

From this macroscopic perspective, some dielectrics may be polar, meaning that they have nonzero stable polarization even if no external field is applied (H_2O, $p = 2 \times 10^{-30}$Cm), or nonpolar when the dominating mechanism of polarization is electron like. Sometimes polar dielectrics can form micro-regions of the same polarization direction, the dielectric domains, similar to magnetic domains. These materials are named ferroelectrics, like $BaTiO_3$ or $PbTiO_3$ compounds.

At the end of these basic considerations, some information about the results of measurements of textile dielectrics in the presence of an oscillating electric field will be provided. Then, the polarization and all underlying quantities, including the relative electric permittivity, are frequency dependent; thus, $\varepsilon(f) = 1 + \kappa(f)$, with the frequency f of the externally applied electromagnetic waves. The response of a typical material has resonance character, meaning that for a certain value of the frequency, the absorption of the wave is maximized. It is worth mentioning that in general $\varepsilon(f)$ is a complex number, namely, $\varepsilon(f) = \varepsilon'(f) - i\varepsilon''(f)$, and the resonance takes place for the imaginary part $\varepsilon''(f)$, while for low frequencies or static situations $\varepsilon''(0) = 0$. Sometimes, the dissipation factor $\tan \delta = \varepsilon''/\varepsilon'$ can be measured and due to measurements of ε' and $\tan \delta$ the ε'' part can be indirectly determined. Table 4.1 provides the results of measurements of electric parameter of selected textile materials. It should be mentioned that all numbers given are only examples for specific fabric thicknesses, surface masses, porosities, etc., and cannot be assumed to be universal for all textile fabrics produced from the same material.

Table 4.1 Electric parameters of diverse textile materials

Sample	Frequency/ Hz	ε' ($\tan\delta$)	References
Banana fiber composite	10^1–10^4	30–5 (2–0.01)	Joseph and Thomas (2008)
Coir fiber-reinforced epoxy composite	10^1–10^4	3.5–6.5 (0.0051–0.0032)	Khan et al. (2015)
Cotton, plain weave		2.077 (0.0314)	Leśnikowski (2012)
Elano-wool, plain weave		1.670 (0.0073)	Leśnikowski (2012)
Hybrid alfa/wool/polymeric	10^{-1}–10^6	100–5 (100–0.01)	Triki et al. (2013)
Jute textiles		1.7–5.5	Mustata and Mustata (2014)
Jute/bamboo	10^3–10^6	6–2 (0.4–0.05)	Jayamani et al. (2014)
Kapok fiber	10^2–10^6	7–4.5 (1.4–0.01)	Mani et al. (2012)
Polyester, plain weave		1.748 (0.0044)	Leśnikowski (2012)
Ramie fibers	10^2–10^7	14–4 (0.4–0.05)	Sao et al. (1990)
Wool, plain weave		1.865 (0.0079)	Leśnikowski (2012)
Wool + polyamide, plain weave		1.529 (0.0052)	Leśnikowski (2012)

4.2   Applications of Dielectric Textiles and Coatings

Dielectric textiles are of special importance for textile capacitors which can be used in different ways. Firstly, textile capacitors offer the possibility to store energy. This energy may stem from a textile or textile-integrated solar cell, from piezo actuators in the shoes, or simply be delivered by plugging in a modified battery charger. Second, textile capacitors can be used as pressure sensors (Sergio et al. 2002; Meyer et al. 2006, 2010; Holleczek et al. 2010; Enokibori et al. 2013; Bansal et al. 2014).

Such capacitors can be built in cylindrical form, as a zigzagging stack or in other shapes (Gu et al. 2010), and can show relatively low capacities of around $70\,\text{nF}\,\text{m}^{-1}$ up to approximately $40\,\text{mF}\,\text{cm}^{-1}$ (Jost et al. 2014). Other textile capacitors are, e.g., inkjet printed (Li et al. 2012) or produced as composites (Liu et al. 2015).

In both cases, an important parameter of the capacitor is given by the dielectric material between the two electrodes, independent of their shape (yarn, textile layer, or coating) and their conductivity.

For a simple parallel-plate capacitor, its capacity C can be calculated as

$$C = \varepsilon\varepsilon_0\frac{A}{d}$$

with the electrode area A and the electrode distance d. The capacity describes the possibility of a capacitor to store charge which can be used afterward, like in a battery.

Other capacitors, such as cylinder capacitor or a capacitor built from two parallel yarns, are mathematically described by more complicated formulas; however, in all

cases the capacity is proportional to ε, the relative electric permittivity of the material between both electrodes.

This formula shows the importance of using materials with high values of ε, especially for capacitors as energy storage systems. It should be mentioned that even for capacitors used as pressure sensors, the sensitivity of these sensors is increased by dielectrics with higher ε_r values (Bansal et al. 2014).

While usual textile fibers already show relative permittivities varying about two orders of magnitude (Table 4.1), other materials offer significantly higher values of ε. For water at room temperature, e.g., $\varepsilon \sim 80$, while this value is approximately between 1250 and 10,000 for barium titanate ($BaTiO_3$) and larger than 250,000 for calcium copper titanate (Young and Freedman 2012; Guillemet-Fritsch et al. 2006). This means that coatings with respective materials offer the possibility to strongly increase the capacitance of a capacitor without changing its geometry.

4.3 Measuring Dielectric Properties of Textiles and Coatings

The easiest way to measure solely the dielectric properties of textiles and textile coatings—without taking into account the influence of conductive textile electrodes with possibly not exact distances due to the production of textile layers and coatings, textile conduction lines, etc.—is using a simple parallel-plate capacitor which is available in most physics laboratories of most universities. Here, it is also often possible to find a capacitance meter which can measure capacitances. Some multimeters may also have a measurement range for farad (F); however, these non-specialized instruments often lack the desired accuracy. For multimeters, measurement errors of approximately 4–5 % are usual, while specialized capacitance meters can reach accuracies of less than 1 %. Depending on the respective application, it must be decided whether a usual multimeter with included capacitance measure function is sufficient or a capacitance meter is necessary.

Figure 4.2 shows the capacitance of air, compared with different textiles, measured for varying distances between the plates of a parallel-plate capacitor. The dielectric constant of glass or glass wool fibers is approximately 5–10 (Bansal et al. 2014), resulting in a significant increase of the capacitance compared with pure air in the capacitor. An additional thin layer of $BaTiO_3$ coating, however, increases the capacitance even stronger.

The measurement values shown here were taken with an inexpensive capacitance meter with a measurement uncertainty of max. 2 % which is apparently sufficient for the development of high-permittivity textiles and coatings.

Fig. 4.2 Capacitance of air and different textile materials
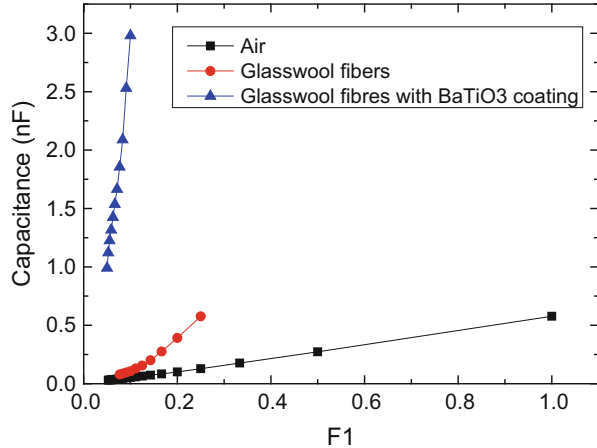
Literature

Bansal, N., Ehrmann, A., Geilhaupt, M.: Textile capacitors as pressure sensors. In: Proceedings of Aachen-Dresden international textile conference (2014)

Enokibori, Y., Suzuki, A., Mizuno, H., Shimakami, Y., Mase, K.: E-textile pressure sensor based on conductive fiber and its structure. In: Proceedings of the 2013 ACM conference on pervasive and ubiquitous computing adjunct publication, pp. 207–210 (2013)

Gu, J.F., Gorgutsa, S., Skorobogatiy, M.: Soft capacitor fibers for electronic textiles. Appl. Phys. Lett. **97**, 133305 (2010)

Guillemet-Fritsch, S., Lebey, T., Boulos, M., Durand, B.: Dielectric properties of $CaCu_3Ti_4O_{12}$ based multiphased ceramics. J. Eur. Ceram. Soc. **26**, 1245–1257 (2006)

Holleczek, T., Rüegg, A., Harms, H., Tröster, G.: Textile pressure sensors for sports applications. Sensors **10**, 732–737 (2010)

Jayamani, E., Hamdan, S., Rahman, M.R., Bakri, M.K.B.: Comparative study of dielectric properties of hybrid natural fiber composites. Proc. Eng. **97**, 536–544 (2014)

Joseph, S., Thomas, S.: Electrical properties of banana fiber-reinforced Phenol Formaldehyde composites. J. Appl. Polym. Sci. **109**, 256–263 (2008)

Jost, K., Durkin, D.P., Haverhals, L.M., Brown, E.K., Langenstein, M., de Long, H.C., Trulove, P.C., Gogotsi, Y., Dion, G.: Natural fiber welded electrode yarns for knittable textile supercapacitors. Adv. Energy Mater. **5**, 1401286 (2014)

Khan, A., Ahmad, M.A., Joshi, S.: A systematic study for electrical properties of chemically treated coir fiber reinforced epoxy composites with ANN model. Int. J. Sci. Res. **4**, 410–414 (2015)

Leśnikowski, J.: Dielectric permittivity measurement methods of textile substrate of textile transmission lines. Electr. Rev. **88**, 148–151 (2012)

Li, Y., Torah, R., Beeby, S., Tudor, J.: An all-inkjet printed flexible capacitor on a textile using a new poly(4-vinylphenol) dielectric ink for wearable applications. IEEE Sens. **2012**, 1–4 (2012)

Liu, L., Yu, Y., Yan, C., Li, K., Zheng, Z.: Wearable energy-dense and power-dense supercapacitor yarns enabled by scalable graphene–metallic textile composite electrodes. Nat. Commun. **6**, 7260 (2015)

Mani, G.K., Rayappan, J.B.B., Bisoyi, D.K.: Synthesis and characterization of kapok fibers and its composites. J. Appl. Sci. **12**, 1661–1665 (2012)

Meyer, J., Lukowicz, P., Tröster, G.: Textile pressure sensor for muscle activity and motion detection. In: 10th IEEE international symposium on wearable computers, pp. 69–72 (2006)

Meyer, J., Arnrich, B., Schumm, J., Tröster, G.: Design and modeling of a textile pressure sensor for sitting posture classification. IEEE Sens. J. **10**, 1391–1398 (2010)

Mustata, F.S.C., Mustata, A.: Dielectric behaviour of some woven fabrics on the basis of natural cellulosic fibers. Adv. Mater. Sci. Eng. **2014**(216548) (2014)

Sao, K.P., Samantaray, B.K., Bhattacherjee, S.: Electrical properties of ramie fibres. J. Mater. Sci. Lett. **9**, 446–469 (1990)

Sergio, M., Manaresi, N., Tartagni, M., Guerrieri, R., Canegallo, R.: A textile based capacitive pressure sensor. Sensors **2**, 1625–1630 (2002)

Triki, A., Omri, M.A., Guicha, M., ben-Hassen, M., Arous, M., Kallel, A.: Correlation between mechanical and dielectric properties of Alfa/Wool/Polymeric hybrid fibres reinforced polyester composites. In: IOP conference series: materials science and engineering, vol. 48, 012008 (2013)

Young, H.D., Freedman, R.A.: University Physics with Modern Physics. Addison-Wesley, San Francisco (2012). ISBN 978-0-321-69686-1

Chapter 5
Optical Examinations of Fibers, Yarns, and Fabrics

For most people, the eyes are their most important sensory organ. Thus, it is no wonder that optical examinations are often an important part of the investigation of textile samples.

Optical examinations can be subdivided into different techniques, resulting in various resolutions and magnifications, respectively, allowing detecting structural features of a sample at different scales.

This chapter gives a short overview of the definitions of the terms "resolution" and "magnification," before frequently used microscopic technologies—optical microscopy, confocal microscopy, and scanning electron microscopy—are described with their advantages and limitations.

5.1 Resolution and Magnification

The angular resolution (or spatial resolution) of a microscope describes how small an object may be to be distinguishable from its neighbors or how large the distance between neighboring point sources may be to realize them as two single objects.

The Rayleigh criterion, defined by Lord Rayleigh, states that two point sources can be just resolved when the principal diffraction maximum of one image overlaps with the first minimum of the other one (Lord Rayleigh 1879). Diffraction effects due to the wave nature of light and the finite apertures of optical instruments can be estimated using the Rayleigh criterion. In this way, it can be shown that the principal maximum spatial resolution of optical instruments, using visible light, is roughly half the wavelength of the used light. As a function of the color of the light, optical microscopes can theoretically reach resolutions between approximately 200 nm and 400 nm. Depending on the details of the optics, the numerical aperture of a microscope can differ, resulting in even increased possible resolutions. If this theoretical limit is reached, the optical instrument is called "diffraction limited."

These theoretical limits, however, cannot be reached by each microscope. But how strongly can a microscope increase the resolution of a sample under investigation, compared with the pure human eye?

If an object is observed in a typical reading distance of about 25 cm, the resolution of the human eye is approximately 40 µm, i.e., 0.04 mm. This can be compared with a human hair which has an average diameter of 50–80 µm for most people, with fine hair having reduced diameters of around 20–40 µm. A typical human hair is thus just visible in a distance of 25 cm. Finer fibers can often be noticed when being moved in front of the eyes. Fibers with diameters of around 10 µm or less, however, are hard to detect with the naked eye, even if it is known where they should be found.

Keeping in mind that the human eye has a resolution of approximately 40 µm, a microscope with a magnification factor of 20 should allow for visualizing features of the order of magnitude 2 µm, and a magnification factor of 200 should result in a resolution of 0.2 µm = 200 nm—which would be the theoretical maximum of the resolution reachable with visible light. But why are there so many inexpensive USB microscopes with magnification 200 times, and what does an optical microscope with 2000 times magnification show?

In all magnifying optical techniques, carefully distinguishing between resolution and (nominal) magnification is necessary.

Principally, the linear magnification is defined as the proportion between the apparent size and the real size of an object.

For an analogue microscope which is used by looking through an ocular with the eye, this means that the visual angle is increased. In this case, the angular magnification is unambiguously given by comparing the angles of sight with and without the microscope.

For a digital microscope, the (nominal) magnification is defined as a linear magnification, comparing the length of the real object with the length of the object on the screen (Hecht 2005). This screen, however, may be changed in size, changing the (nominal) magnification of the microscope without adding or subtracting any information in the picture. Printing the obtained microscopic picture in arbitrary sizes will again result in different magnifications—and can often not even be influenced by authors sending manuscripts to journals for publication.

Thus, the (nominal) magnification of a digital microscope is completely independent of the resolution which can be reached with the respective microscope. This is why in microscopic pictures a length bar (scaling with the image) should be included instead of a figure caption stating the magnification.

Nowadays, often digital microscopes are used. For the digitalization of microscopic images, the so-called Nyquist criterion becomes important.

In order to preserve the optical resolution of a microscopic picture, it is necessary to represent it by an adequate number of pixels so that the latter are spaced closely enough. If two different dark points have to be separated in the digital image, it is necessary to have a darker or a bright pixel between them. Taking this
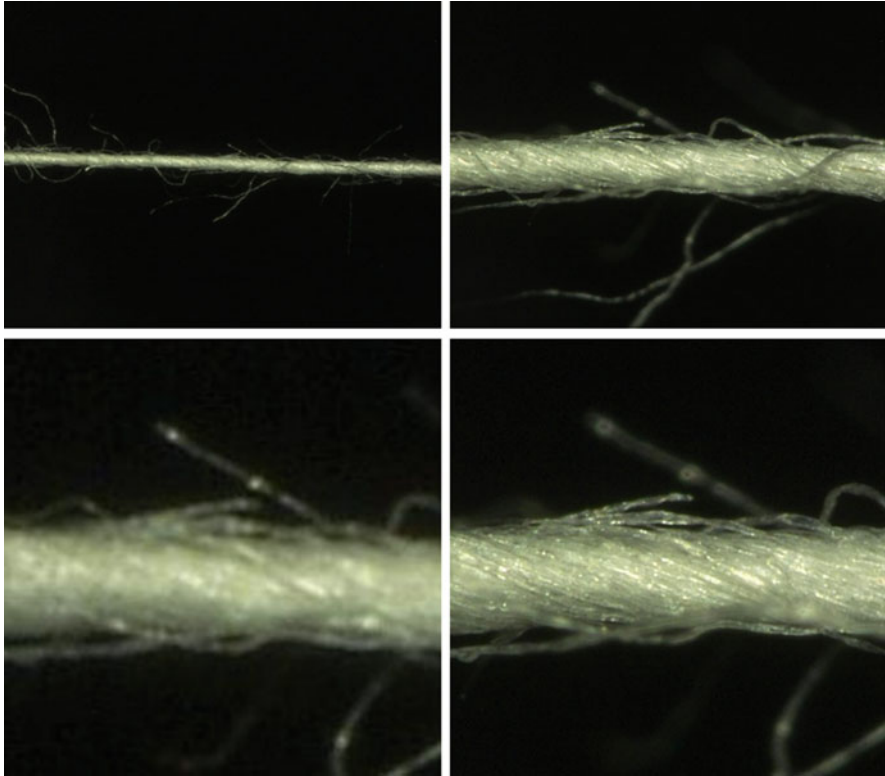
Fig. 5.1 Microscopic pictures of a cotton ring yarn, taken with different magnifications (*upper panels*), and respective details (*lower panels*)

idea into account, the minimum optically separable distance would be represented by 3 pixels.

The Nyquist criterion states that more precisely 2.3 pixels are necessary to depict the minimally separable optical distance. This means that for a possible optical resolution of 460 nm, it is necessary to have pixel widths of 200 nm. A slightly decreased pixel size may make sense in some cases; oversampling with more than 3 pixels, however, only leads to an undesired enlargement of the image file size.

Figure 5.1 depicts two pictures of a cotton ring yarn (upper panels), taken with nominal magnifications of $50\times$ and $200\times$, using a digital optical microscope. These magnifications are related to a $15'$ screen; printing the images in the small sizes used here thus decreases the magnification strongly.

The lower panels show respective details of both images. The left picture, depicting a detail of the yarn examined with $50\times$ nominal magnification, is clearly blurred, while the picture on the right side depicts much more clear details.

The Nyquist criterion can help calculating the maximum resolution of a digital microscopic image. The original pictures shown in Fig. 5.1 (upper panels) have sizes of 1200×1600 pixels. For a nominal magnification of $50\times$ ($200\times$), the

images correspond to object sizes of 4.6 mm × 6.1 mm (1.14 mm × 1.52 mm). Thus, the "longitudinal" resolution of the picture with magnification 50× is 4.6 mm/1200 pixels × 2.3 (due to the Nyquist criterion) = 8.8 μm; the "vertical" resolution is naturally identical. For a magnification of 200×, the resolution is correspondingly 2.2 μm.

Other optical microscopes allow for nominal magnifications of up to 2500×, using otherwise identical values of pixels per image and screen size. Such a magnification would be correlated with a resolution of 176 nm—which is impossible in usual microscopes utilizing light in the visible range (~380–750 nm). Thus, nominal magnifications larger than 2000× are useless if the other parameters (1200 × 1600 pixels, 15′ screen) are kept constant.

Figure 5.2 depicts microscopic images of laser-treated polyester woven fabrics with nominal magnifications of 250× (upper left panel) and 2500× (upper right panel), respectively. The lower panels show details of these photographs, depicting ¼ of the widths and heights of the original images. While in the lower left panel, the resolution is clearly limited by the pixel size, the lower right panel shows blurring effects due to the diffraction limit instead of clearly separable pixels. As calculated above, for the nominal magnification of 2500× the diffraction limit is exceeded, so that further magnification of the picture is not limited by digitalization but by optical diffraction.

Fig. 5.2 Microscopic pictures of laser-treated polyester fabrics, taken with different magnifications (*upper panels*), and respective details (*lower panels*)

Another issue must be taken into account when using inexpensive USB microscopes. The pictures shown above, taken with a professional digital optical microscope, have dimensions of 1200×1600 pixels, i.e., file sizes of 1.92 megapixels. Two megapixels is also a typical value of USB microscopes. However, inexpensive versions with 1 megapixel are also still available, necessarily resulting in lower possible resolutions due to digitalization. On the other hand, USB cameras with nominal magnifications of $200\times$ and 9 megapixels can also be found. Figure 5.3 shows the influence of the image resolution which is varied from 0.48 megapixels (800×600 pixels) to 9 megapixels (3488×2616 pixels), using the same USB microscope. While the upper row depicts the original pictures, the lower row shows details of dimensions ¼ of the widths and heights of the original images. The increasing pixel sizes with decreasing image resolutions are clearly visible.

Additionally, the image quality is limited by several other factors. Firstly, optical issues may occur in inexpensive lens systems, such as spherical aberration, coma, astigmatism, field curvature, or chromatic aberration.

Secondly, the chip size in the camera system also influences the possible resolution in the following way: image sensors consist of several photosensitive photodiodes, e.g., of ~two million photodiodes in a camera with 2 megapixels. Photons emitted from the object which is being photographed are converted into electrical signals on each photodiode. In principle, an increased number of photodiodes is correlated with an increased resolution.

This correlation, however, is only valid if the area of the sensor chip is also increased with the number of photodiodes—which is normally not the case. Instead, each single photodiode normally becomes smaller if the image resolution is increased. This results in less photons impinging on each single photodiode, leading to darker images. The necessity to electronically brighten up these pictures results in increased noise. For an expensive, professional solution, a sensor can be thermoelectrically cooled to reduce this noise. In the worst case, a USB microscope with higher image resolution takes worse pictures than one with a smaller number of megapixels—an effect which gets even enhanced if the picture is taken under inappropriate lighting conditions.

Unfortunately, for most inexpensive USB cameras, the chip size is not even mentioned in the technical specifications. Thus, it is nearly impossible to estimate the quality of microscopic images before buying a USB camera.

5.2 Optical Microscopy

In an optical microscope, the magnification is much higher than in a simple lens, such as a magnifying glass (a loupe). For a magnification of $200\times$, the necessary focal length for a single lens would be equal to the typical good visual distance of 25 cm divided by the desired magnification, i.e., 1.25 mm. This value could only be reached technically by very small lenses. Thus, in a microscope, the magnification is reached by two magnifying steps, as sketched in Fig. 5.4.

Fig. 5.3 Microscopic pictures of a knitted fabric, taken with two different image resolutions (*upper panels*), and respective details (*lower panels*)
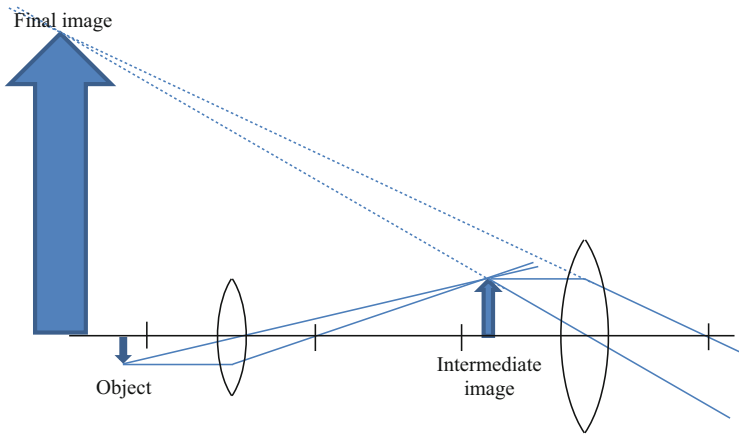
Fig. 5.4 Optical path in an optical microscope

Firstly, a real intermediate image is created by the objective lens (the lens nearer to the object). This image is observed afterward with the ocular lens (the lens nearer to the oculus, i.e., the eye) as if the ocular were a magnifying glass. In this way, the magnifications of both lenses are multiplied to reach the final magnification.
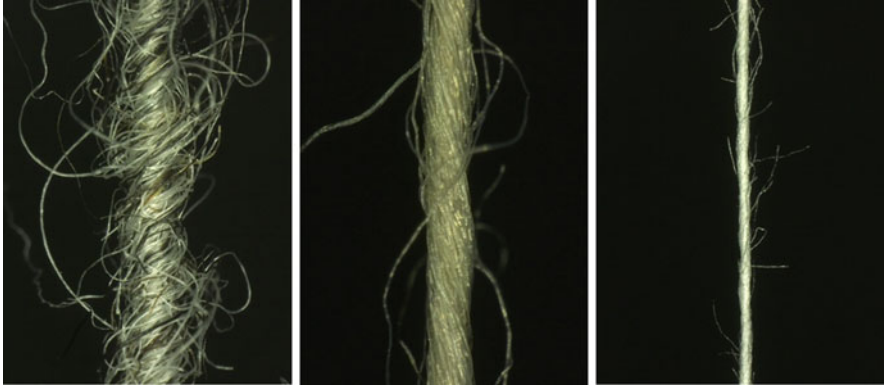
Fig. 5.5 Different yarns imaged by optical microscopy with a nominal magnification of 50×: friction yarn (*left panel*), comb yarn (*middle panel*), and compact ring yarn (*right panel*)

While in theory two lenses are sufficient to build a microscope, in reality optical microscopes are principally built combining more lenses in order to minimize diverse sources of aberrations.

Optical microscopes can be used for diverse applications. Firstly, they help making things visible which are invisible to the naked eye. They can, e.g., allow for distinguishing different yarns and inspecting their details, as depicted in Fig. 5.5. The fibers protruding from the yarns are clearly visible in all cases; their number and length can be estimated from the pictures.

Especially for smaller magnifications, it can be important to separate small objects (e.g., yarns) from the background to avoid that the latter attracts the viewers' attention. By placing the object directly on the microscope table, it may be impossible to make the latter "invisible" due to the large depth of field in small magnifications. This problem is depicted in Fig. 5.6 (left panel) for a compact core yarn which is displayed using a digital microscope with a nominal magnification of 50×.

One possible solution can be described as follows: if a yarn is to be examined, it can be stretched in the air, e.g., between the edges of a bowed cardboard, so that the background is clearly out of focus (Aumann 2013). The result can be seen in Fig. 5.6 (right panel)—now the background is evenly black, as often desired in microscopic pictures.

In some cases, digital optical microscopes allow for estimating the height of a structure under examination. This possibility necessitates two factors: firstly, special software must be used which combines the focused parts of pictures taken in different heights to one focused picture. This principle in turn is based on the microscope software's ability to detect which parts of a picture are focused and which are out of focus. Secondly, the depth of field must not be too large—the smaller it is, the finer is the height resolution. This means that if the height of a structure under investigation is to be estimated using an optical digital microscope,
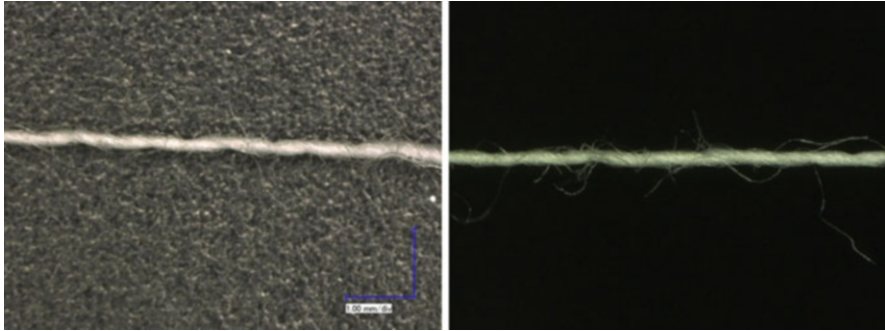
Fig. 5.6 Compact core yarn imaged by optical microscopy with a nominal magnification of $50\times$, fixed on the microscope table (*left panel*) and in the air with several centimeters distance from the microscope table (*right panel*). Photographs: S. Aumann

it can be helpful to use a higher nominal magnification in order to decrease the field of depth. Alternatively, the aperture can be increased to reach a similar effect.

Figure 5.7 (left panel) shows a microscopic picture taken with $200\times$ nominal magnification, depicting a woven fabric composed of carbon yarn and stainless steel wires. Due to the large height differences which extended the field of depth, the picture is composed from 21 single pictures taken in different heights. The streaky areas along the edges are typical for this procedure.

In the right panel of Fig. 5.7, a 3D representation of this picture is calculated by the software, taking into account which areas are focused in pictures taken in which height. The 3D structure looks like expected, with some typical artifacts of this kind of calculation in optical microscopy—especially sharp borders between different areas, such as the transition between stainless steel wire and subjacent carbon yarn, not showing real heights due to averaging effects. However, this method can be used to roughly estimate the surface structure as long as no quantitatively exact values are necessary.

Oppositely, Fig. 5.8 shows the same process for the identical woven fabric, now examined with a lower nominal magnification of $20\times$. In this situation, the depth of focus is much larger than for the previously used magnification of $200\times$.

This results in a significantly worse 3D representation of the woven fabric surface structure (Fig. 5.8, right panel) than with the higher magnification. Apparently, it is impossible for the software to find the best focused height for each spot of the picture in case of such a low nominal magnification.

In principle, if the surface structure shall be estimated from microscopic pictures, it is necessary to create a series of pictures in which focused and defocused areas can clearly be distinguished by the microscope user; else the resulting 3D representation cannot be reliable.

Microscopic images can often be used to investigate not only textile fabrics themselves but also coatings on them. Figure 5.9 depicts TiO_2 layers, coated by a revolving doctor blade with nominal wet coating thickness of 20 μm. The differences in the coating structure due to the different base fabrics are clearly visible.
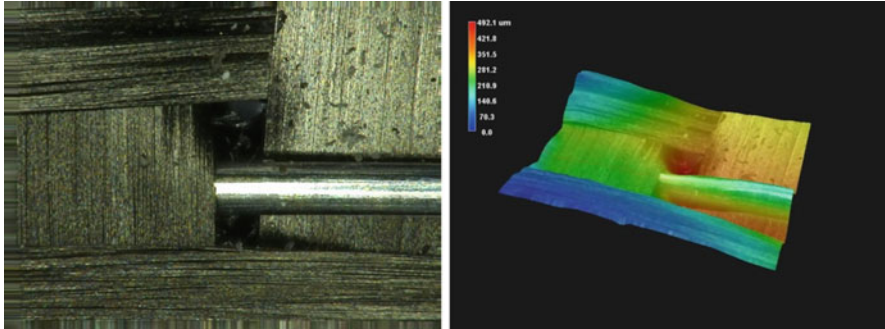
Fig. 5.7 Microscopic picture of a carbon-stainless steel woven fabric, taken with a digital optical microscope with nominal magnification 200× (*left panel*), and respective 3D representation with calculated heights (*right panel*)
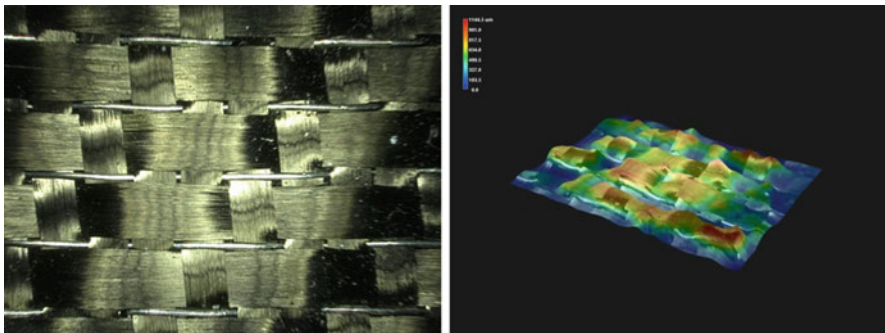
Fig. 5.8 Microscopic picture of a carbon-stainless steel woven fabric, taken with a digital optical microscope with nominal magnification 20× (*left panel*), and respective 3D representation with calculated heights (*right panel*)

In a similar way, typical properties of woven and knitted fabrics, such as yarn spacing and stitch density, can be given easily using a microscope. These parameters can often be calculated more easily and more accurately using a digital optical microscope with a large screen on which distances can be simply measured than in the common way using a weaver's glass.

Finally, an optical microscope which can be tilted by 90° can be used for contact angle measurements. While commercial contact angle measurement systems are expensive and often not reliable for measurements on rough textile surfaces, a simple USB microscope can be used for this task.

Figure 5.10 illustrates how contact angles can simply be measured using a microscope which takes images approximately parallel to the surface of the textile fabric under examination. Independent of the image quality, the most challenging task is always to find the baseline, i.e., the contact line between droplet and fabric. This, however, is not only a problem of image taking—since textile fabrics, opposite to even metal or plastic surfaces, tend to protruding fibers or yarns
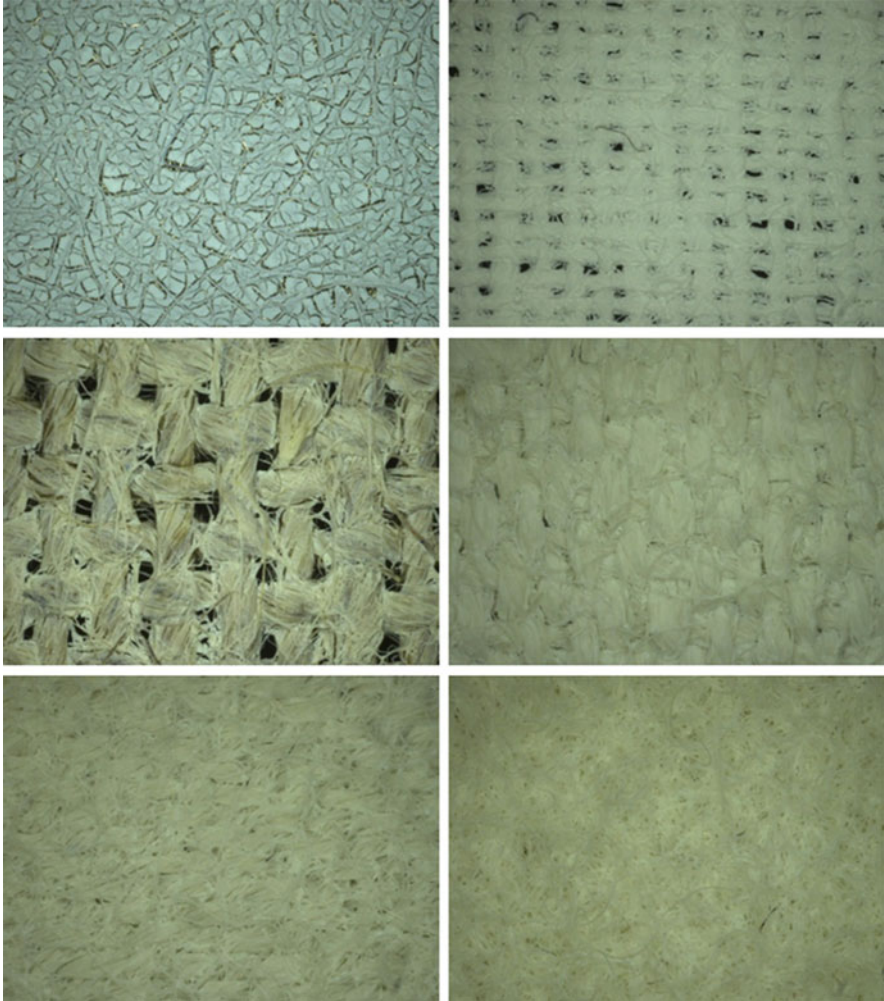
Fig. 5.9 Microscopic picture of a TiO₂ layer with nominal wet thickness of 20 μm on different textiles: stainless steel nonwoven (*upper left panel*), cotton woven fabric (*upper right panel*), linen woven fabric (*middle left panel*), wool–polyester woven fabric (*middle right panel*), wool woven fabric (*lower left panel*), and wool nonwoven (*lower right panel*)

which hide the real contact line—but also of definition (Fiedler and Ehrmann 2015). If measurements are taken carefully, such "self-made" solutions often give more reliable results than commercial devices which are not optimized for textiles.

In spite of all these possible applications of optical microscopy, there are still borders which cannot be overcome due to the limited resolution. Figure 5.11 shows a fabric woven from a wool–polyester blended yarn, examined under a microscope of nominal resolution 200×. Apparently the wool and polyester fibers cannot be distinguished.
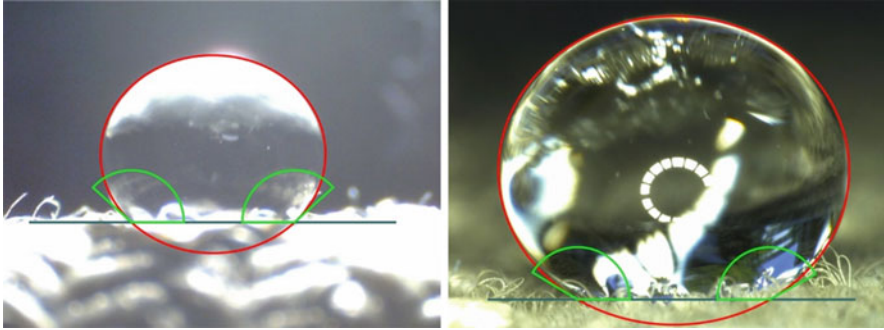
Fig. 5.10 Contact angles, measured on different woven fabrics, using a USB microscope with 1 megapixel (*left panel*) and a digital optical microscope (*right panel*), respectively. Both fabrics are hydrophobic, showing contact angles (*light green*) larger than 90°

Fig. 5.11 Woven fabric consisting of a wool–polyester yarn

In such cases, it can be helpful to use microscopic techniques which are more expensive but also more powerful in terms of resolution, such as confocal laser microscopy.

5.3   Confocal Microscopy

The term "confocal" means "having the same focus" and describes the working principle of a Confocal Laser Scanning Microscope (CLSM): in this special microscopy technique, only beams with the same focus—i.e., being reflected from the sample areas having the same height—are taken for one picture. Afterward, pictures from several focal layers are assembled by software.

Fig. 5.12 Confocal laser scanning microscope with three exchangeable objectives and a visible light beam illuminating a fiber bundle

Confocal laser scanning microscopes contain a common white light source in combination with a laser beam. Since the possible resolution of a picture is proportional to the wavelength of the light used, these lasers often use violet light (e.g., 408 nm wavelength). However, less expensive devices are available with red lasers (658 nm).

Figure 5.12 shows a confocal laser scanning microscope with three objectives which can be changed by rotating them, as in a usual transmitted light microscope. The magnifications given on the objectives usually have to be multiplied by an internal magnification factor of, e.g., 20 (depending on the monitor size), so that in the case depicted here an overall magnification of $1000\times$ is reached.

This magnification is, as described above, related to a specific monitor dimension. In recent equipment, often $23'$ monitors are used. For a maximum resolution of, e.g., 3072×2304, and a minimum image area of 11 µm, this results in a digital resolution of 3.6 nm per pixel. The reproducibility can reach the order of magnitude 20 nm (Keyence 2015).

The working principle of a CLSM is depicted in Fig. 5.13. The light from the laser source is focused in the first aperture to create a point light source. Alternatively, some recent confocal laser scanning microscopes use fiber optics to inject the light instead of this first pinhole.

The laser light is focused by a lens onto the sample. The laser beam reflected from the sample is led via a semipermeable mirror onto a second aperture. Depending on the height of the reflection spot on the sample, this second pinhole either blocks the reflected laser beam or lets it pass. In this way, only light from one defined height is used to create one cross-sectional image.

Fig. 5.13 Setup and working principle of a confocal laser scanning microscope

laser beam

aperture

detector

aperture

semi-permeable mirror

lens
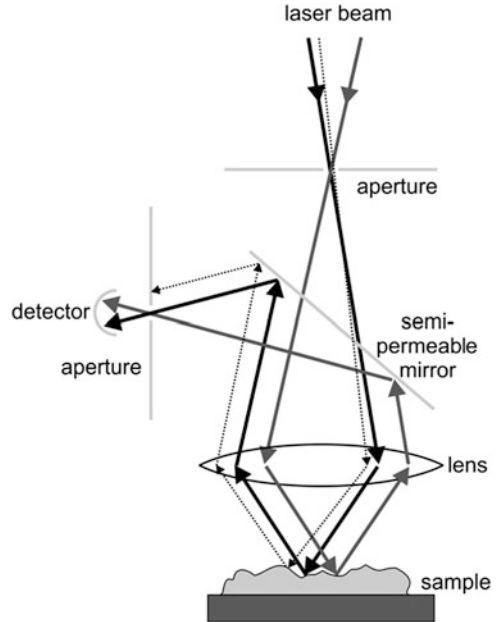
sample

Since the laser beam is focused on a single spot of the sample, it has to be moved relative to the specimen under investigation, i.e., it scans the sample. One complete scan corresponds to the image of one depth of field. Finally, these images are assembled.

While the concept of confocal laser scanning microscopy was already developed in the middle of the twentieth century (Minsky 1961; Minsky 1988), it took some time to develop the first prototypes of working CLSMs (Egger and Petran 1967; Davidovits and Egger 1973). In the 1990s, with advances in laser technology and more stable scanning possibilities, confocal laser scanning microscopes started to be used commercially (Pawley 1995).

Nowadays, confocal laser scanning microscopy is an invaluable tool in biological and medical sciences for the detection of living specimens (Claxton et al. 2006)—which is nearly impossible in the vacuum of scanning electron microscopes. Besides, CLSM can also be used for a variety of problems in other sciences. In textile industry and research, there are several applications where a CLSM is the ideal instrument, compared with common optical microscopy and scanning electron microscopy—and often combining the advantages of both the other instruments.

Typical applications of a CLSM in the textile industry are fiber images. While fiber diameters can often be measured with common optical microscopy, the finer details—such as scales or fiber surface modifications—are normally not visible in usual optical microscopy.

Figure 5.14 shows a laser-treated polyester fabric. Excimer laser radiation can be used to support a chemical hydrophobic finishing, enhancing the longevity of the effect with respect to washing and abrasion (Samm et al. 2009). The sample

Fig. 5.14 Laser-treated
polyester woven fabric

depicted in Fig. 5.14 has firstly been treated with a chemical sol–gel coating, based
on amine-modified polysiloxanes and fluorinated polyacrylates, using a foulard.
Afterward, it was exposed to one excimer laser pulse with a wavelength of 248 nm
and imaging beam shaping, resulting in an energy density of max. 0.5 mJ/cm^2. This
laser treatment results in a thermo-physical process in which the surface melts
without material ablation and a recombination of the polymer molecules during the
following solidification. In the CLSM image, the effect of this treatment becomes
visible: pronounced "valleys" and "mountains" perpendicular to the fiber axis are
generated where the fiber surface was exposed to the excimer laser beam. The
shadowed regions (e.g., the fiber on the left side) stay unaltered.

The CLSM image—here with a nominal magnification of $2000 \times$ —has a high
enough resolution to depict the sub-micron structure on the fiber surfaces clearly. In
this way, confocal laser microscopy enables examination of the effect of abrasion
tests or washing on the protruding structures (Samm et al. 2009).

Another possible application in textile industry is the examination of coatings on
textiles or transparencies. As an example, Fig. 5.15 depicts two different TiO_2
coatings on conductive textiles, both in the anatase modification, which can be used
for textile solar cells. Both were prepared using a revolving doctor blade with a
nominal wet coating thickness of 20 μm.

Figure 5.15 shows the possibilities and limitations of the confocal laser micro-
scope: The different surface structures due to different TiO_2 finishing materials are
clearly visible, comparing the upper and the lower panels. The sintering process,
however, modifies the surface on the nanometer scale, which cannot be visualized
in recent CLSM pictures—no differences are visible between left and right panels
(before and after sintering).

Another advantage of CLSM pictures compared to common optical microscopy
is the possibility to detect surface structures (Ehrmann et al. 2014) and even layer
heights, if a brim is visible in the picture. To illustrate this application, Fig. 5.16
depicts CLSM images of TiO_2 coating on glass. While the upper left panel shows
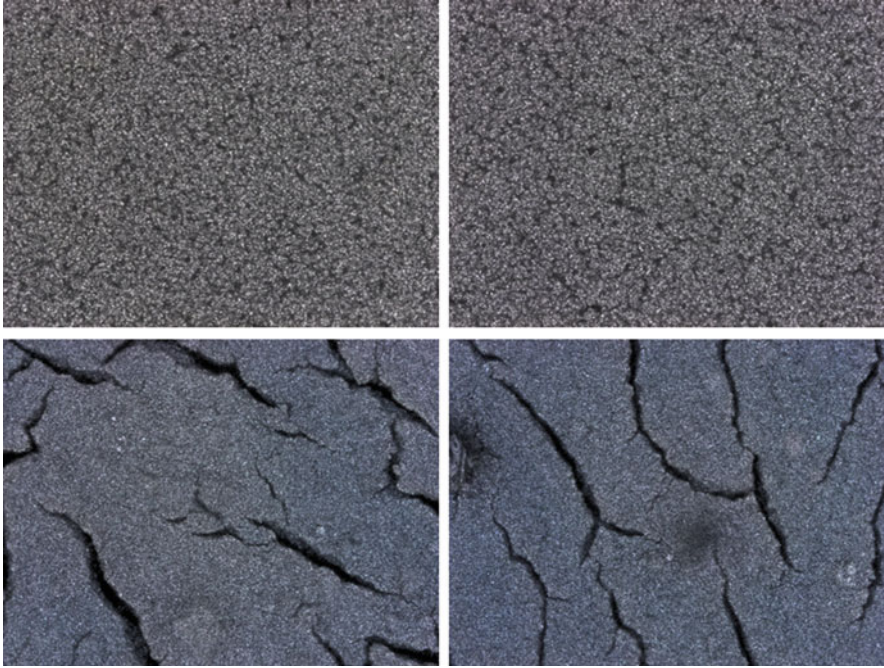
Fig. 5.15   Different TiO$_2$ coatings (*upper/lower panels*) on a conductive woven fabric before (*left panels*) and after sintering at 450 °C (*right panels*)

the usual colored image, the layer heights are depicted as a false color representation in the upper right panel. After defining a crosscut line (lower left panel), the CLSM software calculates the heights along this line (lower right panel).

5.4   Scanning Electron Microscopy

In a scanning electron microscope (SEM), samples are not scanned with visible light but with an electron beam. However, images produced by an SEM offer the possibility of visually inspecting surfaces with high depth of sharpness and high resolution. This is why SEM pictures are included in this chapter.

The advantage of electrons, compared to visible light, in terms of possible image resolutions is based on their wavelength. The de Broglie wavelength of an electron with the energy 1 keV is ~0.04 nm (Watt 2008) which means that the possible resolution of an SEM image is restricted by diffraction effects to a similar order of magnitude—which would be impossible with visible light.

The electrons are emitted by an electron source, either a tungsten wire or a LaB$_6$ crystal in inexpensive systems or a field emission gun in high-class devices. In the
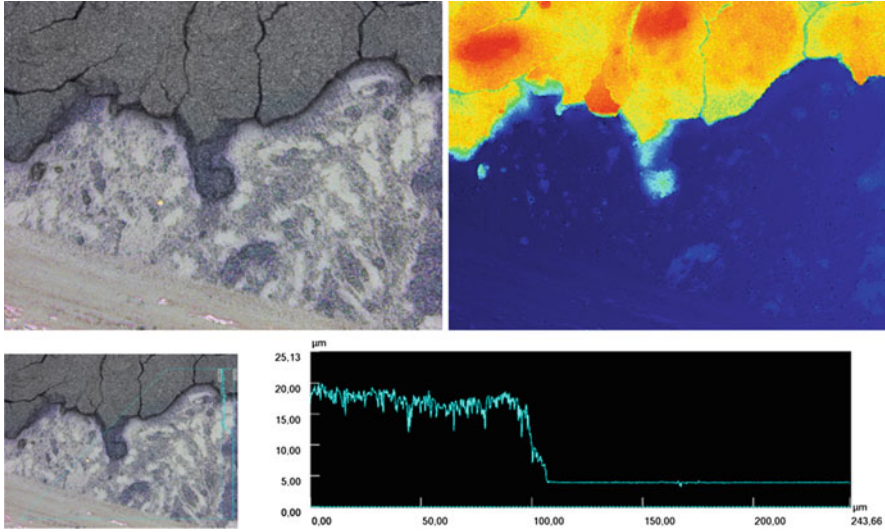
Fig. 5.16 CLSM images of TiO$_2$ coating on glass showing the colored image (*upper left panel*) and the layer heights as a false color representation (*upper right panel*). In the *lower panels*, a *crosscut line* (*left*) is depicted together with the calculated heights along this *line* (*right*)

latter, the electrons have a better defined velocity, resulting in an increased image quality (Colliex 2008).

The resulting electron beam is focused on a spot on the object under examination using magnetic coils. If this object is not conductive, the electron beam can charge it which becomes visible in the picture in the form of bright areas. This problem can be reduced by either sputtering a conductive material on the object under exami-nation or, if this is not possible or not desired, in orienting linear objects, such as fibers, vertically in the pictures, which is usually perpendicular to the electron beam scanning direction.

Scanning is performed line by line, with the signal being converted into gray scale information and synchronously being depicted on a monitor. The resolution of such an SEM picture can reach in practice 1 nm and even smaller values, enabling visualization of smallest sample feature.

In most cases, the secondary electrons originating from the upper layers of a sample are detected, resulting in an image of the surface topography. The contrast in a picture is given by the numbers of secondary electrons detected from each spot and thus defined by the orientation of single areas as well as their material. Secondary electrons have usually energies of some eV (electron-volts).

Backscattered electrons—i.e., primary electrons reflected by the surface—have much higher energies of the order of some keV. Here, the signal intensity depends primarily on the atomic number of the material, allowing for identifying material distribution in a sample. The resolution is lower, of the order of 1 μm.
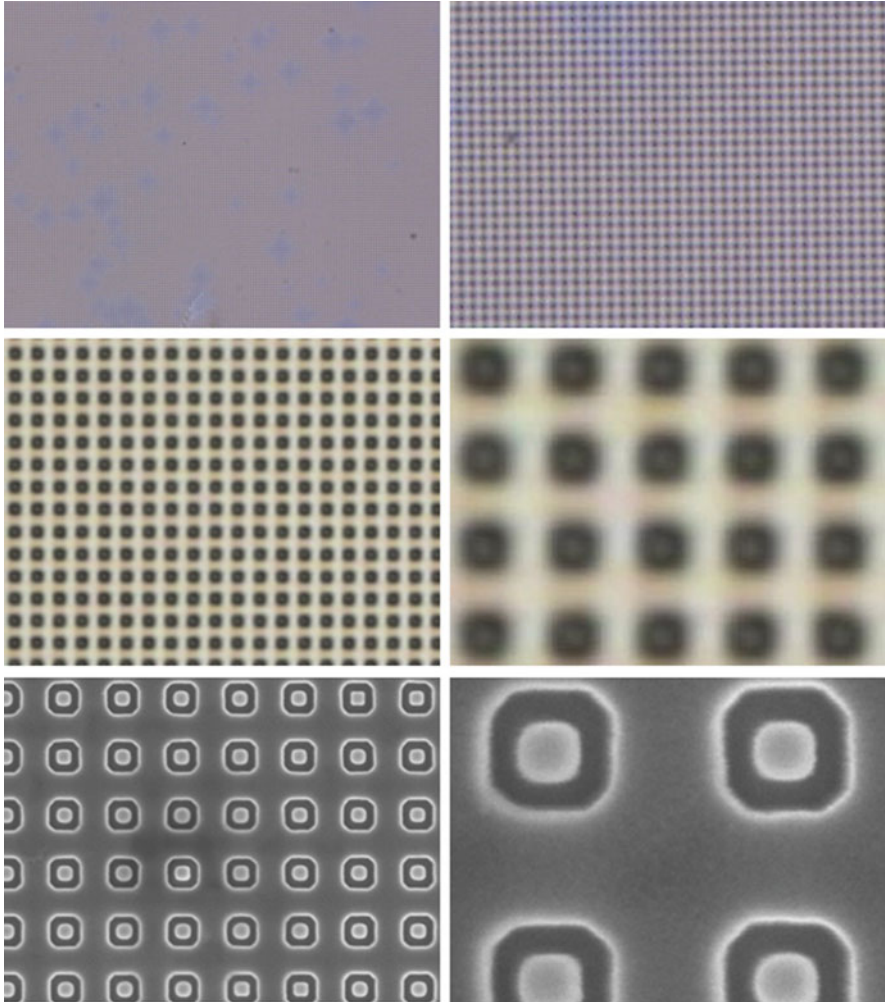
Fig. 5.17 Images of a nanostructured sample with particle diameter 400 nm, taken with a digital optical microscope (*upper row*), CLSM (*middle row*), and SEM (*lower row*). In the right column, details of the original pictures (*left column*) are shown, depicting ¼ of the widths and heights of the original images

Additionally, the energy-dispersive X-ray analysis (EDX) allows for detecting different elements in a sample.

Compared to optical microscopes, SEMs show not only a strongly enhanced resolution but also an increased field of depth. Nevertheless, it should be mentioned that inexpensive tabletop SEM devices have normally significantly lower resolutions, e.g., in the order of 30 nm.

Figure 5.17 shows a comparison of pictures taken from an array of nanostructured particles with diameter 400 nm, using a digital optical microscope (upper

row), a CLSM (middle row), and an SEM (lower row). For a better impression of the possible resolution, the original images (left column) are accompanied by detailed pictures, depicting ¼ of the widths and heights of the original images (right column).

While the optical microscope with a nominal magnification of 2500× only allows for detecting the overall structure of the array, the CLSM image already gives much more information, depicting each single particle in the array similar to a square or a ring. The SEM pictures, finally, clearly show the real structure of the single particles inside the array.

While Fig. 5.17 shows a non-textile example in which the resolution of an SEM has clear advantages, Fig. 5.18 depicts images of fibers, taken with a CLSM and an inexpensive tabletop SEM. As examples of the possibilities and limitations of both techniques, New Zealand wool (left panels) and cashmere fibers (right panels) are compared. CLSM images were taken with a nominal magnification of 1000×, while for the SEM pictures a nominal magnification of 2500× was used. Both magnifications show ideal results for the respective technique, with higher resolutions leading to significantly increased recording times in CLSM and stronger charging of the (nonconductive) fibers in SEM, respectively.

On the one hand, the different scale structure can clearly be seen in all pictures, allowing for differentiating between New Zealand wool with the coarser scales and
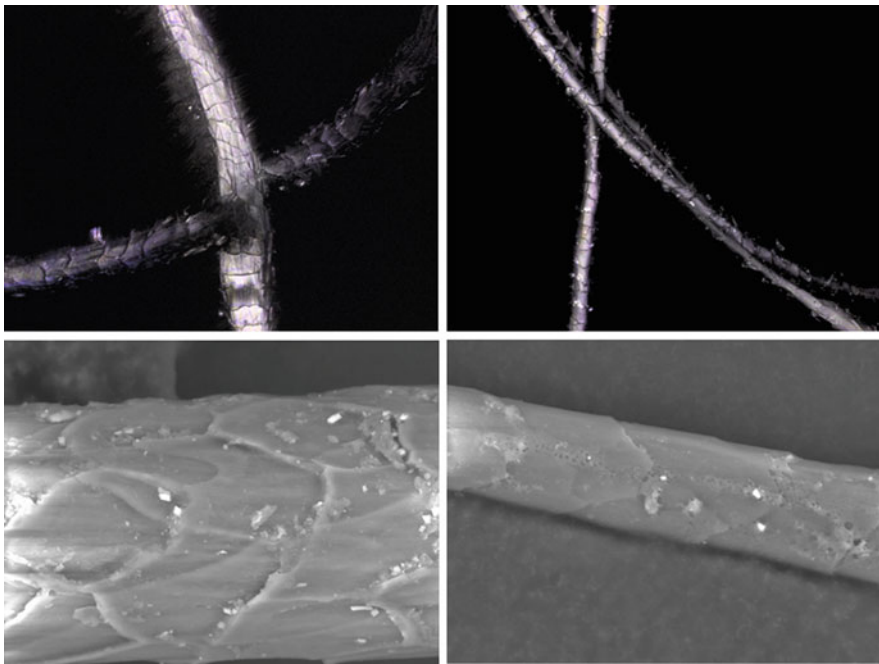
Fig. 5.18 Images of New Zealand wool (*left panels*) and cashmere fibers (*right panels*), taken with a CLSM (*upper panels*) and an SEM (*lower panels*), respectively

cashmere with more even, flat scales which surround the fiber. On the other hand, in the CLSM pictures only a small number of fibers are visible in front of a black background, while in the SEM pictures a background is visible. This shows clearly the large depth of field in SEM images, while in a CLSM, each increase of the depth of field results in a significant increase of the recording time.

Literature

Aumann A: personal communication (2013)

Claxton, N.S., Fellers, T.J., Davidson, M.W.: Confocal microscopy. In: Encyclopedia of Medical Devices and Instrumentation. Wiley, Chichester (2006)

Colliex, C.: Elektronenmikroskopie (trans: H. Kohl). Wissenschaftliche Verlagsgesellschaft mbH, Stuttgart (2008)

Davidovits, P., Egger, M.D.: Photomicrography of Corneal Endothelial Cells *in vivo*. Nature **244**, 366–367 (1973)

Egger, M.D., Petran, M.: New reflected-light microscope for viewing unstained brain and ganglion cells. Science **157**, 305–307 (1967)

Ehrmann, A.: Optical fiber examination by confocal laser scanning microscopy. In: Mondal, M.I.H. (ed.) Textiles: History, pp. 531–546. Properties and Performance and Applications. Nova Science, New York (2014)

Fiedler, J., Ehrmann, A.: Influence of surface micro- and macro-structure on measured and real contact angles. In: Proceedings of Aachen-Dresden International Textile Conference (2015)

Hecht, E.: Optik. Oldenbourg Verlag, 4th edn. (2005) ISBN 3-486-27359-0

Keyence: Konfokales 3D Laserscanning-Mikroskop – Modellreihe VK-X, http://www.keyence.de/products/microscope/laser-microscope/vk-x100_x200/specs/index.jsp (2015)

Lord Rayleigh, F.R.S.: Investigations in optics, with special reference to the spectroscope. Philos. Mag. Ser. **5**(8), 261–274 (1879)

Minsky, M.: Microscopy Apparatus, US Patent 3 013 467 (1961)

Minsky, M.: Memoir on inventing the confocal microscope for viewing unstained brain and ganglion cells. Scanning **10**, 128–138 (1988)

Pawley, J.B. (ed.): Handbook of Biological Confocal Microscopy. Plenum Press, New York (1995)

Samm, K., Kling, R., Korger, M., Tillmanns, A., Janssen, E: Functionalising of textile surfaces with a combination of laser treatment and sol-gel coating. In: Proceedings of the euspen International Conference, San Sebastian (2009)

Watt, I.M.: The principles and practice of electron microscopy, 2nd edn. Cambridge University Press, Cambridge (2008)

Chapter 6
Diffractive Effects in Yarns and Fabrics

Diffraction and interference of light are two fundamental effects in wave optics with many practical consequences. Optics, in general, consists of geometrical, wave, and quantum parts, and light can be treated from these three perspectives (Born and Wolf 1999, Gupta et al. 2015). However, light as a wave and the related wave effects can be directly applied to test textile materials.

Diffraction relies on changing a wave's direction of propagation in the presence of any nontransparent barrier. A yarn or any larger piece of textile materials can surely be treated as a barrier. However, while a yarn is an example of a simple, single barrier, the complete textile is an example of a multibarrier with its own specific structure.

After passing nearby to nontransparent yarns, a light wave generates a whole set of new sources of waves which can interfere with each other producing characteristic interference fringes. In this sense, interference is a secondary effect, while diffraction is the primary one. To be more precise, interference is a type of superposition of waves coming from at least two sources.

In this chapter, we concentrate on diffractive effects, presenting very elementary situations to provide the reader a basic intuition in this field. It should be emphasized that diffraction from a single barrier, like a yarn, also produces characteristic fringes, light and dark places which become visible on a screen placed in the vicinity of the barrier under examination. The obtained diffractive patterns can inform about such parameters as yarn diameter and hairiness, uniformity, and density of yarn distribution.

Now, some basic terms, related to wave behavior in general, will be given in order to support understanding of the next subchapters.

6.1   How to Describe a Wave in a Quantitative Way?

The basic parameters representing a wave are as follows: the wavelength, the wave vector, the wave frequency, and the wave velocity. From the geometrical perspective, the most important parameter for the actual testing applications is the wavelength.

The wavelength can be understood as the closest distance between points in space of the same perturbation (see Fig. 6.1). The perturbation can be of different origin; it can be influenced by pressure changes (acoustic waves), or it can be of electromagnetic origin (light waves). The disturbed points allocated at the same surface form the so-called wave surface. A wave surface can be flat (plain wave), spherical (spherical wave), or quite arbitrary. This depends on the shape of the wave source, the optical system in use, and modifications introduced by barriers.

For light in the visible range, typical values of wavelengths are as follows: 400 nm (violet), 500 nm (green), and 700 nm (red). The whole class of wave optical effects can be explained using a *sinus* trigonometrical function. As it is widely known, this is a periodical function depending on an angle ranging from 0 to 360 angular degrees, or, using more engineering units, it falls into the range between 0 and 2π.

As we know from everyday observations, waves propagate in space, and the sinus function should be somehow calculated using the meter scale, not the angular one. How to overcome this problem? The solution is very easy: One wavelength λ in space is equivalent to 2π in an angular measurement. Then the *sinus* function can be calculated at the arbitrary distance of x, between a light source and a detector, by using the following expression:

$$A \sin \left(2\pi \cdot \tfrac{x}{\lambda}\right) = A \sin \left(k \cdot x\right),$$
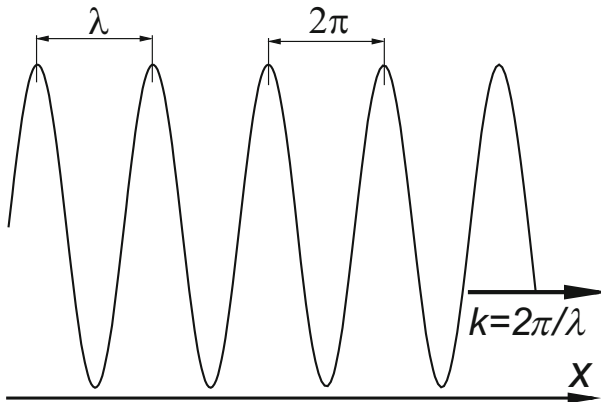
Fig. 6.1   Basic parameters of a wave propagating along the x-axis direction. λ is the wavelength (in meters), and $2\pi/\lambda$ is the wave vector

where *A* is the wave amplitude, which describes the abovementioned disturbance from an equilibrium, and importantly, being a number significantly smaller than the distance *x*. The name of the $2\pi/\lambda$ term is "wave vector," and it is usually represented in literature by the symbol $\vec{k}$. This vector points onto the direction of wave propagation. The internal variable of the *sinus* function is written for generality as the scalar product between $\vec{k}$ and the vector distance $\vec{x}$, and the product is named "wave phase." Thus, the wave can be expressed as

$$A \sin\left(\vec{k} \cdot \vec{x}\right).$$

When we talk about interference of several waves, the same can be said since wave phases of different waves are superimposed.

6.2 Diffraction at Simple Barriers

The presentation of wave-related effects can be carried out in a very graphical way using lines representing wave planes and by understanding how these planes can be drawn, from place to place, imitating the wave propagation in a given direction. In general, this model (see Fig. 6.2a) is simultaneously global and local. It is global

Fig. 6.2 A plain wave propagating from the *left* to the *right* touches a solid barrier, and it is diffracted at it (**a**). The occurrence of curved wave plane can be explained by introduction of local circular waves (**b**). While the real wave planes envelope the *circles*, the *circles* can be interpreted as models of local sources of electromagnetic radiation induced by the incoming wave
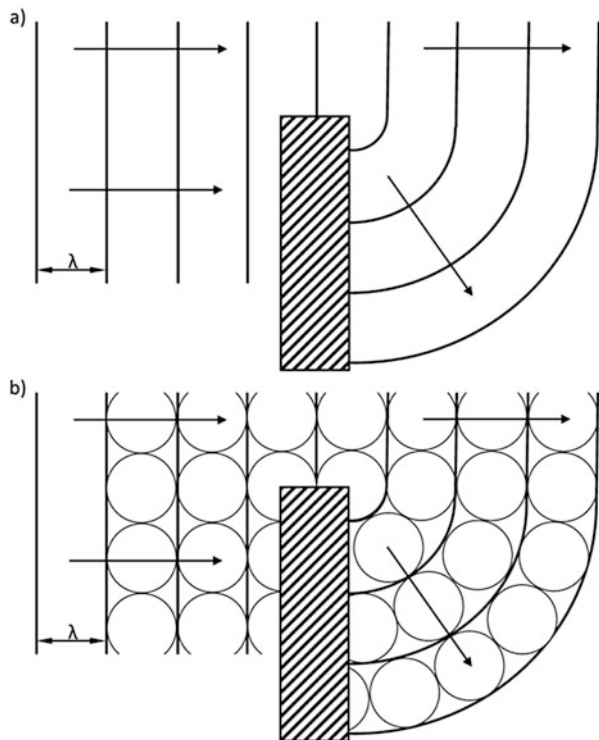
Fig. 6.3 Characteristic
diffractive fringes seen on a
screen positioned about
30 cm from a rectangular
slit of the width 1 μm. The
two *black lines* are only
guides to the eye to give the
reader an idea of the barrier
location. The fringes are
extended along the direction
perpendicular to the slit
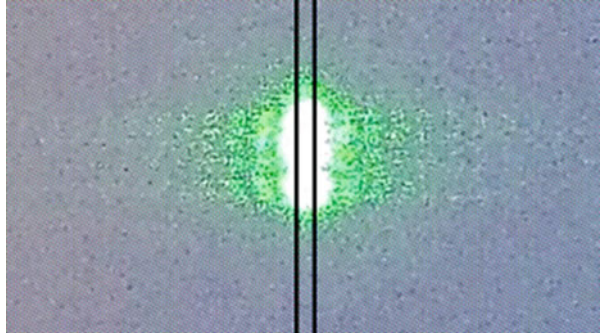
Fig. 6.4 Diffractive pattern
projected on a screen
positioned about 30 cm
from a thin wire of diameter
10 μm. The *black line* is
only a guide to the eye for
the reader to provide a
realistic idea of the barrier
location. The diffracted
light is extended along the
direction perpendicular to
the wire. The *white circular
spot* in the image *center*
represents the diameter of
the laser beam used in the
experiment
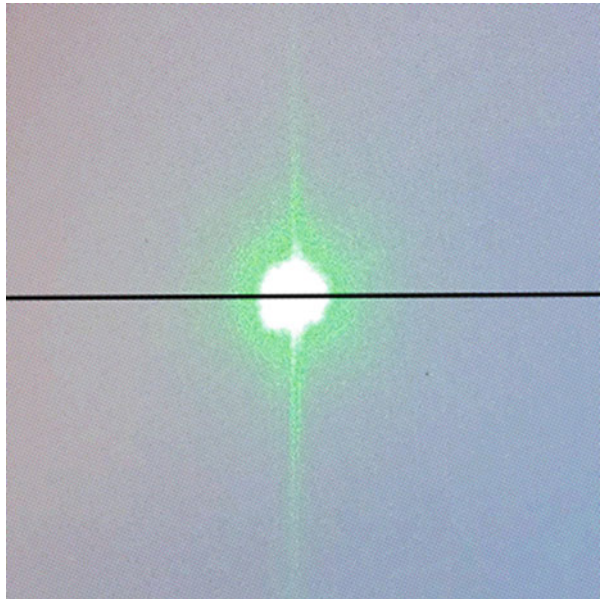
since a wave plane extends in space. It is local, however, since in order to draw
another wave plane, there is a need to introduce local, circular waves emitted by
points allocated in the vicinity of the actual wave plane (Fig. 6.2b).

The basic condition for each wave-like experiment is the wavelength, and the
characteristic dimension of the barrier should be of the same order.

For example, if the green color of light equals about 0.5 μm, then after a passage
through a slit of the width 1 μm, we should succeed in seeing an interference pattern
(Fig. 6.3).

Another elementary example of diffraction is given in Fig. 6.4. Diffraction is
visible in the form of a wide and thin fringe oriented perpendicularly to a wire. The
obtained pattern is almost uniform, since the wire diameter equals about 10 μm
which exceeds 20 times the wavelength.

6.3   Diffraction in Multibarriers

Textiles can be treated, from the perspective of wave optic experiments, as multibarriers or regularly distributed gaps. The examples provided in the previous subchapter were very simple. In the case of textiles, we deal with a superposition of wave phases passing through materials. What is striking, however, is that the obtained diffractive and interference patterns are quite regular in many cases. This happens because textiles are usually regular and high regularity is mostly equivalent to high quality.

   Before we present results of experiments with real samples, let us provide some more complex, physical cases (Figs. 6.5 and 6.6). What is important for real applications is that the obtained patterns keep the spatial symmetry of samples under examination.

   Following these quite regular diffraction object, the next subchapters focus on diffraction at fibers, yarns, and fabrics, showing which information can be gained from diffraction experiments on these parts of the textile chain.

6.4   Applications of Diffraction on Textile Fibers

Natural fibers are relatively expensive, compared to synthetic fibers, with cashmere, silk, and also wool having the highest costs (Nielson 1990). While the fiber industry is steadily aiming at developing man-made fibers further to increase their possible

Fig. 6.5 Diffractive-interference pattern obtained after light-passage through a hole of 2 mm diameter equipped with a regular lattice of wires of density 4 stitches/mm. The *central circle*, with a mesh inside, represents the position of this complex barrier. The obtained pattern has fourfold symmetry, the same as the wire lattice. Inside the main fringes, some weaker, secondary ones are visible
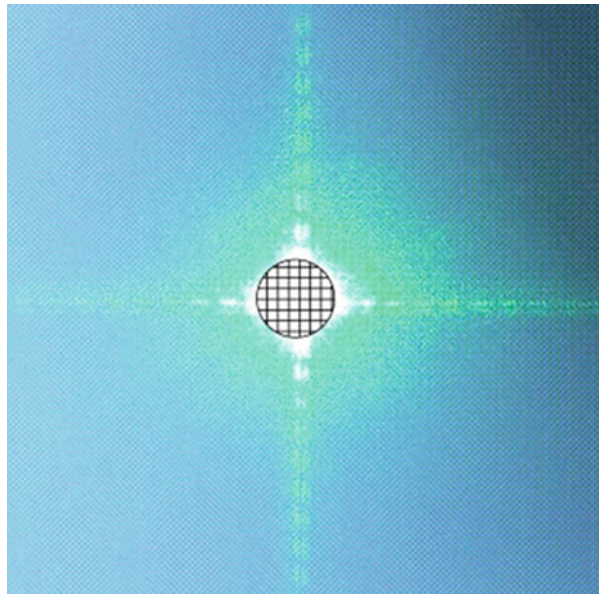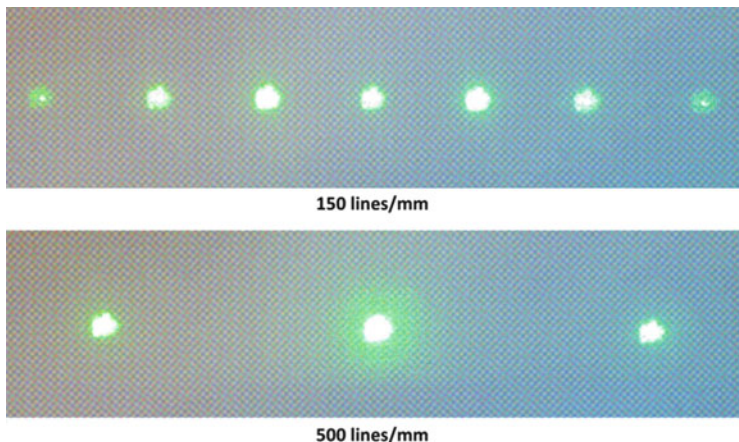
Fig. 6.6 The limiting case of very dense, uniformly distributed parallel slits (*lines*), creating a so-called diffractive grating, for 150 lines per mm (*upper panel*) and 500 lines per mm (*lower panel*), respectively. In the figures only the main diffraction orders can be seen. The laser beam diameter used in the experiment is equal to 3 mm. Thus, a laser beam covers $N_1 = 450$ lines or $N_2 = 1500$ lines, respectively. The theory of light diffraction indicates that between the main diffraction orders, as depicted above, very weak secondary diffractive fringes are located. The number of secondary orders equals $N_1 - 2 = 448$ and $N_2 - 2 = 1498$, respectively. The secondary orders were not registered

applications, the number of imitated fibers, on the other hand, grows rapidly. The German Wool Institute found already in the 1990 about 60 % of their test samples to be mislabeled (Augustin-Jean and Alpermann 2013); an effect which could also be recognized for the expensive cashmere fibers (Phan and Wortmann 2001).

Discovering such counterfeits is often done using a scanning electron microscope (SEM) or a confocal laser scanning microscope (CLSM) since simple light microscopes can only distinguish between man-made fibers and wool or animal hair (Ehrmann 2014). These instruments, however, are not necessarily available in a research institute or even in the incoming goods inspection of a store. Burn tests, on the other hand, which are often used to differentiate between different kinds of fibers, do not allow distinguishing between cashmere and less expensive animal-based fibers, such as common wool (Fabric University 2016).

Thus, it would be interesting to develop a method enabling such a differentiation. Most researchers, however, concentrate on simple diameter measurements of fibers, especially nanocarbon fibers (Brančíiak and Datyner 1977; Siegel and Grundy 1989; Kumar et al. 2002; Demir et al. 2002; Ma et al. 2003; Munawar et al. 2007). The uniformity of different fibers along its length was also investigated by light scattering profiles (Lynch and Thomas 1971). Here we will describe a new method to use the information given in a diffraction pattern in order to distinguish between different fiber materials (Angelow et al. 2015a, b).
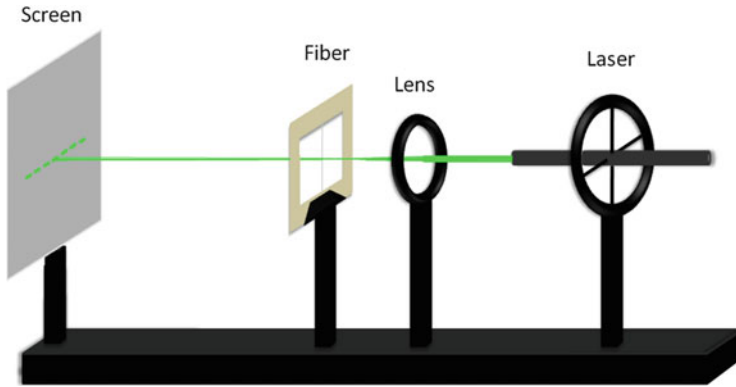
Fig. 6.7 Diffraction pattern on a screen of a fiber on which a laser beam is focused. From Angelow et al. (2015a), modified

The optical setup is depicted in Fig. 6.7. Experiments can be performed using a simple laser pointer, if possible using green light which is better visible to the human eye than red or blue light. The laser is fixed in a mechanical mount; its beam is collimated onto the fiber under investigation using a lens of approximate focal length of 50–200 mm. The fiber can be held in a frame using clamps or simple glue. The main diffraction plane on the white paperboard is oriented 90° to the fiber.

Firstly, the main diffraction pattern allows for calculating the fiber diameter using the well-known formula

$$d = \frac{n\lambda D}{x_n}$$

with the fiber diameter d, the distance x_n between the central maximum and the nth diffraction minimum, the wavelength λ, and the distance D between the slit and the screen. This formula is valid for small diffraction angles, i.e., small ratios x_n/D.

While this relation between d and the dimensions of the diffraction pattern were originally developed for diffraction at a single slit, Babinet's principle states that the Fraunhofer diffraction patterns from complementary screens (i.e., slit and fiber with identical dimensions) are nearly the same. This holds true for Fresnel and Fraunhofer limits of diffraction as long as the area of forward beam intensity is neglected (which is possible here without problems). The Fraunhofer limit is a far-field limit, i.e., the distance D is assumed to be large and the diameter d is small, while in the Fresnel limit, D is small and the diffraction equations can usually only be solved numerically. Thus, calculation of the fiber diameter in this way is easily possible.
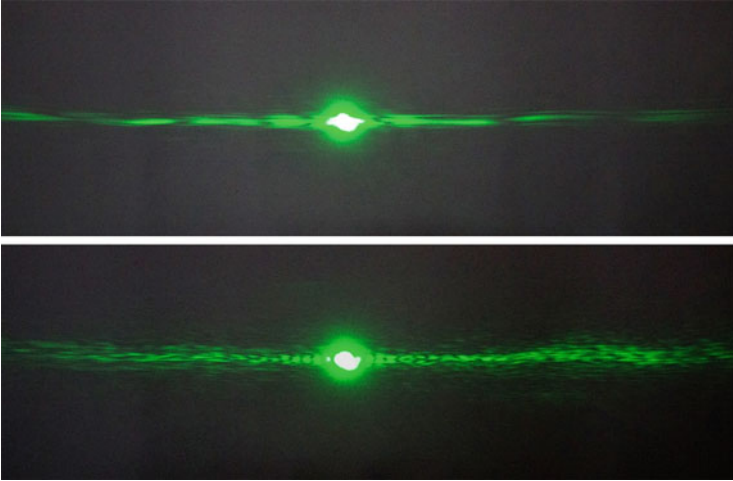
Fig. 6.8 Diffraction pattern of viscose fibers with fineness 0.5 dtex (*upper panel*) and 9 dtex (*lower panel*), respectively

Figure 6.8 depicts an example of two viscose fibers with different diameters, one with 0.5 dtex (upper panel) and the other with 9 dtex (lower panel). Obviously, diffraction at the finer fiber results in significantly larger distances between the nth diffraction minimum and the central maximum. Nevertheless, the irregularity of the fiber makes diameter calculation less simple than for a straight wire.

It should also be mentioned that the main diffraction plane is not absolutely even which can be attributed to slight curves in the fiber. Breaking up the diffraction spots, however, happens due to the fibrils on the viscose surface, making the crosscut formed like a flower instead of round (cf. Fig. 6.9), which would be usual for several other man-made fibers.

Finally, especially Fig. 6.8 (lower panel) shows clearly that the abovementioned requirement for the calculation of the fiber diameter from the diffraction pattern, i.e., small ratios x_n/D, is no longer valid for the outer parts of the image. Instead, the minimum distances are clearly elongated in comparison with the part of the diffraction pattern which is located directly near to the forward beam spot. This means that for calculations of the fiber diameter according to a diffraction pattern, care must be taken to which parts of the image may be used and in which areas the necessary requirements are not fulfilled.

Fibers, however, show even more information in their diffraction patterns, opposite to wires with their even surfaces.

Figures 6.9 and 6.10 show an excerpt of diffraction measurements on different fibers and the corresponding fiber surfaces, detected by SEM. In Fig. 6.9, two different wools are compared with cashmere. It can clearly be recognized that the deviations in the scale structure of the animal fibers are reflected by the deviations in the diffraction patterns, especially *outside* the main diffraction plane. This can easily be understood by the following consideration: The scales of the animal fibers
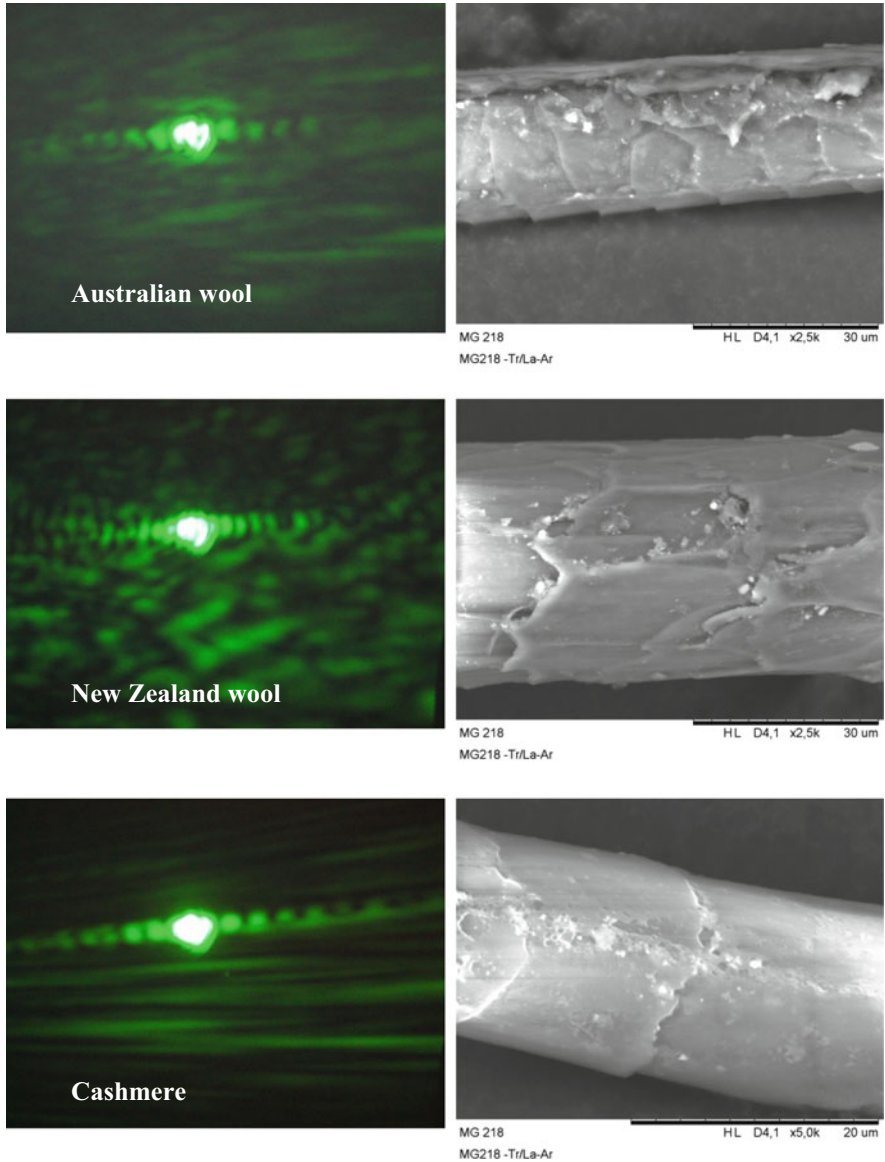
Fig. 6.9 Diffraction patterns of different animal fibers and corresponding SEM images of the respective fibers

can be regarded as several small diffraction slits (or wires) with different orientations since they are slightly canted in comparison with the main fiber axis. This results in several additional diffraction planes being created. On the other hand, this explanation shows that man-made fibers with their typical flat and even surfaces

MG 218
MG218 -Tr/La-Ar

MG 218
MG218 -Tr/La-Ar

MG 218
MG218 -Tr/La-Ar
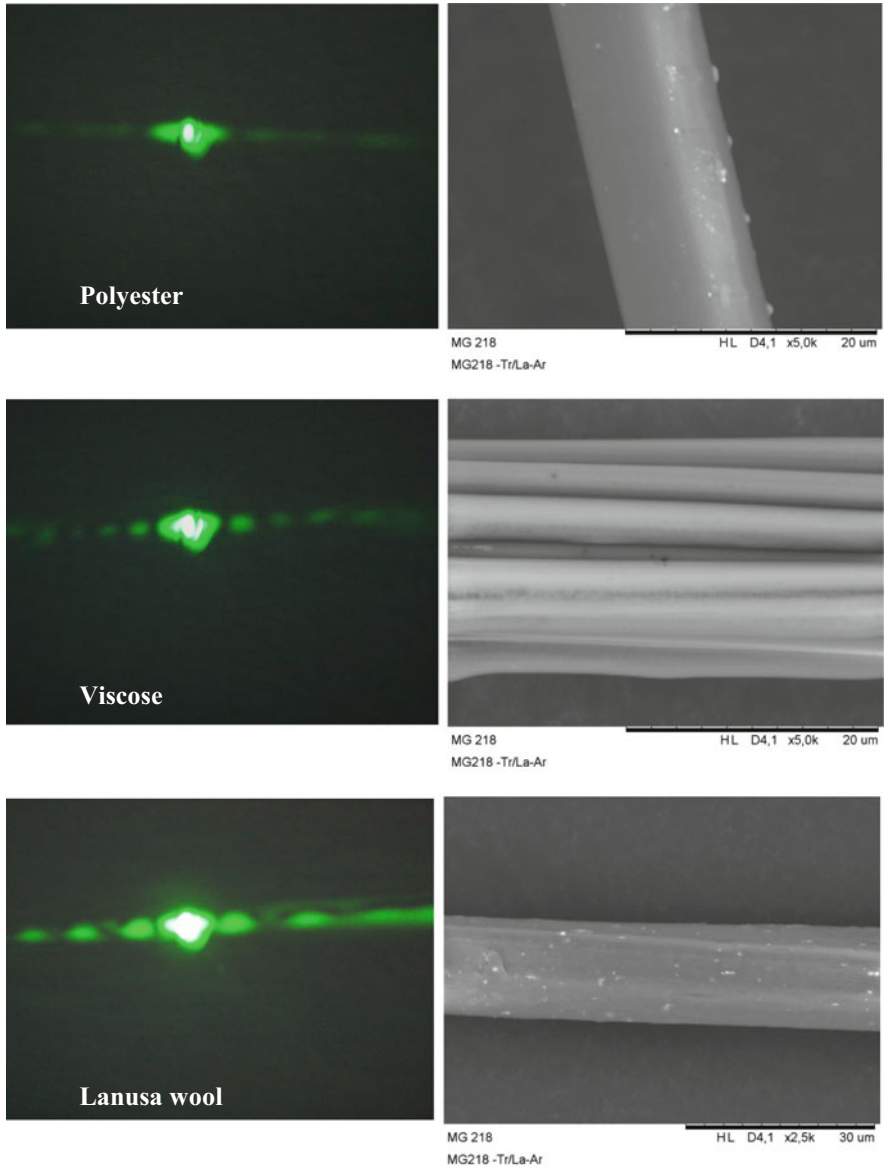
Fig. 6.10 Diffraction patterns of different man-made fibers and corresponding SEM images of the respective fibers

cannot be expected to show strong diffraction patterns below and above the main diffraction plane.

This is what Fig. 6.10 shows: The diffraction spots in the main plane may be disturbed, depending on the exact shape of the fiber surface. Differentiation

between diverse materials by diffraction methods, however, is only possible for significantly different refraction indices or transmission coefficients.

In other words: While diffraction on fibers may be an inexpensive and fast tool for investigations of natural fibers, optical examination – whether direct by microscope or indirect by diffraction – of synthetic fibers is usually not helpful in discriminating different materials.

6.5   Applications of Diffraction on Textile Fabrics

While no reports about laser diffraction on yarns exist in literature, several groups have investigated the possible use of diffraction images of diverse textile fabrics. The bend of the threads in woven fabrics was visualized by laser diffraction (Shlyakhtenko 2000) as well as different geometrical parameters (Sodomka and Komrska 1991). Even the weave structure and other periodic effects could be differentiated by laser diffraction (Toba 1980). The most often used application of such an indirect optical method, however, is defect detection (Mallik-Goswami and Datta 2000; Wood 1990; Ribolzi et al. 1993; Zhang and Bresse 1995; Mallik (Goswami) and Datta 1998a, b).

On the other hand, semifinished textiles, such as fiber mats, can be investigated by laser diffraction, giving rise to the fiber orientation (Shlyakhtenko et al. 2012; Gong and Newton 1996; Xu 1996).

Diffraction patterns of textile fabrics, however, are often hard to interpret. Figure 6.11 depicts different patterns, detected for transmission through fabrics or reflection on their surfaces. Quite regular transmission patterns of fine woven fabrics can be recognized very well (upper right panel) and allow for estimating the warp and weft density, similar to the fiber thickness calculation mentioned above. Less regular or courser fabrics, however, result in quite irregular transmission patterns (upper left panel) which can nevertheless be helpful if weaving errors are to be detected.

Reflection from irregular surfaces without any predominant direction, e.g., given by the fiber orientation, leads to reflection patterns which can only be interpreted using image processing software for the necessary calculations (Fig. 6.11, lower left panel). In this situation, however, outstanding features, such as errors in the surface, can again be recognized from the reflection patterns by eye.

An interesting effect can be found on metal-coated surfaces (lower right panel). Rough metallic planes show a special reflection characteristic, between the diffuse reflection of dull materials, such as most textile fabrics, and the mirror-like reflection of even, shiny materials. The typical reflection cone of metals is more and more approached for thicker metal coatings on textile fabrics (Grecka et al. 2013). Thus, by an angular-dependent measurement of the quantitative reflection, thicknesses of metal coatings can be investigated.

For quantitative evaluation, in the simplest case, Lambert's cosine law can be applied,
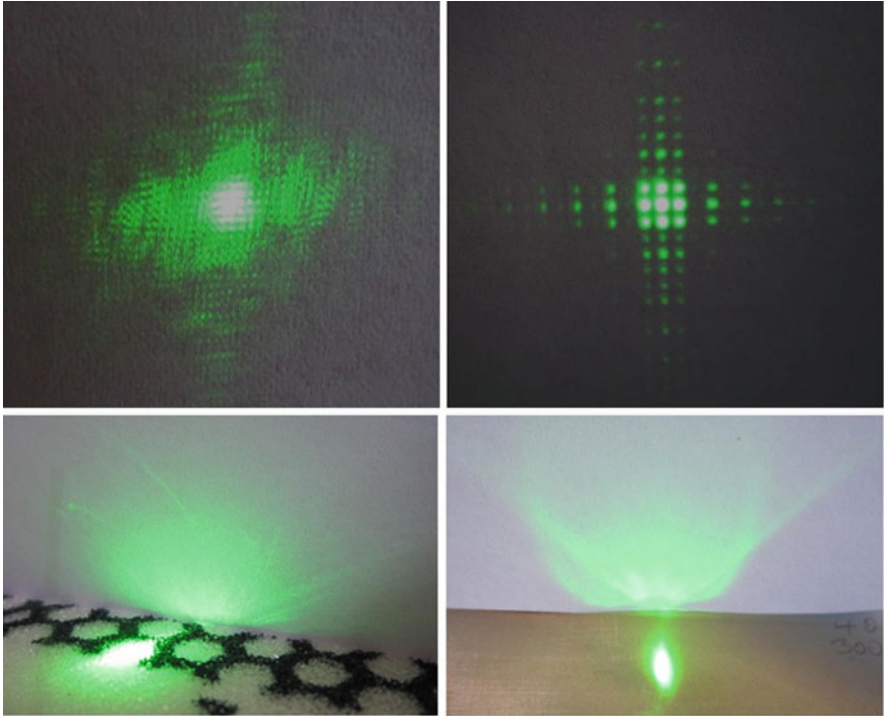
Fig. 6.11 Transmission through woven fabrics (*upper row*), reflection from a foam (*lower left panel*) and a gold-coated woven fabric (*lower right panel*)

$$I = I_0 \cos\beta,$$

with the intensity of reflected light I in a defined direction, the intensity I_0 of the impinging light beam, and the observation angle β measured with respect to the surface normal. More sophisticated models were, e.g., developed by Phong (1975) or Whitted (2005) and often used in computer graphics. Fitting the resulting angle dependences to Lambert's law, however, will be sufficient in several cases.

Literature

Angelow, A., Bednorz, H., Böttcher, S., Schrader, N., Ehrmann, A.: Optical differentiation between cashmere and other textile fibers by laser diffraction. Indian J. Fiber Text. Res. (accepted) (2015a)

Angelow, A., Bednorz, H., Böttcher, S., Schrader, N., Ehrmann, A.: Verfahren zur Art-Bestimmung von Fasern, Patent application DE 10 2015 000 281A1 (2015b)

Augustin-Jean, L., Alpermann, B.: The Political Economy of Agro-Food Markets in China: The Social Construction of the Markets in an Era of Globalization. Palgrave Macmillan, Basingstoke (2013)

Born, W., Wolf, E.: Principles of Optics. Electromagnetic Theory of Propagation, Interference and Diffraction of Light. Cambridge University Press, Cambridge (1999)

Brančíiak, J.V., Datyner, A.: The measurement of swelling of wool fibers in solvents by laser-beam diffraction. Text. Res. J. **47**, 662–665 (1977)

Demir, M.M., Yilgor, I., Yilgor, E., Erman, B.: Electrospinning of polyurethane fibers. Polymer **43**, 3303–3309 (2002)

Ehrmann, A.: Optical fiber examination by confocal laser scanning microscopy. In: Mondal, M.I.H. (ed.) Textiles: History, Properties and Performance and Applications, pp. 531–546. Nova Science, New York (2014)

Fabric University: Burn test. http://www.fabriclink.com/university/burntest.cfm. Last Accessed 15 July 2016 (2016)

Gong, R.H., Newton, A.: Image-analysis techniques Part II: The measurement of fibre orientation in nonwoven fabrics. J. Text. Inst. **87**, 371–388 (1996)

Grecka, M., Rizvi, A., Ehrmann, A., Blums, J.: Influence of abrasion and soaking on reflective properties of Cu and Al coated textiles. In: Proceedings of Aachen-Dresden International Textile Conference (2013)

Gupta, S.D., Ghosh, N., Banerjee, A.: Wave Optics: Basic Concepts and Contemporary Trends. CRC Press, Boca Raton (2015)

Kumar, S., Doshi, H., Srinivasarao, M., Park, J.O., Schiraldi, D.A.: Fibers from polypropylene/ nano carbon fiber composites. Polymer **43**, 1701–1703 (2002)

Lynch, L.J., Thomas, N.: Optical diffraction profiles of single fibers. Text. Res. J. **41**, 568–572 (1971)

Ma, H., Zeng, J., Realff, M.L., Kumar, S., Schiraldi, D.A.: Processing, structure, and properties of fibers from polyester/carbon nanofiber composites. Compos. Sci. Technol. **63**, 1617–1628 (2003)

Mallik-Goswami, B., Datta, A.K.: Optical imaging technique for defect detection in fabric. Indian J. Fibre Text. Res. **23**, 277–280 (1998a)

Mallik-Goswami, B., Datta, A.K.: Fast Fourier transform technique for identification of the structural properties and irregularities in fabric. J. Inst. Eng. India **7**, 1–4 (1998b)

Mallik-Goswami, B., Datta, A.K.: Detecting defects in fabric with laser-based morphological image processing. Text. Res. J. **70**, 758–762 (2000)

Munawar, S.S., Umemura, K., Kawai, S.: Characterization of the morphological, physical, and mechanical properties of seven nonwood plant fiber bundles. J. Wood Sci. **53**, 108–113 (2007)

Nielson, K.J.: Window Treatments. Wiley, New York (1990)

Phan, K.-H., Wortmann, F.J.: Quality assessment of goat hair for textile use. In: Franck, R.R. (ed.) Silk, Mohair, Cashmere and Other Luxury Fibres. Woodhead Publishing Series in Textiles, Cambridge (2001)

Phong, B.-T.: Illumination for computer generated images. Comm. ACM **18**, 311–317 (1975)

Ribolzi, S., Mercklé, J., Gresser, J., Exbrayat, P.E.: Real-time fault detection on textiles using opto-electronic processing. Text. Res. J. **63**, 61–71 (1993)

Shlyakhtenko, P.G.: Diffraction method of monitoring the bend of threads in textile webs. J. Opt. Technol. **67**, 1038–1042 (2000)

Shlyakhtenko, P.G., Vetrova, Y.N., Rudin, A.E., Sukharev, P.A., Nefedov, V.P.: A diffraction method of monitoring the angular distribution of the fibers in the structure of a flat fibrous material. J. Opt. Technol. **79**, 599–602 (2012)

Siegel, M.W., Grundy, R.H.: Apparatus and methods for measuring the diameter of a moving elongated material. US patent 5015867 A (1989)

Sodomka, L., Komrska, J.: Laser diffraction measurements of the parameters of fine-mesh woven textiles. Text. Res. J. **61**, 232–236 (1991)

Toba, E.: Determination of the autocorrelation function of woven fabrics using laser speckle. Text. Res. J. **50**, 238–244 (1980)

Whitted, T.: An improved illumination model for shaded display. ACM Siggraph 2005 Courses 4 (2005)

Wood, E.J.: Applying Fourier and associated transforms to pattern characterization in textiles. Text. Res. J. **60**, 212 (1990)

Xu, B.: Identifying fabric structures with fast Fourier transform techniques. Text. Res. J. **66**, 496–506 (1996)

Zhang, Y.F., Bresse, R.R.: Fabric defect detection and classification using image analysis. Text. Res. J. **65**, 1–9 (1995)

Chapter 7
Image Processing Techniques for Evaluation of Textile Materials

In some situations, the techniques described in the last two chapters may be insufficient to interpret an image correctly – or to gain as much information as possible from a picture taken by a microscope or in another way. Image processing can help to extract additional information from pictures. While these methods often require comprehensive knowledge and expensive databases, there are also possibilities to use common software – partly even without any mathematical knowledge – to find out more about a picture showing a textile material.

This chapter starts with the simple calculation of the cover factor of a textile fabric, followed by different ways to define and measure its roughness, concluding with a detailed mathematical description of a new method to optically measure yarn hairiness especially in knitted fabrics as an example of how to develop similar image processing strategies which may be helpful in other textile related problems.

7.1 The Cover Factor

The cover factor of knitted fabrics is often defined by a calculation suggested by Munden (1962) which can be used as a practical estimation. Similarly, for woven fabrics, the cover factor is often given by other equations related to yarn and fabric parameters (Peirce 1937).

These equations, however, are only estimations of the original definition: The cover factor is the extent to which the area of the knitted/woven fabric is covered by yarn (Gravas et al. 2006). Practically, this simply means that in a photograph of the textile fabric, the ratio of the yarn area to the whole area must be calculated.

Instead of performing complicated measurements on a photograph, this calculation can simply be done using any computer program which is able to calculate a histogram of an image. Figure 7.1 depicts the procedure: A common microscopic picture of a knitted (or woven) fabric (upper left panel) is transferred into a black-and-white image (upper right panel). This can, e.g., be done using Corel Photo-
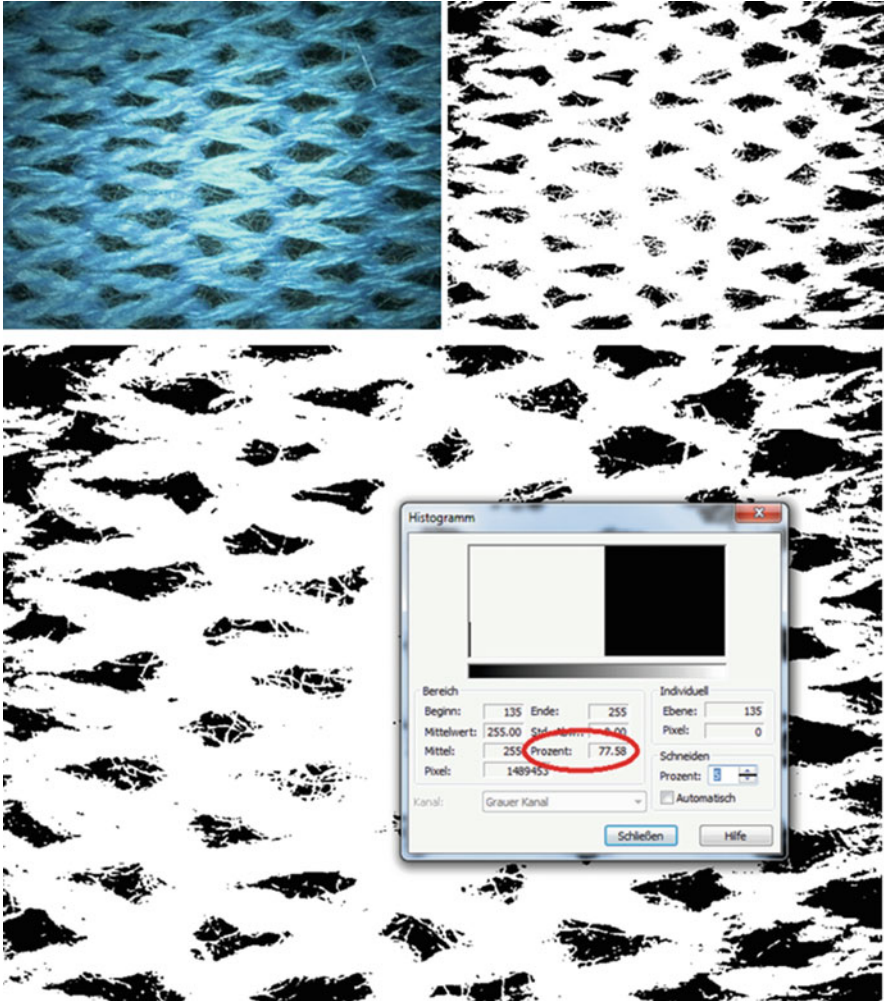
Fig. 7.1 Microscopic pictures of a knitted fabric (*upper left panel*), transferred into a monochrome image (*upper right panel*), and histogram calculation of this image (*lower panel*)

Paint©. Afterward, the monochrome image is transferred back into a grayscale picture in the same program. Then, it is possible to perform a histogram on the picture (Fig. 7.1, lower panel). Depending on the program used for this calculation, the desired color (black or white) can be chosen using the mouse, sliders, input boxes, or the like. Here, the amount of white area (i.e., knitted fabric) is calculated as 77.58 %, i.e., the knitted fabric has a cover factor of 0.78.

It must be mentioned, however, that the quality of the original image significantly influences the results. In the microscopic picture used here, the middle area shows a strongly increased brightness due to the microscope's light. In the

respective monochrome image, the influence of illumination on the borders between black-and-white areas is clearly visible.

Similarly, the borders between "covered" and "open" areas will be shifted by any change in the definition of the limit which separates black from white pixels. Since yarns are no wires with clearly defined borders, the subjective decision where to place the edges of the yarns will always influence the calculated cover factor. The choice of this value has thus to be chosen carefully in order to achieve reliable values.

7.2   Surface Roughness of Textile Fabrics

The surface roughness of a textile fabric strongly influences its haptical properties. Roughness can be evaluated subjectively, i.e., by having trained people compare a textile under examination with another textile to judge its roughness relative to a standard (Mooneghi et al. 2014). This method has shown to allow for a ranking of textiles due to their roughness, even if the testers are not specially selected (Stockbridge 1957), and is thus often chosen in experimental investigations.

Nevertheless, objective measures are always helpful to get unbiased results in experiments. Firstly, it must be mentioned that there are several definitions of the roughness of a surface, e.g., the maximum profile peak height (distance between mean line and highest point of the profile peak), the mean height (mean distance between peak and neighboring valley), the arithmetical mean deviation of a profile (arithmetical average of the absolute distance of profile variations from the mean line), or the root mean square deviation (Mooneghi et al. 2014). It should be mentioned that since each roughness has the unit of a length (usually mm or micron), they can be mixed up easily. When talking about the roughness of a textile surface, care must be taken to define the given value properly.

Objective roughness measurements are possible with contact methods, e.g., the Kawabata evaluation system (Vassiliadis and Provatidis 2004) or the multipurpose fabric tester (Hearle and Amirbayat 1988). Other contacting instruments which are not especially suited for textiles may be available in neighboring institutes and may also be supportive.

Optical methods are usually based on studying light reflection from the fabric surface, detecting either all reflected light or only a certain polarization direction (Mooneghi et al. 2014). Alternatively, bending the textile around a sharp edge and detecting the roughness profile which is illuminated by a line laser can be used for this purpose (Militky and Mazal 2007).

If none of these machines is available, the roughness of a textile surface can often be estimated using a high-resolution digital microscope with the possibility to assemble pictures from different depths of field, as described in Chap. 5, or a CLSM. Especially the latter often has the possibility included to detect height profiles which allow for calculation of the desired roughness.

7.3 Definition and Common Measurement Methods of Yarn Hairiness

One of the most interesting properties of yarns – and often not easy to measure – is their hairiness (Bertaux et al. 2007; Özdil et al. 2005; Omeroglu and Ulku 2007). Similar to the roughness, there are several possibilities how to define yarn hairiness, often correlated with respective measurement devices.

Some research groups have examined the comparability of these different yarn testers and hairiness definitions. Good correlations were found, e.g., between ITQT hairiness tester, Shirley hairiness meter, and Zweigle G565 (Barella and Manich 1989) or between Uster Tester 3, Shirley hairiness meter, and EIB-MTH hairiness tester (Kothari et al. 2004). Other experiments, however, described the correlation between Zweigle G565 and Shirley hairiness tester as good, whereas significantly larger differences occurred between Zweigle G565 and Uster Tester 3 (Basu 1999; Canoglu and Yukseloglu 2008). Some research groups found the correlation between Zweigle G565 and Uster Tester 4 to belong on the yarn under investigation (Alay and Göktepe 2008; Kilic and Okur 2014).

Additionally, these instruments can only be used for pure yarns, not for textile fabrics. This is why only few examinations of hairiness in fabrics can be found (Cherkassky and Weinberg 2010; Carfagni et al. 2005). These studies usually use optical methods, such as laser diffraction (Bueno et al. 2000). Opposite to the optical determination of fabric defects (Malek et al. 2012; Zhu et al. 2014; Xu and Yu 1997), however, no established optical methods exist to evaluate fabric hairiness. Thus, the next subchapter describes a novel optical method based on the evaluation of microscopic images of textile fabrics. This method can not only be implemented relatively easily into different simulation and modeling programs which are commonly used in research institutes but also deal as an example of how to find new possibilities to handle measurement problems for which no solution is commercially available.

7.4 Determination of Yarn Hairiness Based on Microscopic Images and Statistical Analysis

In this subchapter, a detailed explanation is given how to treat common microscopic pictures in order to finally evaluate the complexity of the textile structures depicted using statistical methods.

7.4.1 Information Stored in a Monochromatic Image

To estimate the amount of information stored in a given part of a monochromatic image which also can be called a map, created by only white (background) and black (matter) pixels, we can propose the following expression:

$$p_i = \frac{N_i}{N},$$ (7.1)

where N_i is the number of black pixels in a chosen part of the map and N is the total number of black pixels creating the whole image. The previously mentioned cover factor is an example of such global information. Since the p_i quantity is related to a part of the whole map, it is a measure of local information. Thus, in order to have another type of global knowledge of an image, some probes with the use of Eq. (7.1) should be repeated at different locations.

Another interesting issue is that sometimes we are not sure if the information collected in such a way is rich and representative enough. Additionally, counting all N black pixels requires a lot of computing time. This is why, in practice, a relevant amount of a representative number of pixels should be chosen at random. This is the basic assumption for a typical stochastic experiment leading to proper estimation of information.

It is also worth mentioning that the locally tested region can be quite different from a square; for example, it can be circular and has a given radius R. In order to count pixels in a given circular region, surrounding the position $\vec{x}_i$, the following Heaviside step function can be implemented:

$$N_i = \sum_{j=1}^{N} \Theta \left(R - \left| \vec{x}_i - \vec{x}_j \right| \right)$$ (7.2)

with

$$\Theta \left(R - \left| \vec{x}_i - \vec{x}_j \right| \right) = \begin{cases} 1 & \text{if} \quad R - \left| \vec{x}_i - \vec{x}_j \right| \leq 0 \\ 0 & \text{if} \quad R - \left| \vec{x}_i - \vec{x}_j \right| > 0 \end{cases}.$$ (7.3)

The measure expressed in Eq. (7.1) refers to probability. For example, for a completely black map, $p_i = 1$, if the tested region is the same as the whole map, while for the completely white one, $p_i = 0$ (Fig. 7.2). Similarly, when the black pixels do not cover completely the two-dimensional image, we can obtain $p_i = 1$ (Fig. 7.3) if the tested region covers all the image black pixels; however, in practice this is a very rare situation.

An alternative for Eq. (7.1) can be the arbitrary power of the probability of the qth order, namely,

Fig. 7.2 Amount of
information stored in the
squared images: $p_i = 1$
(*left*), $p_i = 0$ (*right*)

Fig. 7.3 Information stored
within the square of
100×100 dimension
(in pixels) equals $p_i = 1$
since the dimension of the
black square is equal to
20×20, and the tested
region, marked by the
circle, covers all the image
black pixels
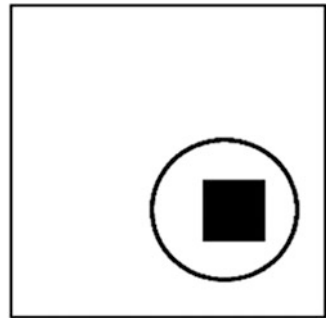
$$p_i = \left(\frac{N_i}{N}\right)^{q-1}, \qquad (7.4)$$

where q can be an arbitrary real number. For $q = 2$, one obtains the standard
expression, and it is clear why the $q - 1$ factor can be seen above. The reason of
this modified expression will be presented later; however, it is easy to notice that
large positive values of q reduce significantly the ratio of N_i/N, while negative
values enhance the small values of this ratio. Thus, one can say the image pixel
distribution is tested at different scales or resolutions, represented here by the
q order. It is worth mentioning, however, that $q = 2$ is practically in use, while
the other orders are important for fractal analysis which is out of the scope of
the book.

As mentioned above, the amount of information can be obtained locally, being
dependent on the position of the local area (Fig. 7.4). However, if the local
experiment is repeated in m separated region, then the simple summation provides
the global information, namely,

$$p^{(m)} = \sum_{i=1}^{m} p_i \qquad (7.5)$$

or

Fig. 7.4 Example of a complex distribution of pixels in the map where the local information $p_i = N_i/N$ is position dependent with $N_1 = 3$, $N_2 = 0$, and $N_3 = 21$. The dimension of the local region under tests, the *square*, equals 13×13 pixels
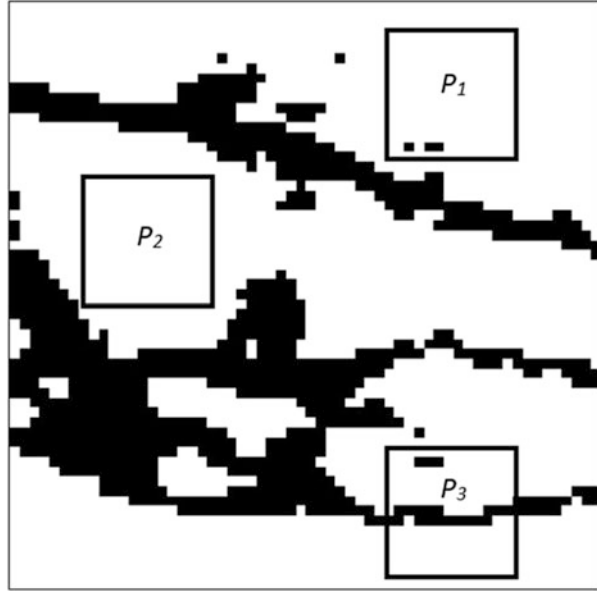
$$p^{(m)} = \sum_{i=1}^{m} p_i^{q-1} \tag{7.6}$$

in its generalized form.

The definitions above are fundamental for textile sample analysis where the nonlocal character of Eq. (7.5) is applied. Counting pixels, the local probabilities and the summation can be calculated using a so-called correlation integral. Its nonlocal character results from summation of local information in the following form:

$$C = \frac{1}{N} \sum_{i=1}^{N} (p_i) \tag{7.7}$$

or

$$C_R = \frac{1}{N} \sum_{i=1}^{N} \left[\frac{1}{N} \sum_{j=1}^{N} \Theta \left(R - |\vec{x}_i - \vec{x}_j| \right) N_i \right] = \frac{1}{N^2} \sum_{i=1}^{N} N_i. \tag{7.8}$$

In other words, a correlation integral is the averaged value of local probabilities read out from a map as a whole. Since these calculations are position dependent, the

question arises how this quantity scales with the radius of the region under examination. In the most general form, it can be written as

$$C_R \sim R^D, \tag{7.9}$$

where D is the correlation fractal dimension (Mandelbrot and van Ness 1968; Havlin and Avraham 1982; Avraham and Havlin 2000). The dimension can be easily read out from the logarithmic relation, for the limiting $R \to 0$ case, as

$$D = \lim_{R \to 0} \frac{\ln C_R}{\ln R}. \tag{7.10}$$

There is another method useful for information analysis of monochromatic images. It is the random walk approach, a method based on statistical algorithms. This is described in the next section.

7.4.2   Random Walk Method

Simply counting black pixels, as described in the previous subchapter, does not inform about the distribution of matter and does not recognize differences in shapes for the same amount of matter.

There is another method which is useful for structural characterization of species, possessing shape-resolving power, based on the so-called random walk algorithm, which removes this inconvenience. A typical implementation of this algorithm leads to quantitative estimation of textile species providing so-called Hurst exponents distribution (Haus and Kehr 1987; Berthelsen et al. 1994; Havlin and Avraham 2002; Ehrmann et al. 2015a, b).

A typical random walk experiment is realized by n random trials performed on a monochromatic map. The trial is a unit spatial step initiated from an arbitrary point, also chosen at random. Every trial has four obvious possibilities: left, right, up, and down. Hence, the trials imitate a time flow during a walk. In other words, time is discretized. Using this method, after n random walks, the following total distance, represented by the two-dimensional displacement vector $\Delta \vec{r}$ (Fig. 7.5), can be reached:

$$\Delta \vec{r} = \left[\sum_{i=1}^{n} \Delta x_i, \sum_{i=1}^{n} \Delta y_i \right], \tag{7.11}$$

with $\Delta x_i = \pm 1$, $\Delta y_i = \pm 1$ being the unit steps in the horizontal direction and the vertical direction, respectively. Obviously, the launched distance strongly depends on the spatial distribution of sample matter (Fig. 7.6). On the other hand, the

Fig. 7.5 Example of a random walk with $n = 1000$ trials on a hypothetical textile structure (*gray*) at randomly chosen region (**a**). Details of the random walk and the displacement vector connecting the starting and the final points (**b**)
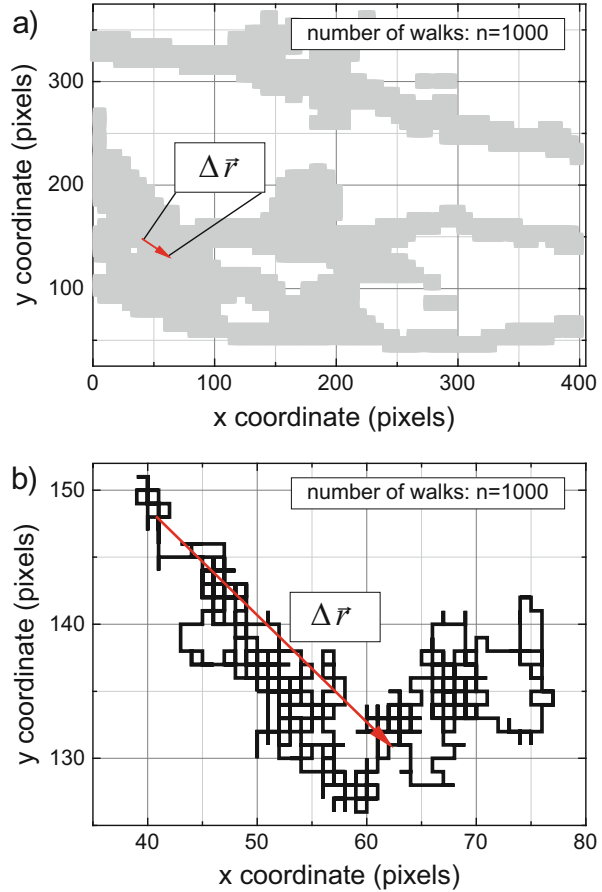
random walk on a completely black map of infinite size is not restricted by spatial distribution of matter and can be treated as a special reference situation.

Next, when the numerical experiment, for the assumed number of the n trials, is repeated many times, starting from the same initial point, then the average displacement vanishes: $< \Delta r > = 0$. Thus, the average distance cannot be useful for our goals. However, the average value of the squared displacement vector $< \Delta \vec{r}^2 >$ never equals zero, since

$$< \Delta \vec{r}^2 > = < \Delta r^2 > = \left\langle \left(\Delta \vec{r}_1 + \Delta \vec{r}_2 + \cdots + \Delta \vec{r}_i + \cdots + \Delta \vec{r}_n \right)^2 \right\rangle$$

$$= \left\langle \left(\sum_{i=1}^{n} \Delta \vec{r}_i^2 \right) + 2 \left(\sum_{i>j}^{n} \Delta \vec{r}_i \Delta \vec{r}_j \right) \right\rangle = \left\langle n + 2 \left(\sum_{i>j}^{n} \Delta \vec{r}_i \Delta \vec{r}_j \right) \right\rangle = < n > = n,$$

$$(7.12)$$

Fig. 7.6 The random walk is shape dependent; especially it depends on the initial point position. The region around point A provides more freedom for the walk, while the region surrounding the B point is more confined
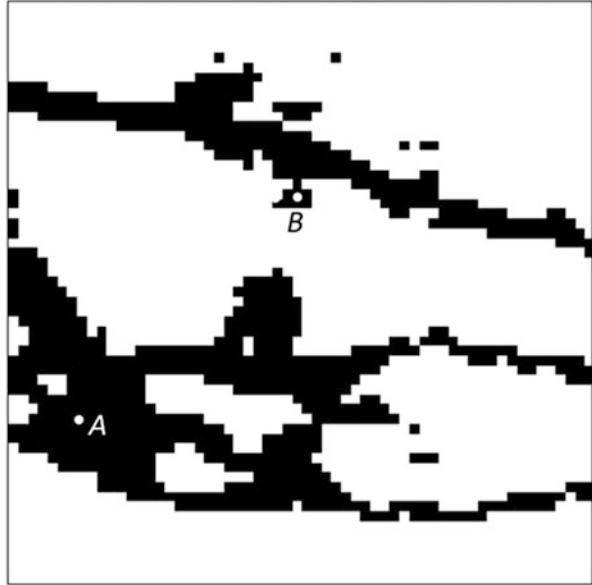
and since the $\sum \Delta \vec{r}_i \Delta \vec{r}_j$ term vanishes – the steps can sometimes be parallel, can sometimes be antiparallel, and in some cases can be perpendicular. Thus, the average value of the squared displacement vector can be treated as a quantitative indicator of the map's structural complexity.

The most striking property of such numerical experiments is that for many real images, the squared displacement vector $< \Delta r^2 >$ is not clearly proportional to n, but to any arbitrary power, namely, for the factor of $2h$ (Eq. 7.13), where h is the so-called Hurst exponent. For $h = 0.5$, one obtains the "normal" linear dependence which occurs only for a walk on infinite and completely black maps. The relation between squared displacement vector and number of steps n is then as follows:

$$< \Delta r^2 >= C \, n^{2h} \tag{7.13}$$

where C is an arbitrary constant of no special importance but required due to mathematical correctness. Practical realization of the random walk algorithm, applied to different types of optically captured maps, will be presented in the subsequent subchapters.

7.4.3   Practical Realization of Random Walk Experiments at Optically Captured Maps

The dependence of the averaged squared distance $< \Delta r^2 >$ on the number of steps n^{2h} can be used for calculations of the h parameter, the Hurst exponent. As mentioned earlier, the h exponent equals 0.5 for an infinite and completely black map. However, other values, obtained for typical images, provide interesting information about the nature of a specific textile pattern. In general, for the $h < 0.5$ case, we have a so-called anticorrelated regime, meaning that after a single step in a given direction, the next one in the same direction is less probable.

This situation occurs especially in small features where steps in the same direction are soon blocked by borders. Similarly, for the $h > 0.5$ case, we have a positively correlated regime, meaning that after a single step in a given direction, the next one in the opposite direction is less probable (Avraham and Havlin 2000). This situation only occurs in dynamical situations, not for evaluation of static pictures.

Calculations of h can be carried out using some elementary derivations. Equation (7.5) can be modified by applying the natural logarithm on both sides:

$$Ln\left(< \Delta r^2 > \right) = Ln(C) + 2h\,Ln(n) \qquad (7.14)$$

with $Ln(< \Delta r^2 >)$ being linearly dependent on $Ln(n)$ and the Hurst exponent being half of the slope of that linear relation. It should be emphasized, however, that in order to obtain information about a map as a whole, the slope in the linear relation above can be obtained by using a range of discrete times. Practically, the linearity is easily accessible if n varies from 1/10 up to 1/2 of the image diagonal. Also, the experiment is repeated for randomly chosen starting points. In real tests with textiles or fibrous samples, the numbers of starting points are chosen from the range 100 to 1000 (Blachowicz et al. 2014, 2015; Ehrmann et al. 2015a).

Now, some examples explaining the working principles of the random walk method will be given. As a sample, the structure depicted in Fig. 7.6 will be elaborated.

Figure 7.7 explains how the number of averages (repetitions) for a fixed starting point influences the results. Figure 7.8 provides distributions of Hurst exponents for increasing numbers of starting points as well as repetitions. The number of repetitions is defined for every starting point for which the experiment was repeated. Thus, the total number of numerical walks equals 100, 10,000, and 1,000,000 for the cases (a), (b), and (c) shown in Fig. 7.8, respectively.

Fig. 7.7 Examples of linear fitting the dependence of averaged squared distance on the number of steps being a measure of time (Eq. 7.14) for a fixed starting point and different numbers of experiment repetitions: 10 (**a**), 100 (**b**), and 1000 (**c**). The results show the increasing accuracy with the number of averaging cycles
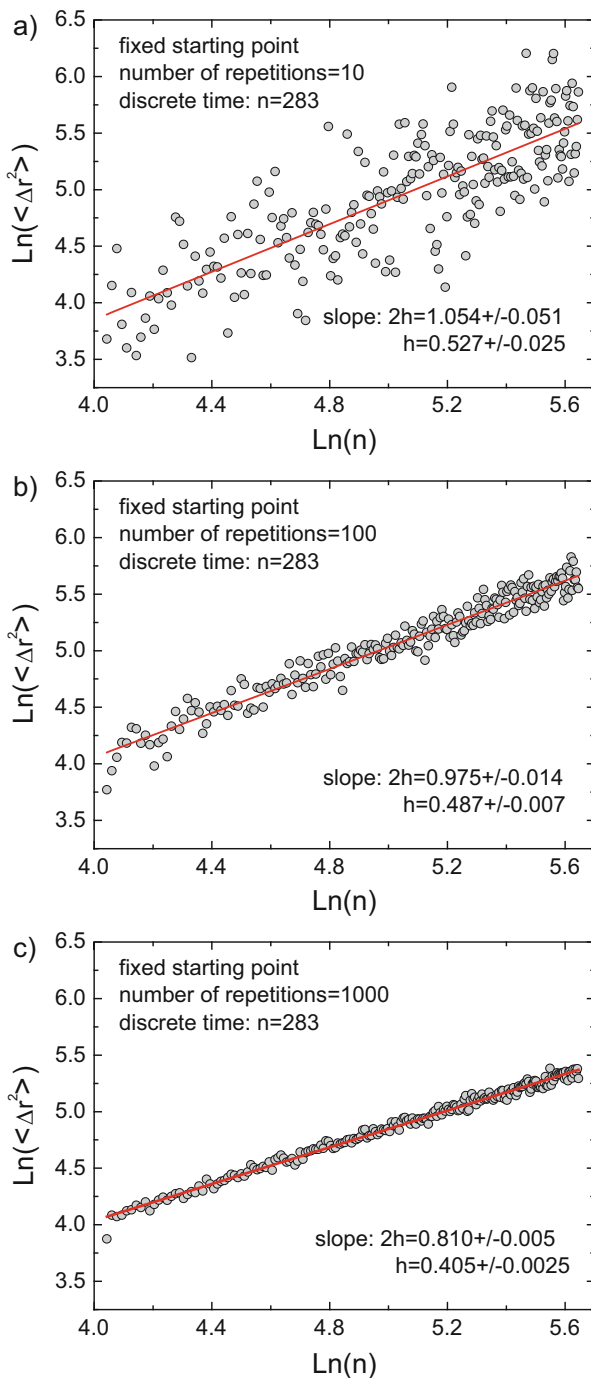
Fig. 7.8 Examples of Hurst exponent distributions obtained for different number of starting points N and repetitions of the experiment: $N = 10$ (**a**), $N = 100$ (**b**), and $N = 1000$ (**c**)
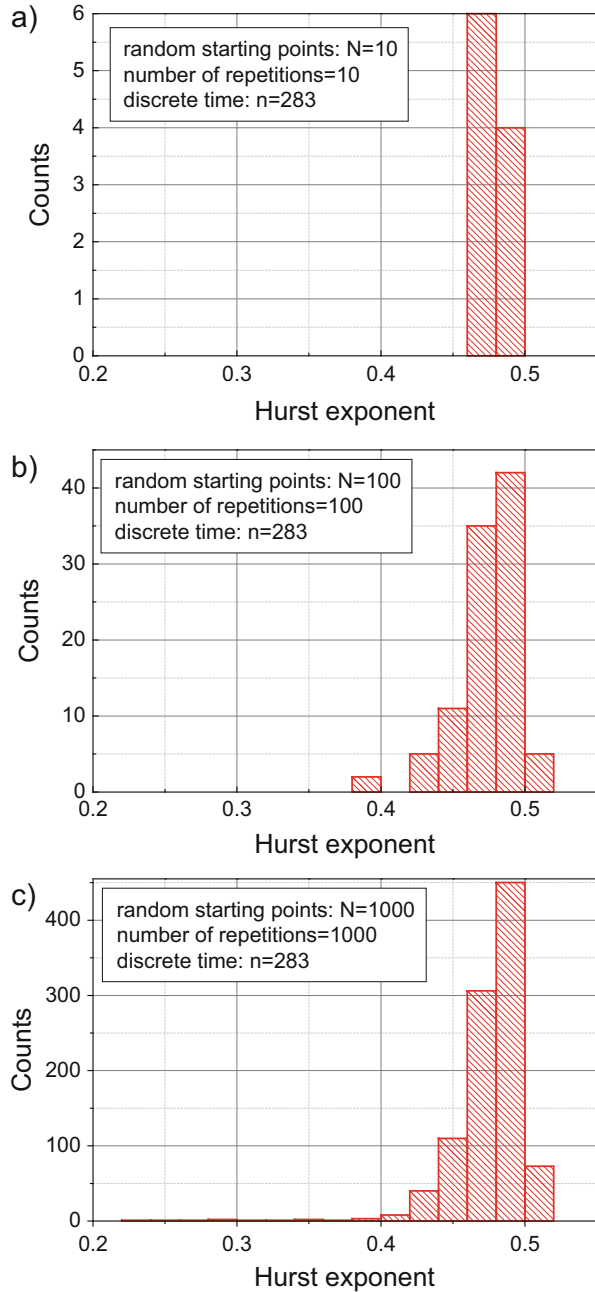
7.4.4 Experiments with Basic Structures

In this subchapter, examples of the random walks carried out on very basic geometrical elements and structures are provided. It should give the reader an opportunity to obtain some elementary intuition related to the method. Two groups of examples are presented. In the first one, a sequence of results carried out on black rectangles is given (Figs. 7.9 and 7.10). The sequence is obtained by a step-by-step reduction of one of the rectangle's sides, leading to the limit of a thin line. In the second example, some differences between patterned structures of different graphical densities are given (Fig. 7.11).
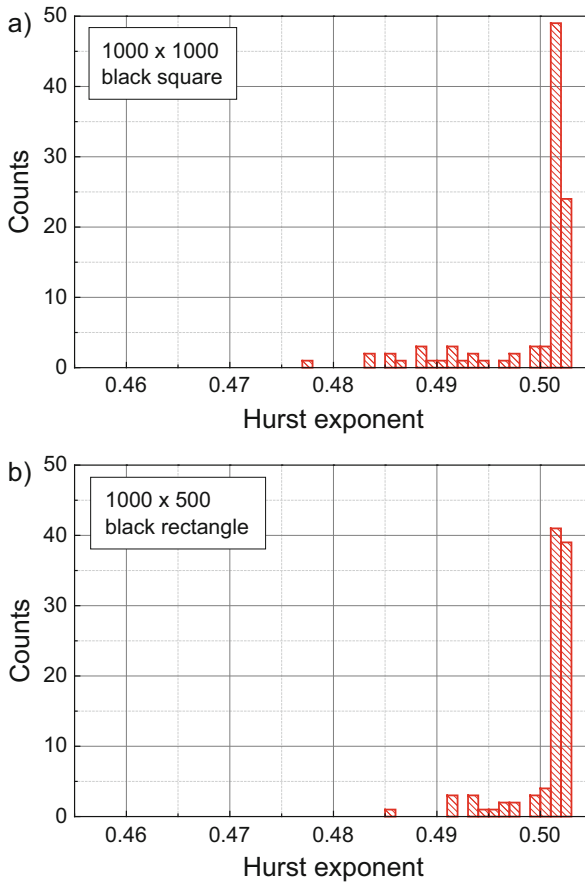
Fig. 7.9 Random walk tests performed at a simple (1000×1000) pixel *black square* (**a**) and *black rectangles* with the dimension of one side gradually reduced (**b, c, d**). This reduction causes a shift in the distribution and a change of its shape. The figure dimensions are given as numbers of pixels. The experiment was carried out at 100 randomly chosen starting points and repeated 1000 times for each starting point
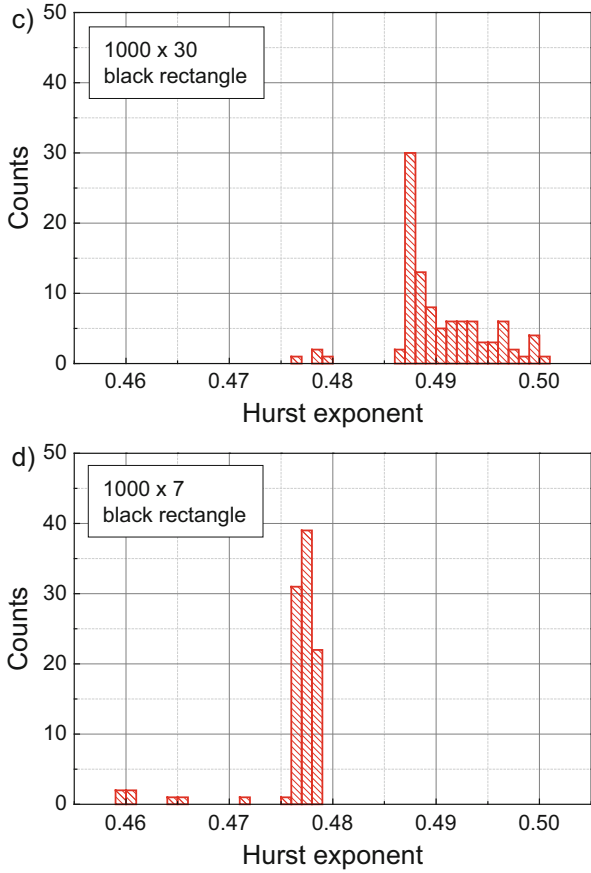
Fig. 7.9 (continued)
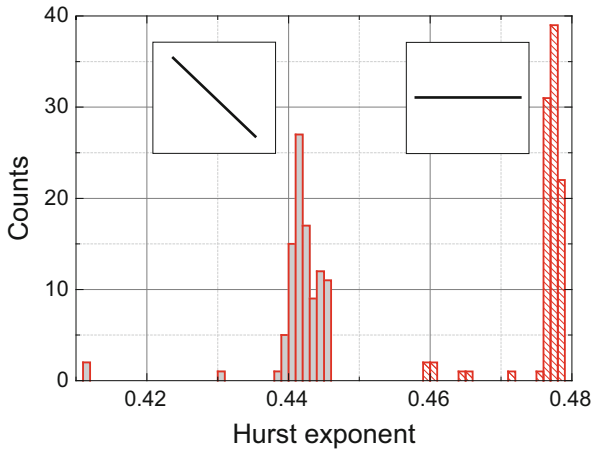
Fig. 7.10 A 45° rotation of a thin line (1000 × 7 pixels) modifies the Hurst exponent distributions. This property of random walk can be described as a directional contrast. The experiment was carried out at 100 randomly chosen starting points and repeated 1000 times for each starting point

Fig. 7.11 Different types of two-dimensional patterns provide specific Hurst exponent distributions. This property of random walk can be imagined as a matter distribution contrast. The size of each sample equals 350×350 pixels. The experiment was carried out using 100 randomly chosen points
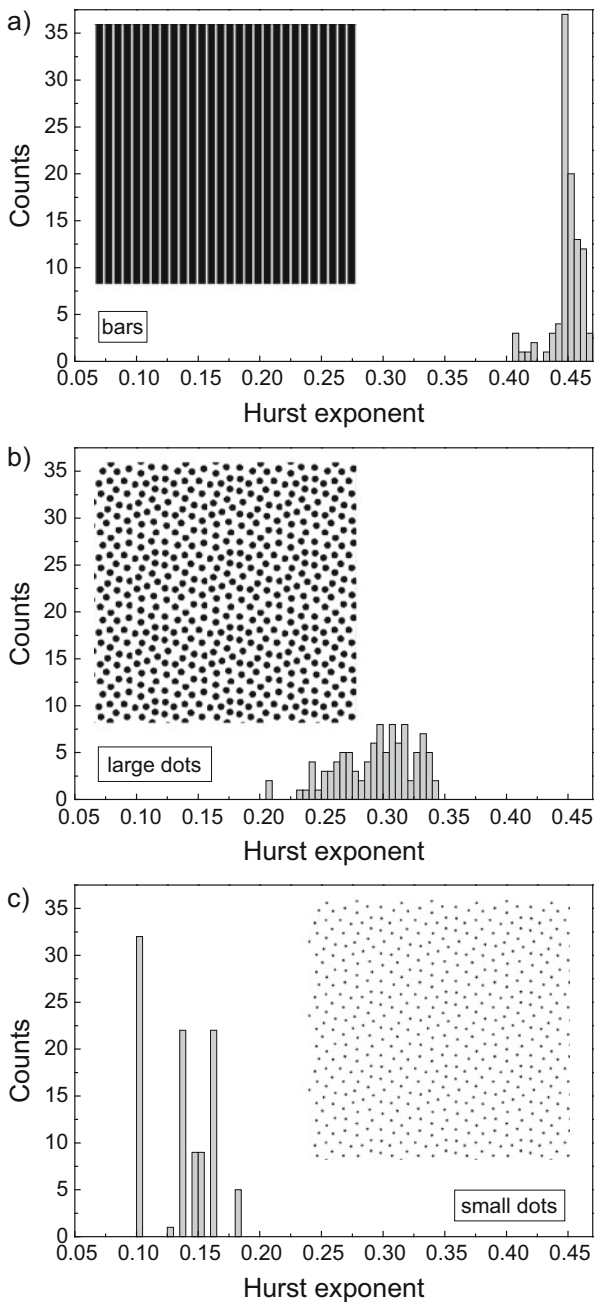
The results seen in the figures above show the spatial resolving ability of the method. Also, in Fig. 7.10, the striking result of the orientation resolving ability proves that the movement along the diagonal is more limited, since it requires two perpendicular movements. Hence, the Hurst exponent reflects a distance covered.

Finally, some examples of two-dimensional samples are given in Fig. 7.11. They show the sensitivity of the random walk on matter density and can be denoted as matter distribution contrast of the method. In Fig. 7.11a, the bars are very closely arranged, thus a sample only slightly differs from a fully black square. Therefore, the distribution is allocated close to the value 0.5. The large dots example (Fig. 7.11b) provides a left-shifted distribution, with a significant shift into the range of 0.25–0.35 Hurst exponent values. The distribution is relatively wide since each single dot has a diameter big enough to be covered by different scenarios of random walks. Hence, a typical single dot is created from about 70 black pixels. Finally, the small dots example (Fig. 7.11c) provides the distribution shifted to small values of the Hurst exponents since the objects under tests are relatively small. It can be said that the obtained values of Hurst exponents are quantized, since the different scenarios for walking at the very small dots are restricted to a few types only. From the image processing perspective, a single dot was created from a number of pixels in the range of 6–9.

In the next two sections, presentations of real industrial examples are provided, especially two qualitatively different types of samples: normal regularly ordered fabrics of industrial origin and completely chaotic hemp fibers. It should convince the reader of the suitability of the method provided in this subchapter. The general ability to classify the very contrary cases reveals the universality of the random walk approach.

7.4.5 Experiments with Two-Dimensional Textile Structures

The species under consideration are single face fabrics knitted using a Stoll flat knitting machine CMS 302 TC with machine gauge E8. Five different types of yarns were used to produce the samples: synthetic fibers of aramid possessing linear mass density of 550 dtex, a blended fiber system of 70 % polyacrylonitrile (PAN) and 30 % virgin wool (WV) (Nm 30/2), ultra-high molecular weight polyethylene (UHMWPE) with a combination of 440 dtex and 220 dtex fibers, high-tenacity polyester (1100 dtex), and a viscose specimen (2×330 dtex). The dtex (decitex) unit measures the mass of fibers in grams per 10,000 m. The metric yarns number (Nm) provides the length in meters per 1 gram. Hence, 1 dtex = 10,000/Nm.

Now, it is a proper moment to mention the photographic image preparation. Images can be captured using a classical optical microscope equipped with a digital camera. For the recent samples, a VHX-600D digital microscope manufactured by Keyence was used. Especially, the VH-Z20R objective enabled making photographs with different magnifications, while here the results for a nominal magnification of $20\times$ are presented.

The transformation into 1-bit black-and-white images can be carried out using commonly accessible free graphical software or self-written computer programs (Vlahos et al. 2008; Nixon 2012). The first ones can use automatic procedures and can lead to significant reduction of information, especially if the sample is not

Aramid
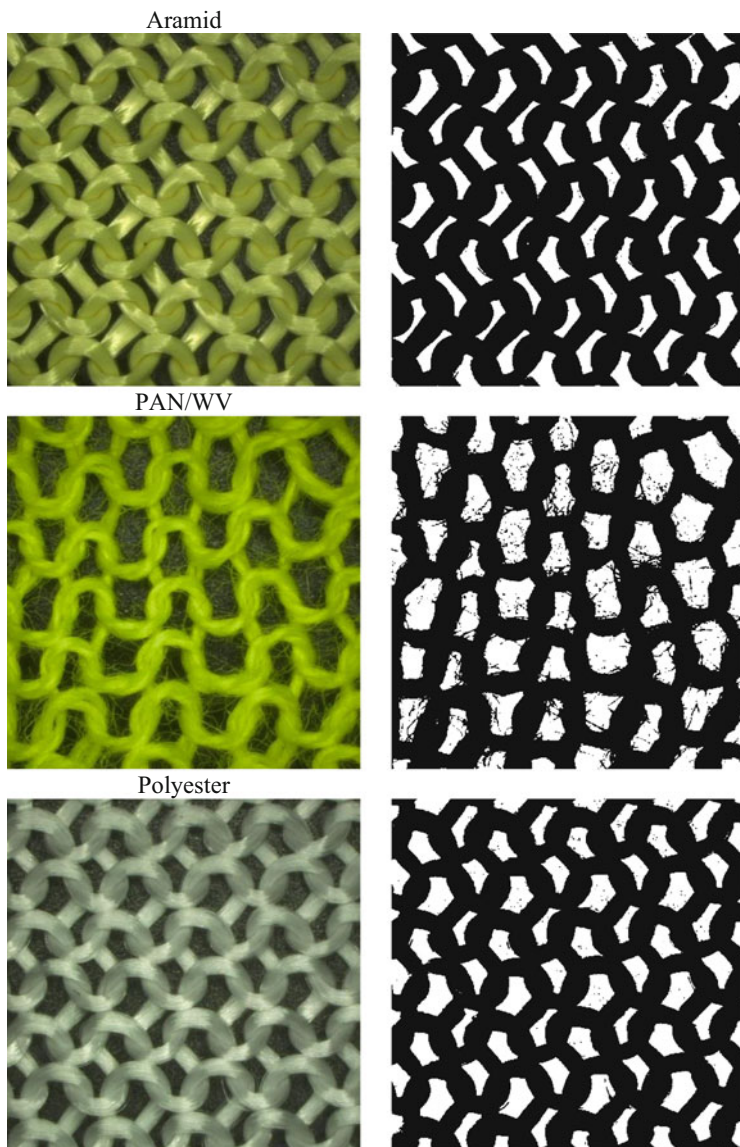
PAN/WV

Polyester

Fig. 7.12 Optically captured images (*left column*) and monochromatic representations (*right column*) of five types of samples: aramid, polyacrylonitrile with virgin wool (PAN/WV), polyester, ultra-high molecular weight polyethylene (UHMWPE), and viscose

UHMW-PE

Viscose
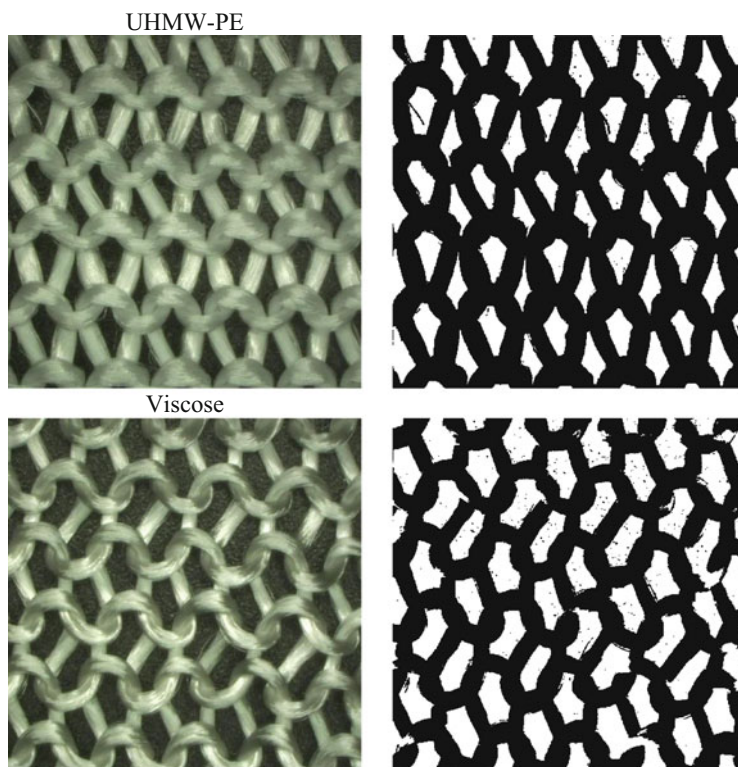
Fig. 7.12 (continued)

uniformly illuminated or if the background is not homogeneous. Self-made codes, on the other hand, are able to obtain optimal amount of data; however, they require deep knowledge of image processing, and they are not universal (Fabiańska and Jackowska-Strumiłło 2012; Zghidi et al. 2015). Such algorithms can consist of several steps, for example, median filtering, unsharp masking, denoising, high-pass filtering, and Gaussian filtering. Next, the whole procedures require several specific decisions, like sampling of the image background, a choice of the extraction threshold and the unsharp-masking proportional factors, as well as tailoring of the other filter parameters.

More details about these image processing steps can be found in computer science literature. Nevertheless, in many practical situations, and also for the images presented here, the automatic solutions warrant rational resolution and contrast. This can be revealed by looking at the PAN/WV sample (Fig. 7.12) where the hairiness is easily distinguishable.

Now, the samples under tests can be examined just from the perspective of hairiness quantitative diagnosis and pattern recognition. The random walk approach, on the base of optically captured and transformed images, can offer
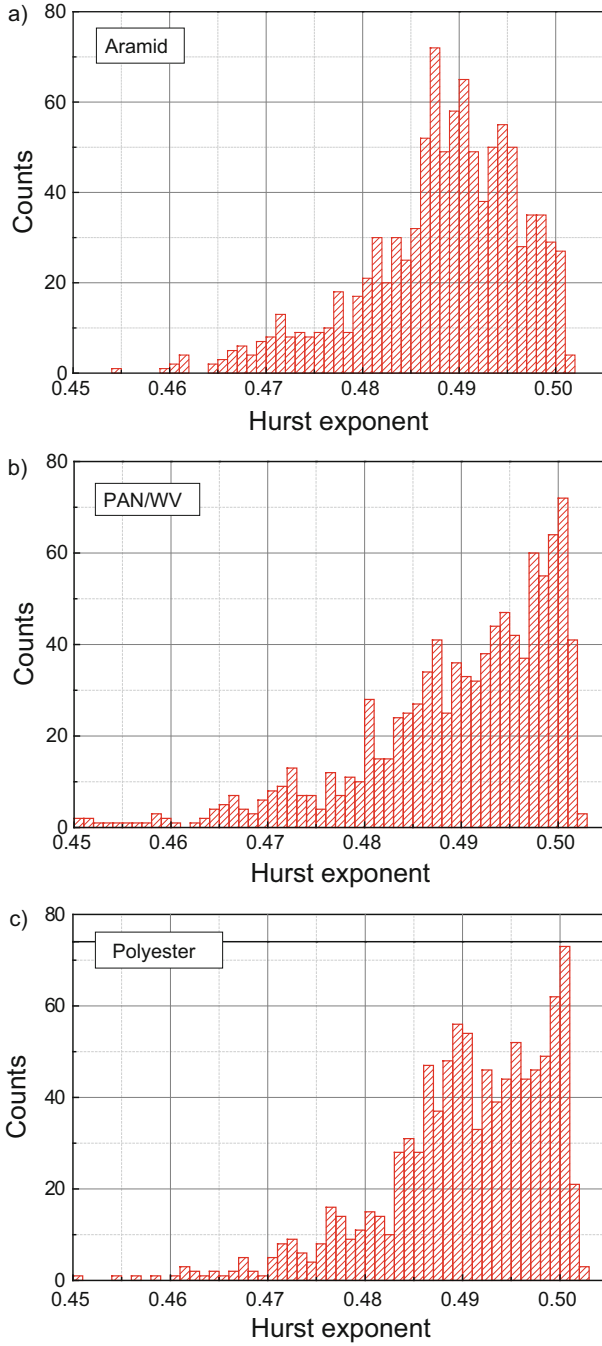
Fig. 7.13 Results of random walk experiments and the Hurst value distributions for the five types of samples: aramid, polyacrylonitrile with virgin wool (PAN/WV), polyester, ultra-high molecular weight polyethylene (UHMWPE), and viscose
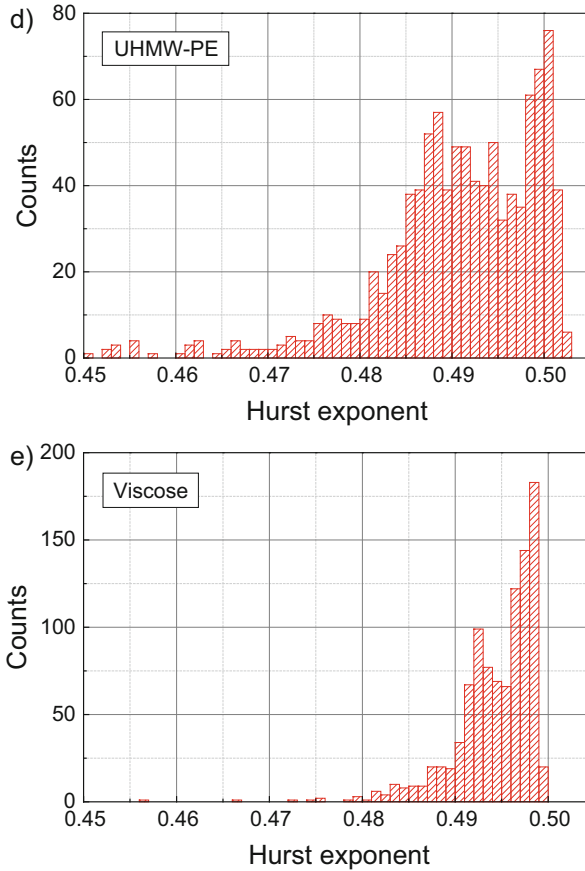
Fig. 7.13 (continued)

another methodology in order to supplement well-established Uster or Zweigle standard tests. Information about hairiness is contained for lower values of Hurst exponents as well as in the overall shape of the obtained distributions. In Fig. 7.12, the original and the transformed images are depicted. The results of simulations are shown in Fig. 7.13.

7.4.6   Experiments with Hemp Fibers

Another example of an application of the random walk method deals with something completely different, i.e., very chaotic species. The images were prepared using similar arrangement as the previous examples of regular textile fabrics. The
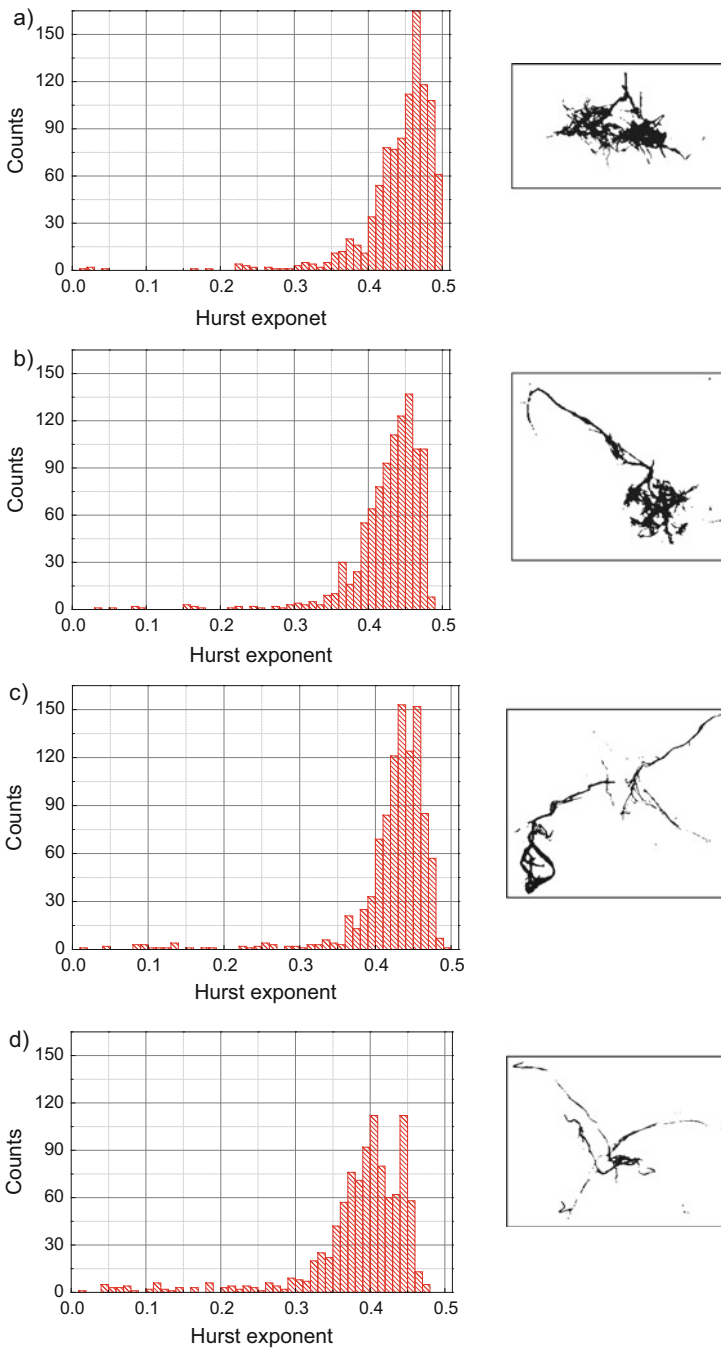
Fig. 7.14 Simulations performed on different hemp samples. Descriptions: a big bulk region with dominating Hurst exponent signal around 0.46 (**a**), dominating single-directional part with a Hurst distribution of reduced amplitude (**b**), a few long fibers and a lack of big bulk parts – the Hurst exponent distribution is split and has the two maxima (**c**), long thin fibers and very short small elements seen as a background extending to the left of 0.3 (**d**)

results are depicted in Fig. 7.14 for four selected species. The samples were chosen on purpose to show the variety of structural properties as well as the capabilities of the numerical treatment.

The results provided enable presenting the resolving ability of the random walk method in application to a variety of textile samples, both regular and chaotic, from the structural point of view. The obtained characteristics represent the diagnostic approach to many different types of species in a quantitative way.

As shown in the examples in this chapter, different methods can be used to gain more information from simple (microscopic) pictures. Depending on the available software and the personal mathematical and programming skills, the level of image processing integration into optical evaluation of samples can be chosen.

Literature

Alay, S., Göktepe, F.: Farklı İplik Tüylülüğü Parametreleri Arasındaki Korelasyonun Araştırılması. Tekst. Konfeksiyon **18**, 28–34 (2008)

Avraham, D. ben-, Havlin, Sh.: Diffusion and Reactions in Fractals and Disordered Systems. Cambridge University Press, Cambridge (2000)

Barella, A., Manich, A.M.: Influence of cotton fiber properties on yarn hairiness. Text. Res. J. **59**, 632–633 (1989)

Basu, A.: Assessment of yarn hairiness. Indian J. Fibre Text. Res. **24**, 86–92 (1999)

Bertaux, E., Lewandowski, M., Derler, S.: Relationship between friction and tactile properties for woven and knitted fabrics. Text. Res. J. **77**, 387–396 (2007)

Berthelsen, C.L., Glazier, J.A., Raghavachari, S.: Effective multifractal spectrum of a random walk. Phys. Rev. **E49**, 1860–1864 (1994)

Blachowicz, T., Aumann, S., Pruß, B., Reiners, P., Ehrmann, A., Weber, M.O., Weide, T.: Optical determination of yarn hairiness using statistical methods. In: Proceedings of the Aachen-Dresden International Textile Conference, Dresden, 27–28 Nov 2014

Blachowicz, T., Ehrmann, A., Zghidi, H., Domino, K.: Optical determination of hemp fiber structures by statistical methods. In: Proceedings of Aachen-Dresden International Textile Conference, Aachen, 26–27 Nov 2015

Bueno, M.-A., Durand, B.D., Renner, M.: Optical characterization of the state of fabric surfaces. Opt. Eng. **39**, 1697–1703 (2000)

Canoglu, S., Yukseloglu, S.M.: Hairiness values of the polyester/viscose ring-spun yarn blends. Fibres Text. East. Eur. **16**, 34–38 (2008)

Carfagni, M., Furferi, R., Governi, L.: A real-time machine-vision system for monitoring the textile raising process. Comput. Ind. **56**, 831–842 (2005)

Cherkassky, A., Weinberg, A.: Objective evaluation of textile fabric appearance part 1: Basic principles, protrusion detection, and parameterization. Text. Res. J. **80**, 226–235 (2010)

Ehrmann, A., Blachowicz, T., Domino, K., Aumann, S., Weber, M., Zghidi, H.: Examination of hairiness changes due to washing in knitted fabrics using a random walk approach. Text. Res. J. **85**, 2147–2154 (2015a)

Ehrmann, A., Blachowicz, T., Zghidi, H., Weber, M.O.: Reliability of statistic evaluation of microscopic pictures taken from knitted fabrics. J. Phys.: Conf. Ser. **633**, 012101 (2015b)

Fabiańska, A., Jackowska-Strumiłło, L.: Image processing and analysis algorithms for yarn hairiness determination. Mach. Vision Appl. **23**, 527–540 (2012)

Gravas, E., Kiekens, P., van Langenhove, L.: Predicting fabric weight per unit area of single- and double-knitted structures using appropriate software. AUTEX Res. J. **6**, 223–237 (2006)

Haus, J.W., Kehr, K.W.: Diffusion in regular and disordered lattices. Phys. Rep. **150**, 263–406 (1987)

Havlin, S., Avraham, D. ben-: Diffusion in disordered media. Adv. Phys. **51**, 187–292 (2002)

Havlin, S., Avraham, D. ben-: Fractal dimensionality of polymer chains. J. Phys. **A15**, L311–L316 (1982)

Hearle, J.W.S., Amirbayat, J.: The design of a multipurpose fabric tester. J. Text. Inst. **79**, 588–598 (1988)

Kilic, M., Okur, A.: Comparison of the results of different hairiness testers for cotton-Tencel blended ring, compact and vortex yarns. Indian J. Fibre Text. Res. **39**, 49–54 (2014)

Kothari, V.K., Ishtiaque, S.M., Ogale, V.G.: Hairiness properties of polyester-cotton blended yarns. Indian J. Fibre Text. Res. **29**, 30–34 (2004)

Malek, A.S., Drean, J.-Y., Bigue, L., Osselin, J.-F.: Optimization of automated online fabric inspection by fast Fourier Transform (FFT) and cross correlation. Text. Res. J. **83**, 256–268 (2012)

Mandelbrot, B., van Ness, J.W.: Fractional Brownian motions, fractional noises and applications. Soc. Indian Appl. Math. Rev. **10**, 422–437 (1968)

Militky, J., Mazal, M.: Image analysis method of surface roughness evaluation. Int. J. Cloth. Sci. Technol. **19**, 186–193 (2007)

Mooneghi, S.A., Saharkhiz, S., Varkiani, S.M.H.: Surface roughness evaluation of textiles fabrics: a literature review. J. Eng. Fibres Fabr. **9**, 1–18 (2014)

Munden, D.L.: Specification of construction of knitted fabrics. J. Text. Inst. **53**, P628–P630 (1962)

Nixon, M.: Feature Extraction and Image Processing for Computer Vision, 3rd edn, p. 114. Academic, Oxford (2012)

Omeroglu, S., Ulku, S.: An investigation about tensile strength, pilling and abrasion properties of woven fabrics made from conventional and compact ring-spun yarns. Fibres Text. East. Eur. **15**, 39–42 (2007)

Özdil, N., Özdogan, E., Demirel, A., Öktem, T.: A comparative study of the characteristics of compact yarn-based knitted fabrics. Fibres Text. East. Eur. **13**, 39–43 (2005)

Peirce, F.T.: The geometry of cloth structure. J. Text. Inst. **28**, T45–T96 (1937)

Stockbridge, H.C.: The subjective assessment of the roughness of fabrics. J. Text. Inst. **48**, 26–34 (1957)

Vassiliadis, S., Provatidis, C.: Structural characterization of textile fabrics using surface roughness data. Int. J. Cloth. Sci. Technol. **16**, 445–457 (2004)

Vlahos, L., Isliker, H., Kominis, Y., Hizanidis, K.: Normal and Anomalous Diffusion: A Tutorial, arXiv:0805.0419 (2008)

Xu, B., Yu, L.: Determining fiber orientation distribution in nonwovens with hough transform techniques. Text. Res. J. **67**, 563–571 (1997)

Zghidi, H., Walczak, M., Blachowicz, T., Domino, K., Ehrmann, A.: Image processing and analysis of textile fibers by virtual random walk. In: Federated Conference on Computer Science and Information Systems, ACSIS IEEE, pp. 729–732 (2015)

Zhu, B., Liu, J., Pan, R., Gao, W., Liu, J.: Seam detection of inhomogeneously textured fabrics based on wavelet transform. Text. Res J. **85**, 1381–1393 (2014)

Chapter 8
Thermal Properties of Textiles

Thermal properties are essential for textile materials due to their common everyday use and protection against cold.

In this chapter, we will concentrate on heat transport through a textile layer or a set of layers. Some fundamental material parameters will be presented and defined. At the end, heat will be presented from the perspective of electromagnetic thermal radiation. This is another mechanism of heat loss, apart from thermal conduction from a body, via textiles, into ambient regions.

8.1 Heat Transport Through Materials

The simplest case, enabling understanding of heat transport via conduction, is the one dimensional energy transport through a single layer (Fig. 8.1). The rule of the transport is very logical. An amount of energy Δq flows between regions of different temperatures. It is proportional to the time and the total area of the layer and inversely proportional to the layer thickness. A more practical quantity expressing the energy flow is the energy flux $\dot{q}_S$. The energy flux is the abovementioned amount of energy divided by layer area and time, and the unit of the heat flux is J/(m^2 s) or W/m^2. It is worth mentioning that a dot over a symbol is the common manner to describe the first time derivative $\dot{q} = dq/dt$, while in practice it can often be approximated by $\Delta q/\Delta t$.

Again, repeating the above mentioned intuitive description in a quantitative way, energy flow Δq (in Joules) is proportional to the area S, the time of heat flow Δt, the temperature difference $\Delta T_{21} = T_2 - T_1$, and inversely proportional to the layer thickness $d = \Delta x$. The proportionality constant κ is the thermal conductivity, a characteristic material parameter expressed in W/m K. The minus sign, on the right side, is obviously required, since $\Delta T_{21} = T_2 - T_1$ is negative, while real energy has to be positive. Thus, we get the mathematical expression

Fig. 8.1 Heat flow through
a single layer from the
region of higher
temperature T_1 to the region
of lower temperature T_2
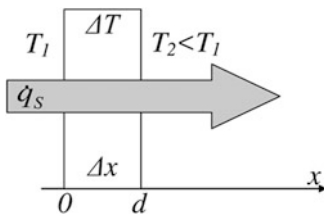
Fig. 8.2 Heat flow through
a double-layer set of
materials from the region of
higher temperature T_1 to the
region of lower temperature
T_3. T_2 denotes the
temperature at the interface
between the materials
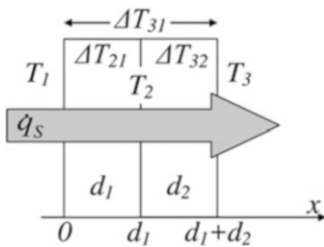
$$\Delta q = -\kappa \cdot \frac{T_2 - T_1}{d} \cdot S \cdot \Delta t$$

and the same rewritten for the energy flux equals

$$\dot{q}_S = -\kappa \cdot \frac{\Delta T_{21}}{\Delta x}.$$

It should be emphasized that the thermal flux is constant across a layer and
across all layers for multilayer materials, respectively. In other words, temperature
distribution inside a material is assumed to be stable across the layer thickness.

The double-layer structure assumes two layers of different thickness and thermal
parameters. As a first approximation, the interface between the layers is assumed to
be perfectly smooth (Fig. 8.2). As we will see later, the introduction of a third
intermediate air layer makes the model more realistic from the perspective of
thermal properties of textiles.

In most situations, the change of temperature across the layers is linear and the
temperature T_2 at the interface equals

$$T_2 = \frac{\kappa_1 d_2}{\kappa_1 d_2 + \kappa_2 d_1} T_1 + \frac{\kappa_2 d_1}{\kappa_1 d_2 + \kappa_2 d_1} T_3.$$

Assuming equality of thicknesses, we have a simple weighted average:

$$T_2 = \frac{\kappa_1}{\kappa_1 + \kappa_2} T_1 + \frac{\kappa_2}{\kappa_1 + \kappa_2} T_3.$$

The important point is that even a complex system can be substituted by a single effective parameter, here by an effective thermal conductivity. It can be derived from the assumption of constant energy flux through the layers, namely,

$$\kappa_1 \cdot \frac{\Delta T_{21}}{d_1} = \kappa_2 \cdot \frac{\Delta T_{32}}{d_2} = \kappa_{\text{eff}} \cdot \frac{\Delta T_{31}}{d_1 + d_2},$$

from where we can derive the effective constant κ_{eff}

$$\kappa_{\text{eff}} = \frac{1}{2} \cdot \frac{d_1 + d_2}{\Delta T_{31}} {}_{31} \left(\kappa_1 \cdot \frac{\Delta T_{21}}{d_1} + \kappa_2 \cdot \frac{\Delta T_{32}}{d_2} \right).$$

Finally, for the simplified case of $d_1 = d_2$ and $\Delta T_{21} = \Delta T_{32} = \frac{1}{2}\Delta T_{31}$, the effective constant is

$$\kappa_{\text{eff}} = \frac{\kappa_1 + \kappa_2}{2}.$$

The thermal conductivity is not the only parameter in use characterizing thermal properties of textile materials. The thermal resistance

$$R = \frac{d}{\kappa},$$

(expressed in m^2 K/W) and the heat transfer coefficient (expressed in W/m^{2}K)

$$U = \frac{\dot{q}\,s}{\Delta T}$$

can also be met in professional literature data. Especially the thermal resistance is applied by textile engineers. This is why we will concentrate on thermal resistance analysis below.

A constant heat flux through a perfectly smooth interface is represented by the subsequent equalities of thermal resistances of the first layer R_1 and the second layer R_2 and consequently by the effective value of thermal resistance R_{eff},

$$R_1 \cdot \frac{1}{\Delta T_{21}} = R_2 \cdot \frac{1}{\Delta T_{32}} = R_{\text{eff}} \cdot \frac{1}{\Delta T_{31}},$$

from which we can derive the additivity condition

$$R_1 \cdot \frac{1}{2\Delta T_{21}} + R_2 \cdot \frac{1}{2\Delta T_{32}} = R_{\text{eff}} \cdot \frac{1}{\Delta T_{31}}.$$

Again, assuming the same temperature difference at each layer, $\Delta T_{\text{layer}} = \text{const}$, we obtain
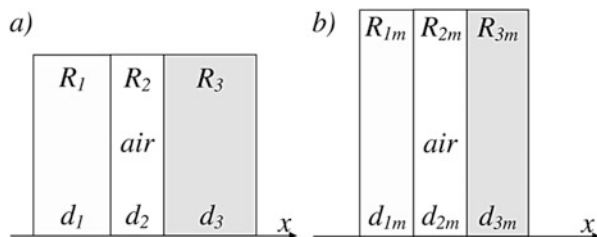
Fig. 8.3 A system of three layers with air in the middle (**a**). In the figure, perfectly smooth interfaces between the layers are assumed. Stretching the layers reduces their thicknesses and thus modifies their thermal resistances (**b**)

$$R_{\text{eff}} = R_1 + R_2 + \ldots + R_n,$$

which means in practice, for an arbitrary number of layers n, that the temperature changes linearly with layer thickness and that the thermal conductivity κ of each layer is temperature independent. This condition, however, is not always fulfilled. This can be better understood by the analysis of a three-layered structure with air as an inner intermediate layer (Fig. 8.3).

For a set of perfectly smooth layers, the additivity condition $R_{\text{eff}} = R_1 + R_2^{(\text{air})} + R_3$ still holds. However, in a more realistic case (Fig. 8.4), the simple summation is broken, and we have $R_{\text{eff}} < R_1 + R_2^{(\text{air})} + R_3$. Some tests regarding dependencies between the number of layers and the respective system's thermal resistance are reported in the literature (Huang 2016). Moreover, the air's thermal conductivity κ, even if it is small, is temperature dependent and with a good approximation proportional to temperature. Additionally, R is strain and thickness dependent, since the recent value of fiber thickness can be reduced due to tensile stresses in a textile material. For such a situation, the modified thermal resistance of the i-th layer R_{im} equals

$$R_{im} = \frac{d_{im}}{d_i} R_i,$$

where d_{im} is the modified (reduced) i-th layer thickness, d_i is the layer thickness, and accordingly R_i is the thermal resistance before stretching.

At the end of this subchapter, some thermal conductivities of textile materials, known from literature, are provided. The data are not fully consistent. The obtained values are strongly dependent on ambient conditions, cleanliness and humidity (Table 8.1).

Fig. 8.4 A system of three
realistic layers where the
total thermal resistance is
not a simple sum of each
material's values
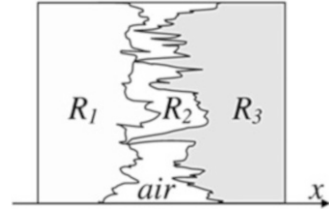
Table 8.1 Thermal conductivities of some textile materials

Material	Thermal conductivity (W/mK)	References
Cotton dry fabrics	$7.6–12.0 \times 10^{-3}$	Romeli et al. (2013)
Cotton wet fabrics	$10.1–14.7 \times 10^{-3}$	Romeli et al. (2013)
Cotton fabrics	6.33×10^{-2}	Lizák and Mojumdar (2013)
Wool	7.0×10^{-2}	Pola et al. (2013)
Polyester fabrics	$2.0–5.0 \times 10^{-2}$	Abdel-Rehim et al. (2006)
Polypropylene fabrics	$2.2–3.4 \times 10^{-2}$	Abdel-Rehim et al. (2006)
Polypropylene fabrics	6.91×10^{-2}	Lizák and Mojumdar (2013)
Polypropylene fibers	$2.2–3.0 \times 10^{-1}$	Lizák and Mojumdar (2013)

8.2   Thermal Radiation of Bodies

It is well known that each body with a temperature above absolute zero
(-273.15 °C) losses its energy via electromagnetic radiation with the characteristic
spectrum depending on its temperature. From this reason, the above-described heat
transport effects have to be extended by inclusion of thermal electromagnetic
radiation.

With a good approximation, every material radiates similarly to some idealized
case of black body radiation. For the black body radiation summarized over the
whole possible range of frequencies, the power per body area P_S (in W/m^2) at a
given temperature T (in Kelvin) is expressed by the Stefan-Boltzmann equation,

$$P_S = \sigma T^4,$$

where σ is a universal constant equal to 5.67×10^{-8} W/(m^2 K^4). However, an
interesting fact is that the radiation spectrum has a maximum introduced by
Wilhelm Wien in 1893 which can be calculated according to

$$\lambda_{\max} \cdot T = \text{const},$$

where the constant equals 2.90×10^{-3} m K (Wien's displacement law). Importantly
the maximum of the radiation at room temperature falls into the infrared (IR) region
of the optical spectrum. From this finding results the possibility to depict temper-
ature distributions using IR thermal cameras. It is worth emphasizing that the

thermal radiation coexists with normal heat transport effects presented at the beginning of this subchapter.

8.3   Standardized Tests of Heat Transfer Through Textile Fabrics

Several standards exist which can be used to measure thermal transmittance through textile fabrics, some of which are related to special applications, such as thermo-protective clothing.

The thermal resistance of a textile between two boxes at different temperatures is defined in ASTM C1363-05 and EN ISO 8990. In this "hot boxes design," two rooms are kept at different temperatures in steady-state conditions. The thermal resistance of the sample placed between both boxes is defined by measuring the necessary energy for keeping the hot box at constant temperature (Asdrubali and Baldinelli 2011; Ricciardi et al. 2014; Yang et al. 2016). This method is also often used for building parts (Mumaw 1974; Adam and Jones 1995).

In the ASTM D1518, e.g., the overall thermal transmission – as the sum of radiation, thermal conduction, and convection – is measured. The overall thermal transmittance is of importance for clothing which is meant to protect people from cold weather. This standard measures the heat transfer from a hot plate held at constant temperature through a textile layer on top of it to a cool atmosphere. Due to the often not directly apparent impacts of small deviations of geometry or measurement procedures, all these parameters are defined quite precisely in the standard to allow for reliable and comparable test results.

Opposite to the dry hot plate used in ASTM D1518, the standards ASTM F1868, ISO 11092, EN 31092, and others use a "sweating" hot plate, determining thermal resistance and evaporative resistance in a stationary state. While ASTM F1868 is suitable for protective clothing, as well as ASTM F1060 which allows for examination of protective clothing at high temperatures up to 316 °C, the other mentioned tests apply to diverse textile fabrics, membranes, coatings, leather, etc. for a variety of applications.

Often used instruments to measure thermal conductivity, thermal resistance, thermal absorptivity, and thermal diffusivity by placing a textile sample between two plates at different temperatures are Alambeta and Permetest, measuring according to ISO 11092, produced by Sensora Instrument (Liberec/Czech Republic). These instruments are used in several scientific publications (e.g., Hes and Dolezal 1989; Hes and Stanek 1989; Hes and Araújo 1996; Hes and Kus 2003; Oğlakcioğlu and Marmarali 2007; Hes 2008; Bhattacharjee and Kothari 2009; Uzun 2014; Mangat et al. 2015; Diswat et al. 2016; Angelova et al. 2016).

Even higher demands are inspected in ASTM F1939 and ASTM F1930, respectively, which are meant to investigate flame-resistant clothing materials. Here, the heat resistance of textile materials are investigated by continuous heating or flash

fire, respectively. Clothing for firefighters is also investigated with respect to the thermal energy stored in a test specimen (ASTM F2702 and ASTM F2703) or combinations of transmitted and stored energy (ASTM F2731).

While ASTM 1930 uses an instrumented manikin, several test standards are based on heated manikins. These tests have the advantage that not only pure textile layers can be compared but also the influence of garment fit; combinations of different garments and fasteners can be tested, and thus the physiological comfort of complete sets of clothing can be estimated. ASTM F1291-05, e.g., investigated the insulation values of garments with respect to dry heat transfer from the manikin "body" to a cool surrounding. Similarly, ASTM F1720-06 and EN 13537 deal especially with the insulation values of sleeping bags. "Sweating" manikins are, e.g., used in ASTM F2370-05 or ASTM F2371-05, testing the evaporative resistance and the heat removal rate of clothing systems, respectively. One example of a sweating manikin is "SAM," the "Sweating Agile Thermal Manikin" developed by EMPA (Richards and Mattle 2001; Morrissey and Rossi 2014).

Opposite to these "standing" manikins, EN 342 describes how to examine garment or clothing ensembles with a "walking" manikin, while in ISO 15831, the thermal insulation of a clothing ensemble in both standing or moving conditions is investigated.

The reason for this large amount of available standards investigating thermal properties of textile layers and complete garments can be attributed to the number of possible distortions in the measurement. While in measurements of mechanical properties the complete experimental setup is usually easy to understand and the measurement procedure can easily be followed, measurements of thermal transmittance through fabrics enable a large number of possible errors to occur which cannot simply be noticed. Meta-studies have shown the deviations of different measurements performed on identical materials (Huang 2016). Performing tests strictly according to a standard is one possibility to allow for comparable measurement results.

Another possibility to reach the same goal is the exact description of all experimental conditions, an approach which is more often used in scientific literature. The next subchapter will thus give an overview of such nonstandardized measurement methods for investigation of the thermal transmittance through textile materials.

8.4   Other Measurements of Heat Transfer Through Textile Fabrics

Depending on the respective application, test conditions of thermal transmittance through textiles can be designed independently of the abovementioned standards.

Hassenboehler and Vigo (1982), e.g., designed an instrument measuring thermal transmittance through textiles in a mixed (laminar/turbulent) flow state of

convection. With the textile under examination placed between a large heated plate (at skin temperature) and a cold plate (slightly below room temperature) in a defined distance to both plates, not only heat transport but also moisture transport, relative humidity, and air temperature were measured in real time. Even more realistic was an experiment in which the thermal insulation of textile draperies was measured by placing the draperies under investigation in front of a window in a cold chamber and detecting the thermal transmission depending on humidity (Epps et al. 1984).

An optical method, using a spectrophotometer with an integrating sphere, was used to identify directional transmittance and hemispherical reflectance and transmittance and to calculate water content and thermal parameters of textile materials (Limare et al. 2003).

Heat transfer through silk cocoons was tested in an artificial air flow by Jin et al. (2015). The ventilation system was composed of a fan and a connected duct in whose center the cocoon was located. During the test, the temperatures were measured inside and outside the cocoon by needle-type temperature probes, while the wind speed was measured using a hot-wire anemometer.

A very naturalistic study design can be found in some projects dealing with real probands wearing garments and being monitored by different sensors (e.g., Kofler et al. 2013).

A completely different method is based on using a thermal imaging camera, often connected with simulations to avoid misinterpretations of the thermo-camera pictures. Puszkarz and Krucinska (2016), e.g., placed knitted double-layer fabrics from different materials on a flat plate held on skin temperature in a room with constant air temperature and humidity and measured the upper layer temperature by thermal imaging.

Figure 8.5 shows how this method works. Here, for better visualization, two fabrics were placed on a hand (instead of a hot plate of defined, constant temperature, as usual), and images were taken with a thermo-camera FLIR E8.

The temperature distribution on the surface of the textile fabrics is clearly visible; using the respective software, temperatures can in principle be read out for each single point. Nevertheless, it must be mentioned that optical temperature measurements require knowledge of the emissivity ε which can be assumed to be approximately 0.95 for human skin and several other surfaces but deviates strongly, e.g., for metal surfaces. Thus, before reliable measurements with a thermo-camera are possible, calibration by a contact-measurement method is necessary to avoid possible large errors.

Besides the above-described macroscopic measurements of thermal transmission, investigations on the nano- or microscale are possible by special atomic-force microscopes (AFMs). They may be used to investigate, e.g., heat transport along the fiber axis in comparison with other directions. These instruments, however, are usually not available in textile laboratories.

Fig. 8.5 Thermographic images, taken of a hand under a knitted (*upper panel*) or woven fabric (*lower panel*)
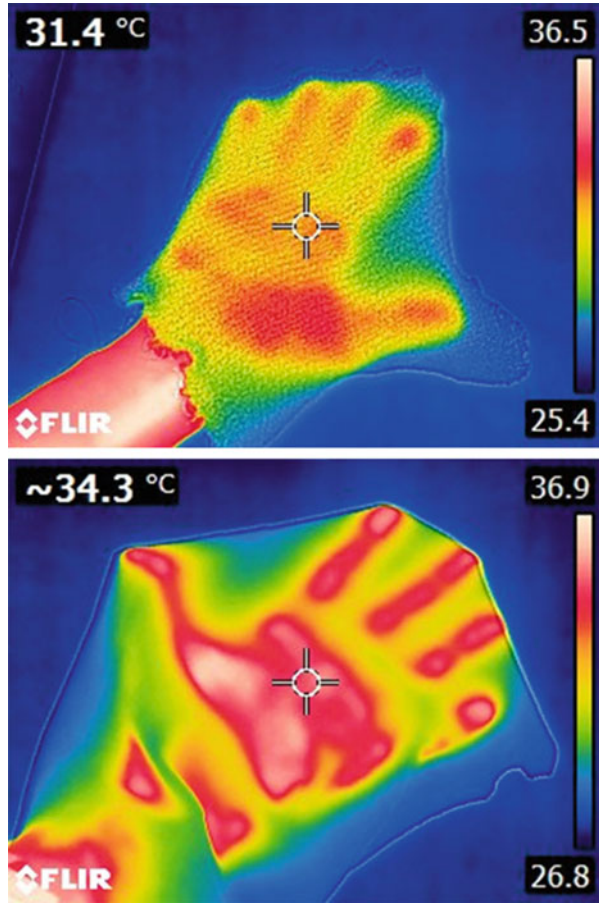
Literature

Abdel-Rehim, Z.S., Saad, M.M., El-Shakankery, M., Hanafy, I.: Textile fabrics as thermal insulators. AUTEX Res. J. **6**, 148–161 (2006)

Adam, E.A., Jones, P.J.: Thermophysical properties of stabilised soil building blocks. Build. Environ. **30**, 245–253 (1995)

Angelova, R.A., Reiners, P., Georgieva, E., Konova, H.P., Pruss, B., Kyosev, Y.: Heat and mass transfer through outerwear clothing for protection from cold: influence of geometrical, structural and mass characteristics of the textile layers. Text. Res. J. online first (2016)

Asdrubali, F., Baldinelli, G.: Thermal transmittance measurements with the hot box method: calibration, experimental procedures, and uncertainty analyses of three different approaches. Energy Buildings **43**, 1618–1626 (2011)

Bhattacharjee, D., Kothari, K.V.: Heat transfer through woven textiles. Int. J. Heat Mass Transf. **52**, 2155–2160 (2009)

Diswat, J., Hes, L., Bal, K.: Thermal resistance of cut pile hand tufted carpet and its prediction. Text. Res. J. online first (2016)

Epps, H.H., Goswami, B., Hassenboehler Jr., C.B.: The influence of indoor relative humidity and fabric properties on thermal transmittance of textile draperies. ASHRAE Trans. **90**, 104–115 (1984)

Hassenboehler Jr., C.B., Vigo, T.L.: A mixed flow thermal transmittance tester for textiles. Text. Res. J. **52**, 510–517 (1982)

Hes, L.: Non-destructive determination of comfort parameters during marketing of functional garments and clothing. Indian J. Fibre Text. Res. **33**, 239–245 (2008)

Hes, L., Araújo, D.M.: Effect of mutual bonding of textile layers on thermal insulation and thermal contact properties of fabric assemblies. Text. Res. J. **66**, 245–250 (1996)

Hes, L., Dolezal, I.: New method and equipment for measuring thermal properties of textiles. J. Text. Mach. Soc. Jpn. **42**, 124–128 (1989)

Hes, L., Stanek, J.: Theoretical and Experimental Analysis of Heat Conductivity for Nonwoven Fabrics. INDA-TEC Transactions, Philadelphia, PA (1989)

Hes, L., Kus, Z.: Non-destructive testing of thermophysiological properties of protective clothing. In: ECPC International Conference on Protective Clothing, Montreaux (2003)

Huang, J.: Review of heat and water vapor transfer through multilayer fabrics. Text. Res. J. **86**, 325–336 (2016)

Jin, X., Zhang, J., Hurren, C., Li, J., Rajkhowa, R., Wang, X.: The effect of fibrous structural difference on thermal insulation properties of biological composites: silkworm cocoons. Text. Res. J. online first (2015)

Kofler, P., Herten, A., Heinrich, D., Bottoni, G., Hasler, M., Faulhaber, M., Bechtold, T., Nachbauer, W., Burtscher, M.: Viscose as an alternative to aramid in workwear: influence on endurance performance, cooling, and comfort. Text. Res. J. **83**, 2085–2092 (2013)

Limare, A., Duvaut, T., Henry, J.F., Bissieux, C.: Non-contact photopyroelectric method applied to thermal and optical characterization of textiles. Four-flux modeling of a scattering sample. Int. J. Therm. Sci. **42**, 951–961 (2003)

Lizák, P., Mojumdar, S.C.: Thermal properties of textile fabrics. J. Therm. Anal. Calorim. **112**, 1095–1100 (2013)

Mangat, M.M., Hes, L., Bajzik, V.: Thermal resistance models of selected fabrics in wet state and their experimental verification. Text. Res. J. **85**, 200–210 (2015)

Morrissey, M.P., Rossi, R.M.: The effect of wind, body movement and garment adjustments on the effective thermal resistance of clothing with low and high air permeability insulation. Text. Res. J. **84**, 583–592 (2014)

Mumaw, J.R.: Calibrated hot box: an effective means for measuring thermal conductance in large wall sections. In: American Society for Testing and Materials, ASTM STP 544, Heat transmission measurements in thermal insulations, West Conshohocken, pp. 193–211 (1974)

Oğlakcioğlu, N., Marmarali, A.: Thermal comfort properties of some knitted structures. Fibres Text. East. Eur. **15**, 94–96 (2007)

Pola, T., Häkkinen, T., Hännikäinen, J., Vanhala, J.: Thermal performance analysis of 13 heat sink materials suitable for wearable electronics applications. Sci. Technol. **3**, 67–73 (2013)

Puszkarz, A.K., Krucinska, I.: The study of knitted fabric thermal insulation using thermography and finite volume method. Text. Res. J. online first (2016)

Ricciardi, P., Belloni, E., Cotana, F.: Innovative panels with recycled materials: thermal and acoustic performance and life cycle assessment. Appl. Energy **134**, 150–162 (2014)

Richards, M., Mattle, N.: A sweating agile thermal manikin (SAM) developed to test complete clothing systems under normal and extreme conditions, RTO-MP-076, pp. 1–7 (2001)

Romeli, D., Barigozzi, G., Esposito, S., Rosace, G., Salesi, G.: High sensitivity measurements of thermal properties of textile fabrics. Polym. Test. **32**, 1029–1036 (2013)

Uzun, M.: Processing and characterisation of the copper treated polylactic acid and cotton fabrics: thermophysiological comfort properties. Mater. Sci. **20**, 67–72 (2014)

Yang, C., Wang, J., Li, L.: A novel approach for developing high thermal conductive artificial leather by utilizing smart electronic materials. Text. Res. J. online first (2016)

Chapter 9
Hydrophobic and Hydrophilic Textiles

Textiles can be finished to gain certain properties, e.g., by dyestuff to reach a desired look, by flame retardant, and by antibacterial or antimicrobial coatings. One property which is addressed very often, not only in technical textiles but also for garments or home textiles, is the behavior of the fabric surface when exposed to water. In some cases, textiles should be hydrophobic (water repellent), while other applications require hydrophilic (hygroscopic) properties.

The hydrophobic or hydrophilic characteristics of textiles can be estimated easily; however, measuring them exactly is often hard. This chapter gives an overview of simple and specialized, commercially available measurement equipment allowing for evaluation of contact and roll-off angles as well as other methods to define the water-repellent properties of a textile surfaces. Additionally, a closer look will be taken at the problems arising from typical textile surface structures.

9.1 Hydrophobicity

The term "hydrophobic" is combined from the Greek words for "water" and "fear" and thus means "avoiding water." Hydrophobic substances do not mix with water; here, nonpolar substances such as waxes, alcohols with long alkyl radicals, alkanes, etc. should be mentioned, while alcohols with short alkyls – such as methanol, ethanol, or propanol – do not belong to the typical hydrophobic materials. Hydrophobicity is often combined with lipophilic (also known as oleophilic, i.e., highly soluble in fats and oils) properties; however, some substances are at the same time hydrophobic and lipophobic, such as fluorocarbons or silicones.

A typical measure of the hydrophobicity of a surface is the contact angle, as depicted in Fig. 9.1. For contact angles smaller than 90°, a material is referred to as hydrophilic, while hydrophobic surfaces have contact angles larger than 90°. With contact angles much higher than 90° (typically larger than 140°), a surface is called super-hydrophobic.

Fig. 9.1 The contact angle as a measure of the hydrophobicity of an even sample. Contact angles smaller/larger than 90° allow for defining the sample as hydrophilic/ hydrophobic
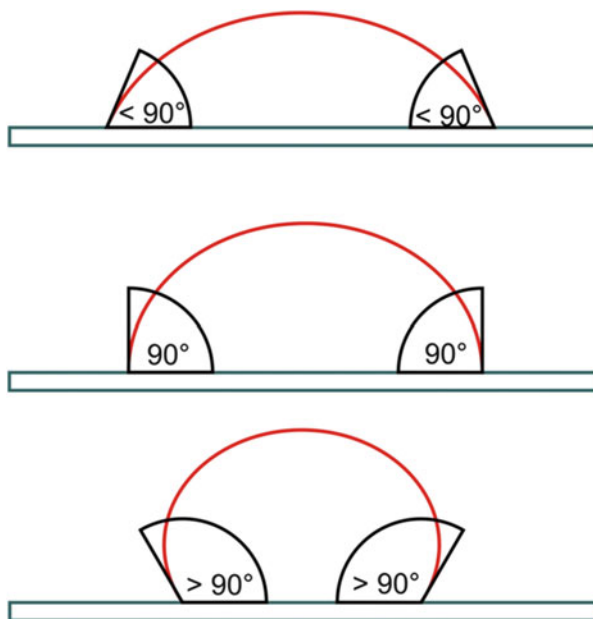
Super-hydrophobic surfaces can be found in nature, e.g., on lotus leafs – resulting in the name "lotus effect" according to the study of super-hydrophobic and self-cleaning properties (Barthlott and Ehler 1977; Barthlott and Neinhuis 2001) – and other less well-known plants, insects, etc. Due to the extremely reduced contact area between a droplet and the super-hydrophobic material, droplets rolling over a dirty surface will pick up dirt particles, resulting in a self-cleaning effect. This is of importance for plants as well as animals to prevent pollution of their surface by pathogens.

Rough technical surfaces with a hydrophobic coating can also result in super-hydrophobic surface properties (Johnson and Dettre 1964). As shown in several investigations (Guo et al. 2005; Mueller 2008; Solga et al. 2007), super-hydrophobicity and self-cleaning properties do not only stem from pure chemical characteristics but are supported by the surface roughness at microscopic to nanoscopic scales. This is why not only metals (Vorobyev and Guo 2015) but also textiles can be radiated by pulsed laser light to achieve a nanostructured surface supporting its hydrophobic properties (Samm et al. 2009a, b).

Hydrophilic surfaces, oppositely, can also be supportive for some applications. If a textile surface is dirty, it can be cleaned easier if water and other cleaning agents can penetrate deeper into the textile, i.e., if they are hydrophilic. The question whether a textile should be hydrophobic to avoid contamination or hydrophilic to allow for cleaning it after a contamination has occurred, depends on the exact area of application, e.g., where the textile is used, which sort of dirt can be expected to pollute it, etc.

A simple approach for the connection between surface tension and contact angle is given by the Young equation

$$\gamma_{SG} = \gamma_{SL} + \gamma_{LG} \cos\theta$$

with the surface tensions γ_{xy} between the three phases solid (S), liquid (L), and gas (G) as well as the contact angle θ (Young 1805). On real surfaces with a certain roughness, this equation has to be modified by introducing the receding and the advancing contact angle (Tadmor 2004) as well as the models of Wenzel and Cassie-Baxter, taking into account whether the "valleys" of a rough surface are wetted by the fluid or not (Marmur 2003; Whyman et al. 2008). In some cases, the line tension has additionally to be taken into account, too (Chen et al. 2012).

The different measurement methods which are commonly used in laboratories to examine the hydrophobicity or self-cleaning properties of textile fabrics are based on different principles and thus investigate partly varying parameters. In particular, static and dynamic methods probe partly different properties of the textile samples. Thus, the investigation method should be chosen with respect to the planned application.

9.2 Spray Test

The spray test is a simple method to get an impression of the hydrophobic properties of a textile. The spray test is described in AATCC 22-2005 and often examined since it only necessitates a simple and inexpensive setup (American Association of Textile Chemists and Colorists 2005). The spray test measures the water-repellent properties of a textile surface, i.e., the resistance to wetting by falling water. For this, water is sprayed onto a fabric under defined conditions, and the wetting pattern of the sample is optically evaluated. The results are not only influenced by a water-repellent coating but also by fiber and yarn as well as fabric construction.

The spray tester setup is depicted in Fig. 9.2. The sample under examination is fixed on the sample holder by a metal double ring under an angle of 45° to the horizontal plane. The test area has a diameter of 15.5 cm. Fifteen centimeters above the middle of the specimen, the middle of the spray nozzle can be found. The funnel on top must be able to collect at least 250 ml of distilled water. This amount of water is sprayed on the fabric through the nozzle in a time of 25–30 s if a water temperature of 27 °C is used. After the spray test, the specimen is taken from the test stand with the double ring which is tapped firmly against a solid object from both sides. Directly afterward, the wetting pattern is compared with a series of images given in AATCC 22-2005. In this way the sample under examination can be rated using values between 100 (no sticking or wetting of the textile surface) and 50 (complete wetting, also beyond the spray points) as well as 0 (complete wetting of the whole surface).

Fig. 9.2 Spray tester
according to AATCC
22-2005
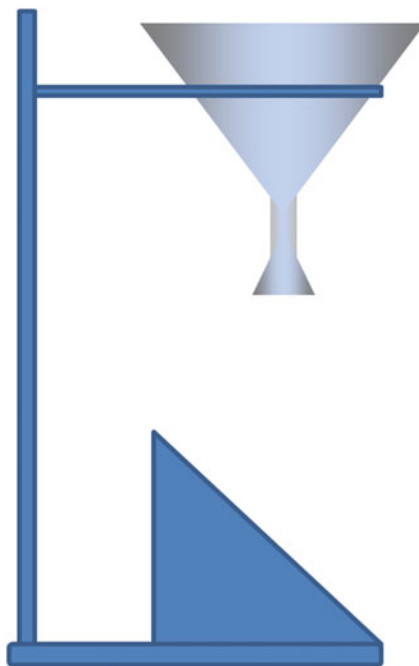
Since this evaluation procedure is necessarily subjective, the results may depend on the tester's experience with this method. Especially if many testers are included in a study, care must be taken to avoid a possible bias. This can be done by letting all involved people evaluate identical samples, either with comparing their individual results afterward or discussing their rating values during the evaluation process. In this way, differences in the rating can be leveled out before the actual samples are being evaluated.

It should be mentioned that although in the spray test the water falls down on the tested sample, resulting in a certain impact on it (opposite to the contact angle measurement in which a water drop is laid down on the surface), this test is not suggested to be used as a measure of the rain penetration. Instead, AATCC 35-2013 explicitly measures the penetration of water by impact (American Association of Textile Chemists and Colorists 2013), e.g., the rain penetration resistance. In this test, the amount of water leaking through a sample during 5 min of water spraying is measured.

Table 9.1 Rating of 3 M water drop test II

Grade	Distilled water/%	Isopropanol/%
W	100	0
1	90	10
2	80	20
3	70	30
4	60	40
5	50	50
6	40	60
7	30	70
8	20	80
9	10	90
10	0	100

9.3 Drop Test

Another typical test of the water repellency of textile fabrics was developed by 3 M and is known as "water drop test II" or "water/alcohol drop test." This method tests the resistance of textiles after a water-repellent finishing against water stains.

Samples of at least 20 cm × 20 cm are laid flat on a table. Drops of different fluids (cf. Table 9.1) with a diameter of approximately 5 mm are laid on three positions of the sample which differ about more than 5 cm. The drops are inspected for 10 s. Each step of the test procedure is passed if two of the three drops are still visible after 10 s.

The test procedure starts with pure distilled water and ends with pure isopropanol (cf. Table 9.1). The grade of the highest passed test step is given in the test report.

The idea behind this test is that isopropanol has a significantly smaller surface energy (~21.3 mN/m for isopropanol, ~72.7 mN/m for water at 20 °C) and can thus easier penetrate into a hydrophobic textile, as can be recognized from the Young equation.

However, this test, although regularly referred to as "water drop test," is indeed a "water/alcohol drop test," as its name mentions. In some cases, the drop test values may result in a different rating than other methods which are based on pure water.

9.4 Contact Angle Measurements

Principally measuring the contact angle, as depicted in Fig. 9.1, gives a good estimation of the hydrophobicity and water repellency of textile fabrics. This is why the contact angle is often used in the literature to define the quality of hydrophobic or hydrophilic coatings and finishings (e.g., Lim et al. 2016; Rahimi et al. 2016; Przybylak et al. 2016).

Several commercial contact angle measurement devices can be bought to carry out contact angle measurements on smooth surfaces. Other instruments are explicitly constructed for the measurement of contact angles on textile fabrics, e.g., by Krüss (2016) or DataPhysics (2016).

Contact angle measurement instruments work as follows: In the static case, a droplet of defined volume is laid down on a surface. A digital camera is used to take a photograph from the side, i.e., parallel to the surface under examination. This image is evaluated by image processing techniques to obtain the contact angle.

While this procedure is simple in theory, the reality of measuring contact angles on textile fabrics has some challenges. Opposite to measurements on flat surfaces, such as metals, plastics, etc., the contact angle on a textile surface is not even well defined, not to mention the practical problems during measuring.

Since textile surfaces normally exhibit a macroscopic roughness due to their woven or knitted structure, protruding fibers of hairy fabrics, etc., defining the baseline is not easy. Often this baseline will differ for both sides of the drop, as depicted in Fig. 9.3. The image is taken under an angle of 60° with respect to the surface normal (instead of 90° as usual in contact angle measurements) to ensure that the contact points are clearly visible and not hidden in the textile. The "contact angles" taken from these images are thus different from the actual contact angles.

Next, differences may occur between microscopic and macroscopic contact angle due to the surface roughness (Drelich et al. 1996). This issue is depicted in Fig. 9.4.

The image shows exactly the same situation as Fig. 9.3; only the magnification is increased. In Fig. 9.3, the "contact angles" are measured by fitting an ellipse to the droplet and a line to the contact line between droplet and textile surface. In Fig. 9.4, the real "edge" which becomes visible now is used to determine the "contact angle." Comparing both values (black angles in both pictures), they differ strongly (143° for the macroscopic angle in Fig. 9.3, 128° for the microscopic angle in Fig. 9.4). Apparently macroscopic and microscopic contact angles are different.

Fig. 9.3 Contact angle measurement of a droplet on a textile surface. From Fiedler and Ehrmann (2015)
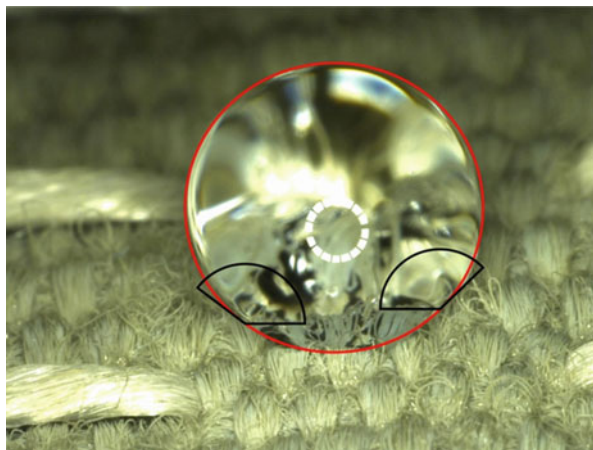
Fig. 9.4 Contact angle measurement of the same droplet as in this figure, image taken with higher magnification. From Fiedler and Ehrmann (2015)
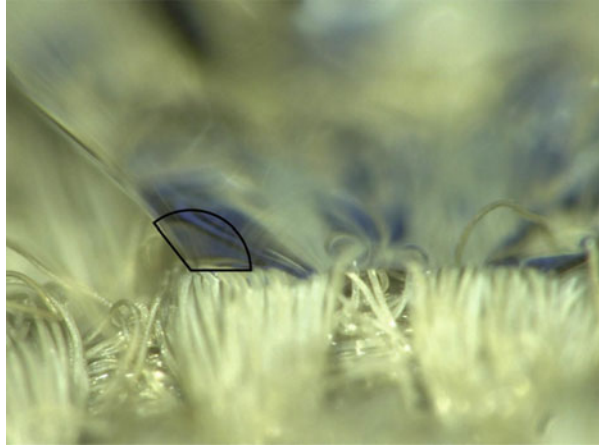
This effect is visible using simple manual fitting of lines and ellipses to the images, while image processing techniques will normally not allow the user to get an insight into these possibly problematic decisions during contact angle evaluation.

The next problematic effect is also correlated with the surface roughness. The contact angle is defined as the angle built between the liquid/vapor interface and the liquid/solid interface. To be measured, it is necessary that both interfaces are visible at the "triple point" where all three phases (solid, liquid, and vapor) touch each other. On the other hand, the contact angle is defined for images taken parallel to the fabric, i.e., under an angle of 90° to the surface normal. For rough surfaces, such as woven or knitted fabrics, both conditions are contradictory.

Figure 9.5 shows a series of images, taken from the same droplet on a woven fabric under different angles to the surface normal.

Apparently, for an angle of 88° to the surface normal, the contact line between droplet and textile fabric is not completely visible, so that the position of the baseline cannot be estimated. In the picture taken under an angle of 85°, the front of the droplet reveals first contact areas. Going to even higher positions of the camera, the angle of 82° allows for seeing more parts of the contact line between droplet and textile. Finally, at an angle of 77°, the contact areas on both sides of the water droplet become visible.

As can be recognized from this series of images, contact angle pictures of droplets on textile surfaces can easily be misinterpreted. If the contact line is not completely visible, the contact angle will be underestimated. This effect results in contact angle measurements on textiles, especially with commercially available equipment without the possibility to adjust the angle between camera and surface normal, being significantly error prone.

Finally, this problem can be increased by single fibers protruding from the textile fabric, as depicted in Fig. 9.6. The contact lines between textile and droplet as well as between droplet and air are strongly distorted by such fibers. Former experiments have shown the significant influence of the interactions between liquid and solid
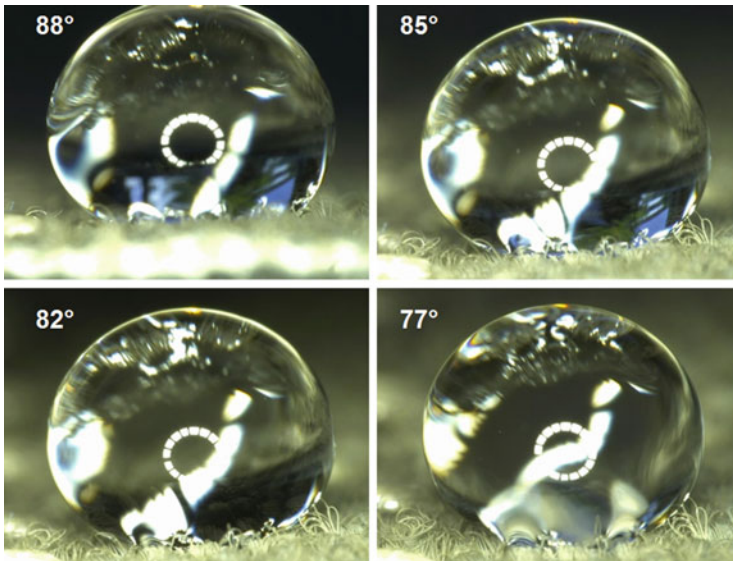
Fig. 9.5 Contact angle measurement of a droplet on a woven surface, using different angles to the surface normal (cf. insets). From Fiedler and Ehrmann (2015)
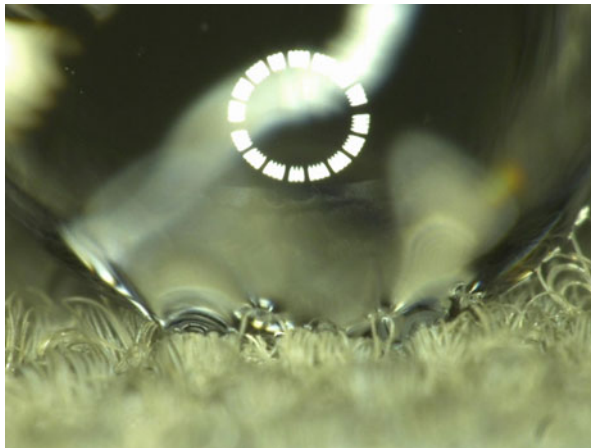
Fig. 9.6 Contact line between water and textile. Image taken under an angle of 77° to the surface normal. From Fiedler and Ehrmann (2015)

along the three-phase contact line, while inhomogeneities of the interfacial area inside the drop can be ignored (Gao and McCarthy 2007). Depending on the position of the fibers, the microscopic contact angles vary strongly.

This effect may be negligible for textiles with relatively even surfaces, created from yarns which are not too hairy. However, it can also be enhanced for measurements on knitted fabrics, textiles with broken fibers after Martindale tests, very

hairy fabrics, etc. This problem has to be taken into account, too, when contact angles on textile surfaces are to be measured.

Due to the large number of attempts to create hydrophobic or hydrophilic textile fabrics by coating wool (Mura et al. 2015), nylon (Du et al. 2015), cotton, polyester (Periolatto and Ferrero 2015), or leather (Türk et al. 2015), using either chemical, physical, or combined surface modifications (Molina et al. 2015; Popescu et al. 2014; Samm et al. 2009a, b), several theoretical approaches deal with reliably measuring contact angles on textile and other rough surfaces.

Contact angles on rough surfaces were modeled by introducing the surface roughness into the Young equation (Bico et al. 2002) or by extending the Wenzel and Cassie-Baxter formulas to multi-equilibrium drop shapes (Patankar 2003). For geometrically inhomogeneous substrates, a more generalized form of the Young equation was developed (Swain and Lipowsky 1998). Other calculations concluded that if the line tension (i.e., the excess energy per unit length of the three-phase contact line) must not be ignored, the microscopic contact angles on rough surfaces differ from those given by the Young equation (Wolansky and Marmur 1998).

Alternatively, an experimental approach is given in the form of the captive-bubble technique, measuring the contact angles of an air bubble in water under a textile surface, instead of the usual sessile-drop technique, using water on a textile surface (Drelich et al. 1996). Opposite to the usual technology, however, this technique necessitates a more complex and thus more expensive setup and can thus not be used in all cases.

To conclude, while contact angle measurements are in principle easy to perform experimentally, care must be taken to do these measurements in a reliable way. Very often, simple pictures taken with a microscope allow for evaluating the three-phase contact line easier than commercial systems which can be less flexible, if they are not specialized for rough textile surfaces. After several measurements on different textile substrates, the evaluators' experience will enable them to distinguish between trustable measurement values and others. Performed with the necessary diligence, contact angle measurements can be a very helpful tool to distinguish between different hydrophobicity qualities or to evaluate the process of change of the hydrophobicity of a sample.

Finally, it should be mentioned that in this subchapter, only the static contact angle was discussed. Dynamic contact angle measurements, giving rise to the advancing and receding contact angles, are introduced in the next subchapter.

9.5   Dynamic Measurements: Contact Angles and Roll-Off Angle

The roll-off angle of a textile fabric is defined as the smallest inclination angle at which a drop rolls off the sample. It is especially used for super-hydrophobic surfaces but can also be an interesting tool in other cases.

Fig. 9.7 Advancing (*upper panel*) and receding (*lower panel*) contact angles
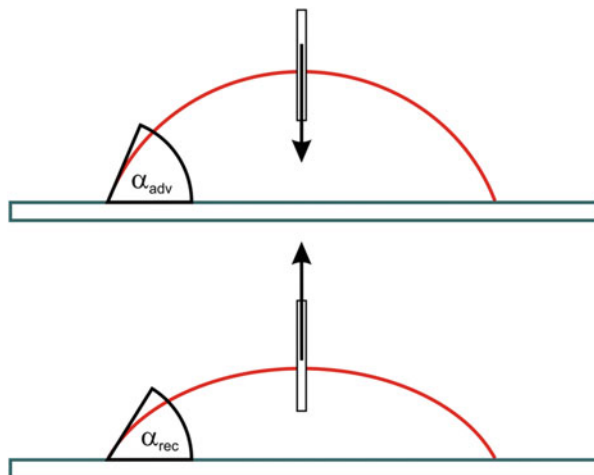
The roll-off angle is furthermore proportional to the contact angle hysteresis (Dussan and Chow 1983). This hysteresis describes the difference between contact angles of advancing and receding droplets. It is usually attributed to surface roughness and/or chemical inhomogeneities and stems from a pinning of the three-phase contact line. When the droplet volume is increased or decreased, the contact line tries to stick at the previous position, until it finally has to slip to a new position. This process is repeated again and again as long as the droplet volume is changed (Shanahan 1995).

Sticking of the contact line on a certain position of the surface results from energetic minima due to physical and chemical inhomogeneities and the respective neighboring energy maxima which have to be overcome to allow for the contact line slipping (Johnson and Dettre 1964; Collet et al. 1997). The contact angle hysteresis thus depends on these energy barriers (Chen et al. 1991).

One possibility to measure advancing and receding contact angles is given by a static measurement method which is depicted in Fig. 9.7. Water volume is either added to (upper panel) or subtracted from a static droplet (lower panel) using a small syringe or a micropipette. In this way, the advancing and receding contact angle can be measured, respectively.

Alternatively, the fabric can be tilted, similar to a roll-off angle measurement (Fig. 9.8). In the moment directly before the drop starts moving, the advancing and receding contact angles are measured taking a photograph and extracting both angles from it, as depicted in Fig. 9.8.

Both methods do not give perfectly identical results (ElSherbini and Jacobi 2006) but can nevertheless be used to compare samples within a test series. Oppositely, roll-off angles can easily be measured using a common (digital) angle meter with a broad enough upper surface to fix the textile under examination on it.

Similar to the friction coefficient describing the interaction between contacting solid objects, a so-called pinning parameter can be defined for the description of wetting behavior on a solid-liquid interface which is proportional to the contact angle hysteresis (Varanasi et al. 2008).

Fig. 9.8 Advancing and
receding contact angles on a
tilted surface, measured in
the moment before the drop
rolls off the fabric
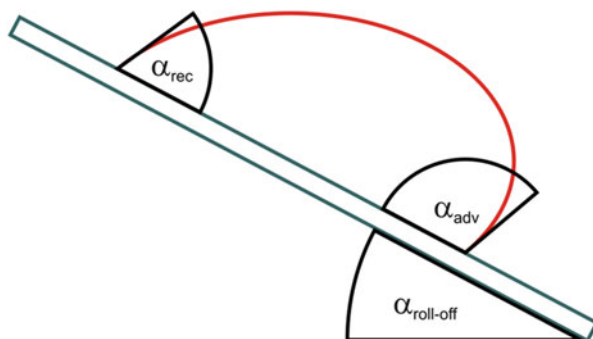
9.6   Comparison Between Different Hydrophobicity Measures

Since the above-described test methods measure hydrophobicity in different ways,
the results will also differ, and the influence of the fabric under examination and of
washing or abrasion tests will be of different significance.

Figure 9.9 depicts a test series of ten washing cycles, performed by colored
washing at 40 °C with spin cycles of 1400 min^{-1}. After each washing cycle, the
sample was refreshed in a drying oven at 130 °C for 30 s.

To create hydrophobic surfaces, woven polyester samples were treated with the
sol-gel product Sogetec 047 by Comp-tex (Düren, Germany), based on amine-
modified polysiloxanes and fluorinated polyacrylates, which was applied to the
samples using a foulard and dried at 130 °C. This coating has been shown to
produce ideal hydrophobic and oleophobic behavior on polyester samples (Torre
et al. 2007; Samm et al. 2009a, b).

The spray rating of this test series, depicted in the upper panel, shows a
significant decrease of the hydrophobicity. Although being a subjective test, the
error bars are relatively small due to three samples having been tested after each
number of washing cycles.

The water/alcohol drop test (second panel) depicts the same trend, although the
curve is less smooth, and the error bars are slightly higher. It should be mentioned
that while in both cases the graphs show the complete range of possible values on
the y-axis, in the spray rating, no values between 50 and 0 exist, which makes the
decrease of the spray rating relatively smaller than the decrease in water/alcohol
drop test rating.

The contact angle, depicted in the third panel, shows again decreased error bars
but connected with a strongly decreased range of values taken during these tests.

While the contact angle also shows a clear trend of decreasing values, the change
during the washing tests is so small that it cannot be regarded as significant.

Finally, the fourth panel depicts the roll-off angle measured during this test
series. While a clear trend is visible again, the difference between first and last
values is not significant, too.

This comparison shows that sometimes the simple subjective methods provide more information about changes of a sample during a test series or about differences between diverse samples. However, the choice of the best measurement techniques must take into account that all of them evaluate slightly different situations, as well as the other test procedures which have not been described here in detail.

In some cases, these test methods even seem to produce contradictory results, e.g., in case of the so-called sticky hydrophobicity, describing (super) hydrophobic surfaces with large contact angle hysteresis and correspondingly large roll-off angles which may even be above 90°, i.e., water droplets stick to the fabrics even with the surface being turned upside down (Wang and Weiss 2012; Bakli and Chakraborty 2015).
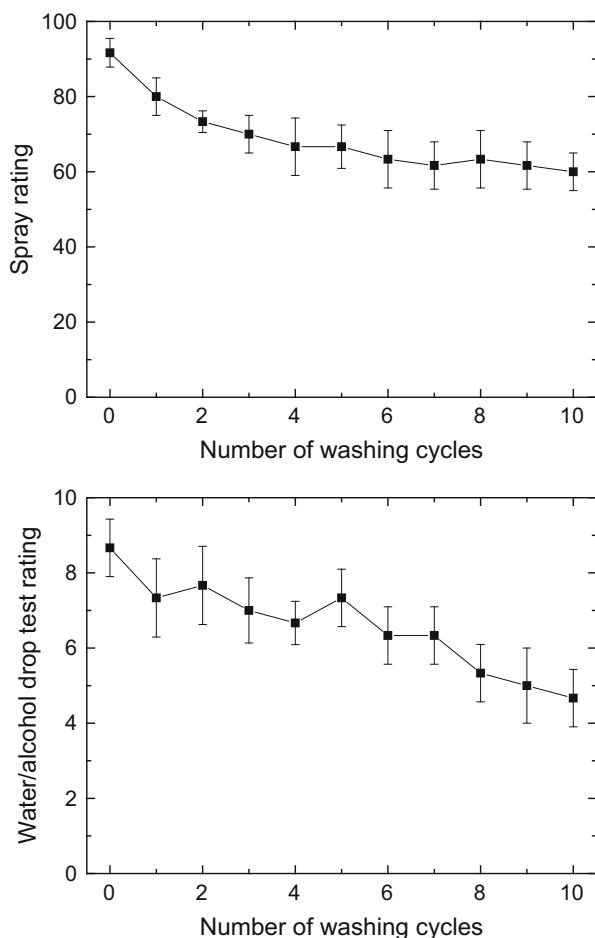
Fig. 9.9 Spray rating, water/alcohol drop test rating, contact angle, and roll-off angle, measured for ten washing cycles on woven polyester samples with hydrophobic finishing
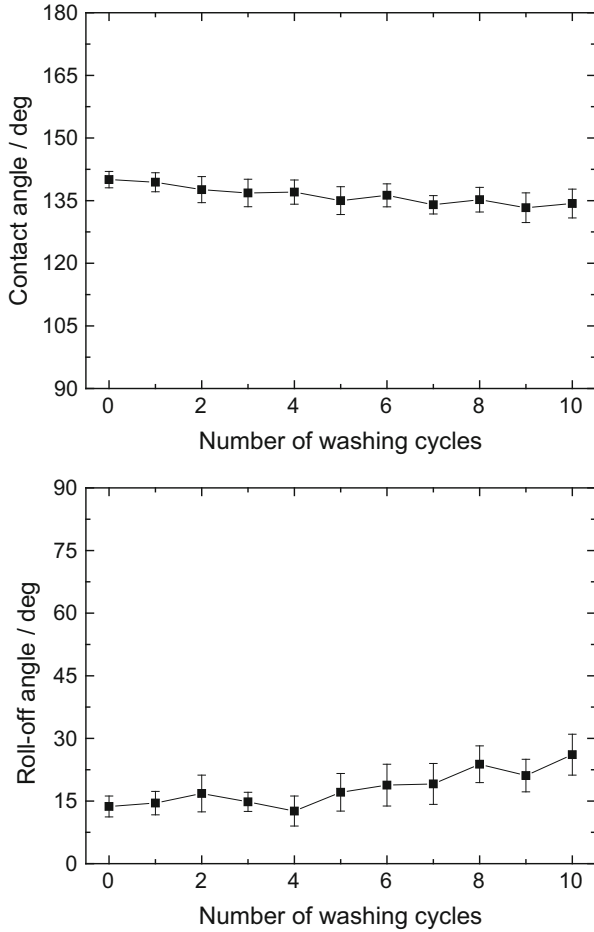
Fig. 9.9 (continued)

Literature

American Association of Textile Chemists and Colorists: Water Repellency: Spray Test. AATCC Test Method 22-2005 (2005)

American Association of Textile Chemists and Colorists: Water Resistance: Rain Test. AATCC Test Method 35-2013 (2013)

Bakli, C., Chakraborty, S.: Slippery to sticky transition of hydrophobic nanochannels. Nano Lett. **15**, 7497–7502 (2015)

Barthlott, W., Ehler, N.: Raster-Elektronenmikroskopie der Epidermis-Oberflächen von Spermatophyten. Akademie der Wiss. u. d. Literatur, Mainz (1977)

Barthlott, W., Neinhuis, C.: The lotus-effect: nature's model for self cleaning surfaces. Int. Text. Bull. **1**, 8–12 (2001)

Bico, J., Thiele, U., Quéré, D.: Wetting of textured surfaces. Colloids Surf. A Physicochem. Eng. Asp. **206**, 41–46 (2002)

Chen, Y.L., Helm, C.A., Israelachvili, J.N.: Molecular mechanisms associated with adhesion and contact angle hysteresis of monolayer surfaces. J. Phys. Chem. **95**, 10736–10747 (1991)

Chen, X., Ma, R., Li, J., Hao, C., Guo, W., Luk, B.L., Li, S.C., Yao, S., Wang, Z.: The evaporation of droplets on superhydrophobic surfaces: surface roughness and small droplet size effects. Phys. Rev. Lett. **109**, 116101 (2012)

Collet, P., De Coninck, J., Dunlop, F., Regnard, A.: Dynamics of the contact line: contact angle hysteresis. Phys. Rev. Lett. **79**, 3704 (1997)

dataphysics – Understanding Interfaces: Products. http://www.dataphysics.de/2/start/products/contact-angle-measuring-and-contour-analysis-systems/. Accessed 6 Aug 2016

Drelich, J., Miller, J.D., Good, R.J.: The effect of drop (Bubble) size on advancing and receding contact angles for heterogeneous and rough solid surfaces as observed with sessile-drop and captive-bubble techniques. J. Colloid Interface Sci. **179**, 37–50 (1996)

Du, J.M., Luo, X.F., Fu, Z., Xu, C.H., Ren, X.H., Gao, W.D., Li, Y.: Improving the hydrophobicity of nylon fabric by consecutive treatment with poly(acrylic acid), tetraethylorthosilicate, and octadecylamine. J. Appl. Polym. Sci. **132**, UNSP 42456 (2015)

Dussan, E.B., Chow, R.T.P.: On the ability of drops or bubbles to stick on non-horizontal surfaces of solids. J. Fluid Mech. **137**, 1–29 (1983)

ElSherbini, A.I., Jacobi, A.M.: Retention forces and contact angles for critical liquid drops on non-horizontal surfaces. J. Colloid Interface Sci. **299**, 841–849 (2006)

Fiedler, J., Ehrmann, A.: Influence of surface micro- and macro-structure on measured and real contact angles. In: Proceedings of Aachen-Dresden International Textile Conference, Aachen, 26–27 Nov 2015

Gao, L., McCarthy, T.J.: How Wenzel and Cassie were wrong. Langmuir **34**, 3762–3765 (2007)

Guo, Z., Zhou, F., Hao, J., Liu, W.: Stable biomimetic super-hydrophobic engineering materials. J. Am. Chem. Soc. **127**, 15670–15671 (2005)

Johnson Jr., R.E., Dettre, R.H.: Contact angle hysteresis. III. Study of an idealized heterogeneous surface. J. Phys. Chem. **68**, 1744–1750 (1964)

Krüss – Advancing your Surface Science: Drop Shape Analysis. http://www.kruss.de/services/education-theory/glossary/drop-shape-analysis/. Accessed 6 Aug 2016

Lim, J., Powell, N., Lee, H., Michielsen, S.: Integration of yarn compression in modeling structural geometry of liquid resistant-repellent fabric surfaces and its impact on liquid behavior. J. Mater. Sci. **51**, 7199–7210 (2016)

Marmur, A.: Wetting of hydrophobic rough surfaces: to be heterogeneous or not to be. Langmuir **19**, 8343–8348 (2003)

Molina, J., Fernandez, J., Fernandes, M., Souto, A.P., Esteves, M.F., Bonastre, J., Cases, F.: Plasma treatment of polyester fabrics to increase the adhesion of reduced graphene oxide. Synth. Met. **202**, 110–122 (2015)

Mueller, T.: Biomimetics, design by nature. Nat. Geo. Mag. **68** (2008)

Mura, S., Greppi, G., Malfatti, L., Lasio, B., Sanna, V., Mura, M.E., Marceddu, S., Luglie, A.: Multifunctionalization of wool fabrics through nanoparticles: a chemical route towards smart textiles. J. Colloid Interface Sci. **456**, 85–92 (2015)

Patankar, N.A.: On the modeling of hydrophobic contact angles on rough surfaces. Langmuir **19**, 1249–1253 (2003)

Periolatto, M., Ferrero, F.: Cotton and polyester surface modification by methacrylic silane and fluorinated alkoxysilane via sol-gel and UV-curing coupled process. Surf. Coat. Technol. **271**, 165–173 (2015)

Popescu, V., Sandu, I., Muresan, E.I., Istrate, B., Lisa, G.: Effects of the pre-treatment with atmospheric-air plasma followed by conventional finishing. Rev. Chim. **65**, 676–683 (2014)

Przybylak, M., Maciejewski, H., Dutkiewicz, A., Dabek, I., Nowicki, M.: Fabrication of superhydrophobic cotton fabrics by a simple chemical modification. Cellulose **23**, 2185–2197 (2016)

Rahimi, M., Zinadini, S., Zinatizadeh, A.A., Vatanpour, V., Rajabi, L., Rahimi, Z.: Hydrophilic goethite nanoparticle as a novel antifouling agent in fabrication of nanocomposite polyethersulfone membrane. J. Appl. Polym. Sci. **133**, 43592 (2016)

Samm, K., Kling, R., Korger, M., Tillmanns, A., Janssen, E.: Functionalising of textile surfaces with a combination of laser treatment and sol-gel coating. In: Proceedings of the euspen International Conference, San Sebastian (2009a)

Samm, K., Hustedt, M., Stein, J., Klug, U., Korger, M., Tillmanns, A., Janssen, E.: Potential applications of lasers in the textile industry. In: Proceedings of the 3rd Aachen-Dresden International Textile Conference, Aachen 26–27 Nov (2009b)

Shanahan, M.E.R.: Simple theory of "stick-slip" wetting hysteresis. Langmuir **11**, 1041–1043 (1995)

Solga, A., Cerman, Z., Striffler, B.F., Spaeth, M., Barthlott, W.: The dream of staying clean: lotus and biomimetic surfaces. Bioinspir. Biomim. **2**, 1–9 (2007)

Swain, P.S., Lipowsky, R.: Contact angles on heterogeneous surfaces: a new look at Cassie's and Wenzel's laws. Langmuir **14**, 6772–6780 (1998)

Tadmor, R.: Line energy and the relation between advancing, receding and young contact angles. Langmuir **20**, 7659–7664 (2004)

Torre, C., Rabe, M., Janssen, E.: Superhydrophobe und superhydrophile textile Oberflächen. Textilveredlung 7/8 (2007)

Türk, M., Ehrmann, A., Mahltig, B.: Water-, oil-, and soil-repellent treatment of textiles, artificial leather, and leather. J. Text. Inst. **106**, 611–620 (2015)

Varanasi, K.K., Deng, T., Hsu, M.F., Bhate, N.: Design of superhydrophobic surfaces for optimum roll-off and droplet impact resistance. ASME Int. Mech. Eng. Cong. Expo. **13**, 637–645 (2008)

Vorobyev, A.Y., Guo, C.: Multifunctional surfaces produced by femtosecond laser pulses. J. Appl. Phys. **117**, 033103 (2015)

Wang, X., Weiss, R.A.: A facile method for preparing sticky, hydrophobic polymer surfaces. Langmuir **28**, 3298–3305 (2012)

Whyman, G., Bormashenko, E., Stein, T.: The rigorous derivation of Young, Cassie–Baxter and Wenzel equations and the analysis of the contact angle hysteresis phenomenon. Chem. Phys. Lett. **450**, 355–359 (2008)

Wolansky, G., Marmur, A.: The actual contact angle on a heterogeneous rough surface in three dimensions. Langmuir **14**, 5292–5297 (1998)

Young, T.: An essay on the cohesion of fluids. Philos. Trans. R. Soc. Lond. **95**, 65–87 (1805)

Chapter 10
Mechanical Properties of Yarns, Fabrics, and Coatings

Mechanical properties of textiles are fundamental to be known for practical reasons. Mechanical properties include elastic properties which are most often used for descriptions of textiles, but also bending stiffness, drapability, etc. Elasticity is quite a general term. It is linked with the more precise terms of strain and stress. Stress can be unidirectional or multidirectional. The response on stress is strain. This response can be linear (reversible) or nonlinear (nonreversible). The strains are associated with deformations. If the stress is small, then the deformation is small, or in other words, the situation is reversible. Deformations can be normal (tensional), shear (tangential), and torsional (twisted). The Poisson's ratio is a fundamental metric for elastic properties, giving rise to normal and unusual reaction of a fabric on strain, the latter being known as auxetic fabrics. This chapter gives an overview of different mechanical properties of textiles and possibilities to measure them.

10.1 What Is the Reason for Elasticity?

Even if elasticity seems to be an everyday effect associated with our activity, it has, however, a molecular origin. Elastic properties result from electromagnetic interactions between individual atoms and molecules inside materials. In Fig. 10.1, a single fiber stretching due to externally applied axial forces is shown from this perspective. The number of molecular connections is obviously proportional to the cross section S. The cross section is an easily measurable quantity, while the number of the connections can be estimated from material parameters, such as density or molar mass. Namely, the volume concentration n of atoms in a given material can be calculated from the following expression:

Fig. 10.1 The axial
deflection Δl is cross-
sectional dependent due to
the existence of molecular
forces of electromagnetic
nature. Hence, $\Delta l \sim 1/S$
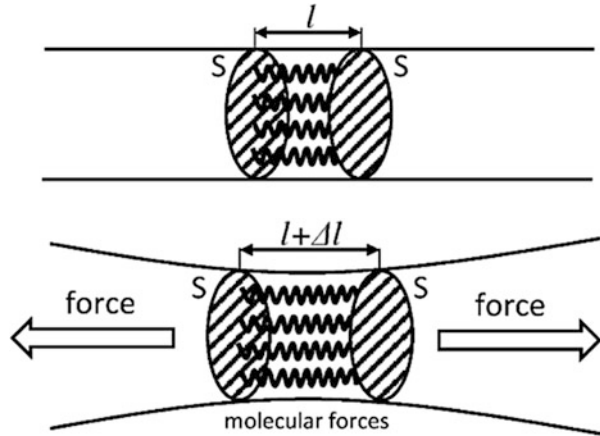
$$n = \frac{N}{V} = \frac{N\,m}{m\,V} = \frac{N\rho}{m} = \frac{N_A\rho}{\mu},$$

where N is the total number of atoms in a sample (in practice an unmeasurable
quantity), ρ is the material density, m is the sample mass, and μ is the mass of a
single mole (which can easily be found in chemical tables), while $N/m = N_A/\mu$, since
N_A is the Avogadro constant (6.022×10^{23} mol^{-1}) counting the number of atoms or
molecules in a single mole.

Since for an isotropic substance all directions are the same, i.e.,

$$n = n_x n_y n_z = \left(\frac{N_A\rho}{\mu}\right)^{1/3} \left(\frac{N_A\rho}{\mu}\right)^{1/3} \left(\frac{N_A\rho}{\mu}\right)^{1/3},$$

the aerial part of the above expression, being a measure of the surface density of
intermolecular connections, is equal to

$$n_S = n_x n_y = \left(\frac{N_A\rho}{\mu}\right)^{2/3}.$$

The above quantity is of the order 10^{19} molecules/m^2 for many substances.

In practical laboratory and industrial situations, the measurable quantity is not
the number of atomic connections per area, but the externally applied force F per
area S. The ratio F/S is named stress and usually marked by the Greek letter σ. The
stress causes an elongation of the object on which it is applied.

Robert Hooke, an English scientist, in the seventeenth century properly formu-
lated the fundamental mechanical law that the elongation is proportional to the
applied force.

The recent commonly used version of the Hooke's law interconnects the stress
with the relative change of the initial length l_o

Fig. 10.2 The linear part of
the stress and strain relation
constitutes Hooke's law.
Above the proportional
limit stress, the relation is
nonlinear, and the
maximum possible stress
(ultimate) determines the
tensile strength of the
sample
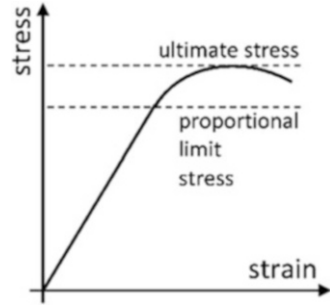
Fig. 10.3 The longitudinal
deformation in the
x direction is accompanied
by a compression effect in
the perpendicular
y direction
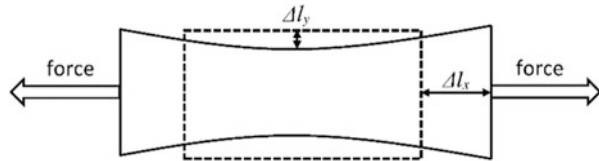
$$\frac{F}{S} = E\frac{\Delta l}{l_o}.$$

The relative change of length $\varepsilon = \Delta l / l_o$ is called strain, while the proportionality constant E is the Young modulus expressed in units of pressure (1 Pa $= 1$ N/m^2).

The proportionality $\sigma = E\varepsilon$ is not unlimited. Above a certain value of the strain, the relation can become nonlinear, and the elongation process is no longer reversible (Fig. 10.2).

The occurrence of a strain is very rarely a one-dimensional effect. A longitudinal deformation in one direction usually causes lateral compression in the other one (Fig. 10.3).

The above property can be quantitatively expressed as a ratio of the lateral $\varepsilon_{\text{lateral}}$ to the axial $\varepsilon_{\text{axial}}$ strains, namely,

$$\nu = -\frac{\varepsilon_{\text{lateral}}}{\varepsilon_{\text{axial}}}.$$

This is the Poisson's ratio, a fundamental quantity for all elastic phenomena (Sun et al. 2005; Ajeli and Jeddi 2014). The minus sign underlines the fact that axial elongations usually stand in contradiction to lateral ones.

The same can be expressed more precisely for the three-dimensional case, based on the linear Hooke's relation. Thus, the strain along the *x*-axis is reduced due to the negative strain along the *y*-axis, and vice versa the strain along the *y*-axis is reduced due to the reversed strain along the *x*-axis. Accurate relations are as follows:

$$\varepsilon_x = \frac{\sigma_x}{E} - \nu\frac{\sigma_y}{E}, \ \text{ and } \ \varepsilon_y = \frac{\sigma_y}{E} - \nu\frac{\sigma_x}{E}.$$

What is even more interesting, for a thin piece of material, the common in-plane elongations along x and y directions cause strain in the perpendicular-to-plane directions, namely,

$$\varepsilon_z = -\nu\frac{\sigma_x}{E} - \nu\frac{\sigma_y}{E},$$

and the same can be written down in the more simplified form of $\varepsilon_z = -\nu\,\varepsilon_{xy}$, where the combined strain equals $\varepsilon_{xy} = (\sigma_x + \sigma_y)/E$. To underline the generality of the Poisson's ratio, it is worth mentioning that the ratio was measured even for paper (Szewczyk 2008).

In order to keep a more general perspective of elastic phenomena, in the next paragraphs, three more commonly used elastic parameters will be introduced. These are the bulk modulus K, the shear modulus G, and the torsional stiffness of fibers being proportional to the G modulus.

The bulk modulus measures the volumetric effect of bulk compression or decompression under the influence of a pressure p. The formal definition of K is

$$K = -\frac{p}{\Delta V/V},$$

where the minus sign results from that fact that under an externally applied pressure ($p > 0$) a typical body decreases its volume, thus $\Delta V < 0$, while the K modulus is a material parameter and defined to be positive. For linear-elastic and isotropic materials, this equation can be transferred into

$$K = \frac{E}{3(1 - 2\nu)}.$$

Thus the bulk modulus K can be calculated from the Young modulus E and the Poisson's ratio ν. The bulk modulus is not so important for typical textile materials which consist of thin fibers and yarns and usually form one-dimensional or two-dimensional structures.

The notion of the shear modulus requires more explanation. The idea of a shear stress and subsequent deformation is explained in Fig. 10.4. Obviously, it has molecular origin; however, the process of deformation is now different from normal elongation. In case of shear stress, a pair of forces is imposed tangentially to the external sample planes.

Thus, the planes are shifted causing a tilt which can be described by an angle β. As can be seen in Fig. 10.4, the thickness h is kept constant, while the upper layer is shifted by Δl, and the shear angle (shear strain) can be expressed by the tangent, i.e., $\tan\beta = \Delta l/h$, while in practice, the angle is very small and $\tan\beta \approx \beta = \Delta l/h$.

Fig. 10.4 The molecular origin of the shear effect (*upper panel*) and the shear strain measured by the ratio of upper layer shift to sample thickness, $\beta = \Delta l / h$ (*lower panel*)
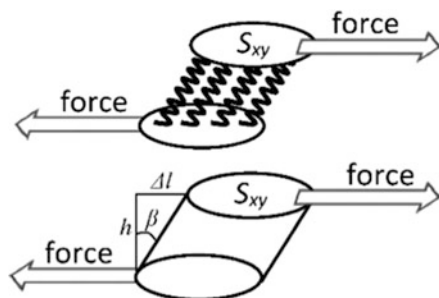
The usage of the angle β is very rational, since this angle is directly proportional to the shear stress τ, understood as the ratio of the force to the sheared surface $\tau = F/S_{xy}$, i.e.,

$$\tau = G\beta.$$

The constant G is the shear modulus. Interestingly, the relation between shear stress and shear strain is very similar to Hooke's law, namely,

$$G = \frac{E}{2\,(1+\nu)}.$$

Modeling and analysis of the shear strain of woven fabrics is quite a challenging task due to the spatial complexity of real textile samples (Sun and Pan 2005).

The aforementioned relations between bulk modulus, shear modulus, and the Poisson's ratio enable general classification of elastic materials (Fig. 10.5). Plain woven fabrics have Poisson's ratios in the range of 0.2–0.6. Rubber has a Poisson's ratio around 0.5 and thus no defined bulk modulus. Another interesting class are auxetic materials. They have negative Poisson's ratios. In other words, the longitudinal elongation in one direction is accompanied by an elongation in the perpendicular direction. This seemingly incredible fact results from special internal structure of materials and can arise in different crystals as well as in specially designed structures (Liu et al. 2010; Ugbolue et al. 2012; Zhou et al. 2013; Rant et al. 2013, 2014).

Finally, the last issue of this paragraph is related to a special type of deformation, namely, the twist of a fiber. The effect can be realized by an applied torque (Fig. 10.6). There are several conventions and quantities describing the underlying effects.

First of all, the angular strain γ, or twist, is a response to the applied moment of force T, the torque. Thus, the underlying relation, again mathematically similar to Hooke's law, is as follows:

Fig. 10.5 The shear and bulk moduli as functions of the Poisson's ratio. The moduli are determined by the Poisson's ratio and Young moduli E. Here, for simplicity, E equals 1. Plain woven fabrics have usually Poisson's ratio values in the range of 0.2–0.6, and auxetic materials have negative values
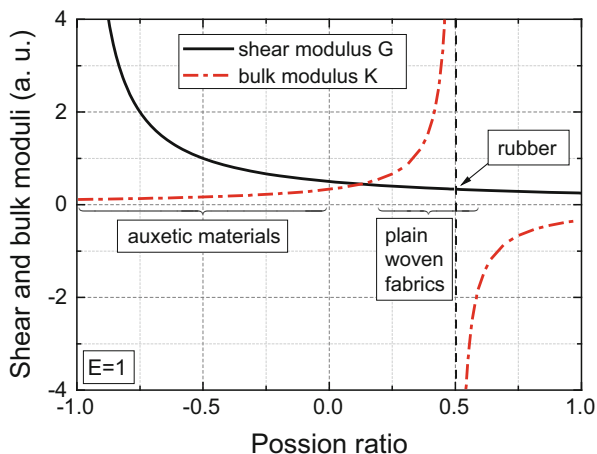
Fig. 10.6 The twist of the cylindrical fiber of length l measured by the angle γ, with the point A' being shifted from its initial position at A. The bottom base of the fiber is fixed
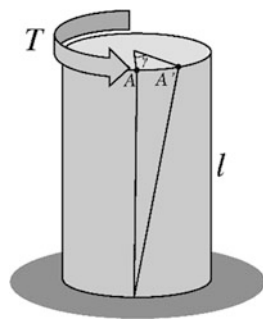
$$T = \frac{J\,G}{l}\gamma,$$

where G is the shear modulus (shear effects also occur in twist), l is the fiber length, and J is the so-called torsional constant which is dependent on the fiber cross-section shape. For a circular cross section, $J = 0.5\,\pi \cdot r^4$, with the fiber cross-section radius r. There are some additional conventions related to the formulas above; e.g., the product $J \cdot G$ is the torsional rigidity, while $(J \cdot G)/l$ is the torsional stiffness.

From the perspective of elastic properties, real textile materials are complicated physical systems (King et al. 2005; Gao and Wang 2015) with great number of interconnections, weavings, internal friction effects, and correlated deformations (Fig. 10.7). For such systems, an important parameter during elasticity experiments is the angular orientation of the in-plane elongation direction with respect to any main high-symmetry direction of the textile sample, for example, related to the direction of warp or weft (Penava et al. 2014). For example, the Poisson's ratios measured in the range of in-plane angles between 0° and 90°, for cotton, wool, wool plus Lycra, and polyester (PES), were equal to (0.57. . .0.24), (0.71 . . . 0.28), (0.07

Fig. 10.7 Plain wave fabric. The elastic properties of the structure are directional dependent
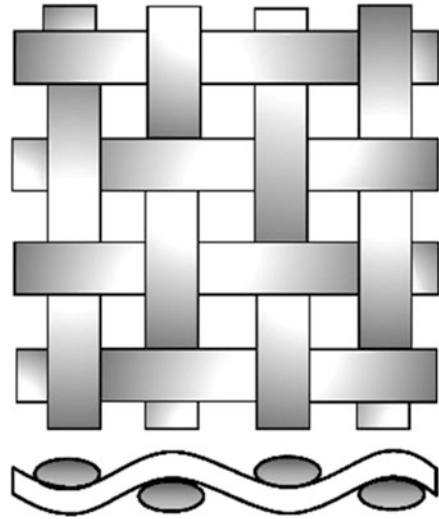
... 0.20), and (0.38 ... 0.78), respectively. The Young modulus shows a similar directional dependence. The measured values (in MPa) for the in-plane range between 0° and 45° were equal to (32.6 ... 0.8), (21.9 ... 0.2), (0.25 ... 0.08), and (5.2 ... 0.5), for cotton, wool, wool plus Lycra, and polyester (PES), respectively.

10.2   Measuring Elastic Properties

One of the most important instruments to measure elastic properties of textiles and other materials is a so-called universal testing machine, as depicted in Fig. 10.8. It consists of a stable base and head plate, connected by guide pillars (not shown here), including a vertically moving traverse which is guided along elevating screws. The (textile) sample is clamped in sample holders, one of which is connected with a load cell which measured the force related to a defined displacement of the moving traverse. If a single fabric is fixed in the sample holder and elongated, the resulting curve gives the stress-strain relation of the respective material.

Such stress-strain measurements are described in different standards, e.g., EN ISO 2062 and EN ISO 13934-1 for woven fabrics or EN 29073-3 for nonwovens, which differ as a function of the desired tests and the materials under examination. One example of the resulting curves is given in Fig. 10.9.

Here, the universal testing machine was used to stretch the samples under examination from a relaxed state until a defined maximum elongation was reached. Afterward, the elongation was reduced to zero again. This procedure can be

Fig. 10.8 Universal testing machine, used for measurement of elastic and other properties of textile fabrics
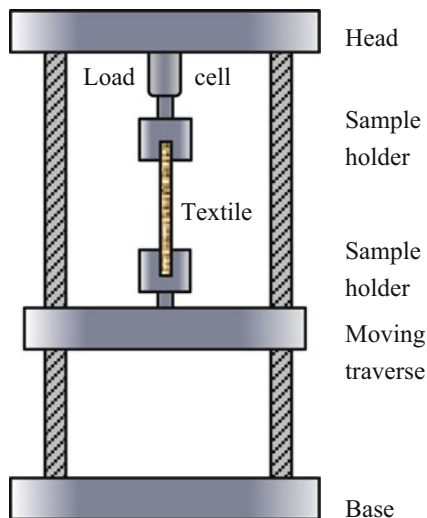
Fig. 10.9 Stress-strain measurement, applied on a pure polymer film and a polymer coating of identical thickness on a knitted fabric
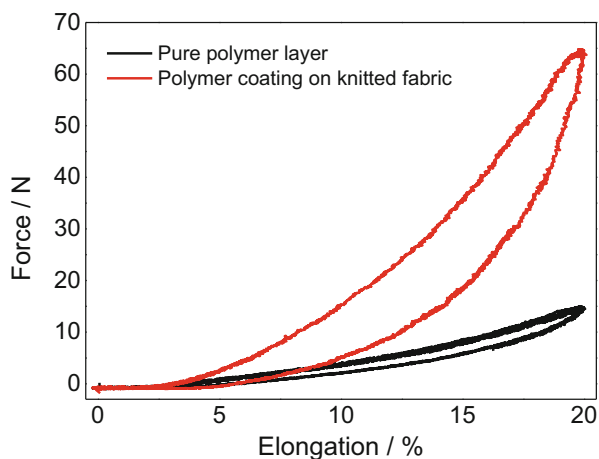
repeated several times to allow for investigation of a possible training effect, i.e., a difference between the first loops and the following ones.

In Fig. 10.9, a significant hysteresis loop is visible, especially in case of the polymer coating on a knitted fabric. This means that the elongation and the relaxation processes behave differently, in other words, the samples wear out. Continuing these measurements can thus give an insight into the "wearing out" of elastic textiles, such as knitted fabrics or samples containing elastic materials like elastane. This relaxation process is important to be investigated not only for garments but also for elastic technical textiles.

Examinations of nonelastic textiles (especially woven fabrics and nonwovens, but also yarns or fibers) are usually performed until the sample breaks (Fig. 10.10).

Fig. 10.10 Stress-strain measurement on a woven fabric until (partial) failure
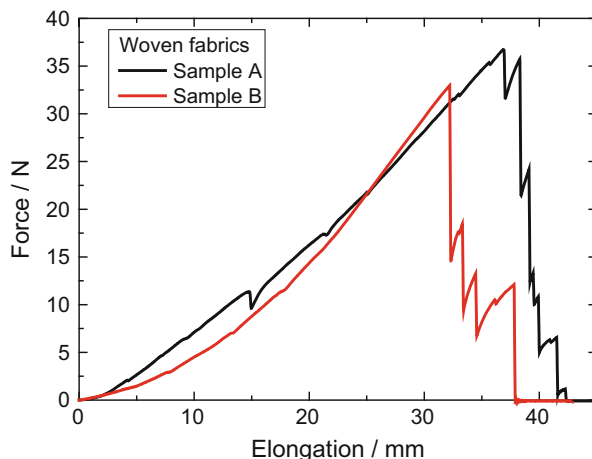
In this way, breaking forces and elongations at break can be measured as well as the elastic modulus which is defined as

$$E = \frac{\Delta\sigma}{\Delta\varepsilon},$$

i.e., as the slope of the stress-strain curve in the elastic part at the beginning of the elongation process, before plastic deformation starts.

In a similar way, the seam resistance (or seam slipping resistance) of fabrics can be examined by a universal testing machine. The force-travel diagram of a specimen which is fixed in the clamps of a universal testing machine can either be evaluated on its own or in comparison with the results of a sample prepared from the identical material without seam. In this way, the influence of the seam can exactly be determined.

The elastic properties of knitted fabrics are usually not examined using universal testing machines, but burst testers which enable isotropic stretching, so that the knitwear is elongated in all directions at the same time. This method is also useful for fabrics which are subject to stress in all directions during their use, such as filters or parachutes. Typical standards for bursting tests are ASTM D 3786, ISO 1328-2:1999, or ISO 13938-1:1999.

The working principle of a burst tester is depicted in Fig. 10.11. A rubber diaphragm with defined diameter (often 30 or 113 mm) is bulged by a fluid below. The sample clamped above will burst in a defined time range, allowing for measuring the extension and force necessary for the fabric break.

Burst tests do not work for fabrics with very high stretchability, since the diaphragm must be able to be elongated more, or for high-tenacity fabrics (e.g., from aramid or ultra-high molecular-weight polyethylene) which may destroy the diaphragm.

Liquid
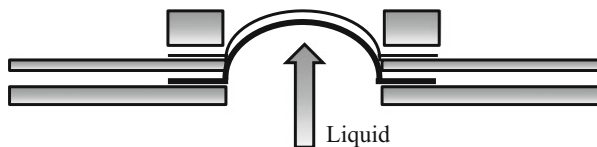
Fig. 10.11 Burst tester with rubber diaphragm (*thick black line*) stretched by a fluid below, elongating a textile fabric above (*thin black line*) isotropically

It should be mentioned that in all cases it is essential to use the correct load cell. The upper and lower values of load cells can differ significantly, with ranges of 40–2000 N which are suitable for several usual woven fabrics up to load cells which can be used for metals or down to very small forces necessary for fiber or yarn tests. Using a load cell with too small upper force will simply prohibit measuring the necessary forces, while using a load cell with too high minimum force may result in incorrect measurements.

10.3   Measuring Adhesive Forces by a Universal Testing Machine

In case of composites, it is often interesting to investigate the adhesive forces between the different materials. Textile composites can consist of fibers, woven fabrics, nonwovens, etc. impregnated with a resin matrix, of a textile and a coating, of a 3D printed polymer on a textile fabric, or of two or more textile layers which are glued together.

For this test, a sample of defined dimensions has to be prepared, e.g., of 25 mm width and minimum 150 mm length, according to DIN 53530. At one end of the composite, both materials must be separated to allow for clamping them in the sample holders. Afterward, separation forces are measured for a haul-off speed of 100 mm/min.

Figure 10.12 shows the results of adhesion force tests of nylon coatings on fabrics woven from polyester yarn. The forces are given in the unit N/cm to take into account the fabric width to which the overall force is proportional.

The evaluation of these tests occurs in different way, depending on the measurement results, as described in DIN 53539 (or in DIN 53357 in case of synthetic leather) or the newer DIN ISO 6133, dealing with the analysis of multi-peak results obtained in adhesion force measurements. In accordance with this standard, evaluation depends on the number of peaks (less than five, five to twenty, or more). The evaluation methods differ if the peaks are too tight to be counted or the curve is undulating rather than showing distinct peaks. For more than 20 peaks, e.g., nine equidistant vertical lines are introduced in the graph (cf. Fig. 10.12), and for each line, the height of the nearest peak is measured.

Fig. 10.12 Adhesion tests of different nylon coatings on polyester woven fabrics
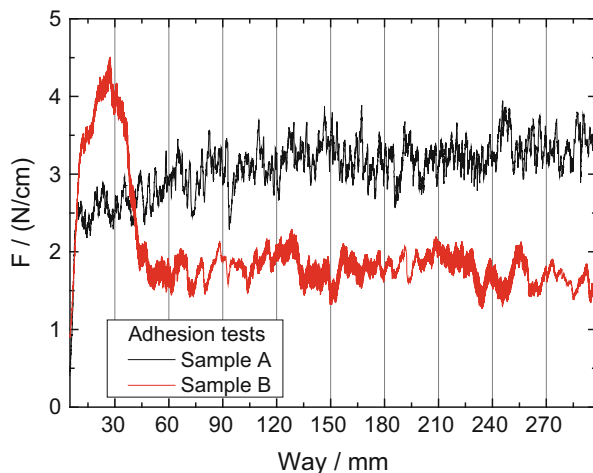
Apparently, the evaluation method can influence the results. Thus, in adhesion force test, not only the measurement itself but also the evaluation has to be performed carefully, taking into account the possible effects of the chosen method, especially if results of different groups are to be compared.

10.4   Bending Strength

Examination of the bending stiffness of textile materials is especially important for composites created from fibers, nonwovens, or woven fabrics which are impregnated by a resin. The bending stiffness, however, is also defined and in some cases important for pure textile fabrics, yarns, or fibers.

Depending on the textile object under examination, different methods are usually used and described in test standards. Often used methods are two-point, three-point, and four-point bending stiffness measurements.

The two-point bending test is correlated with ISO 2493-1, DIN 53121, and ISO 5628. It can be used to evaluate paper and cardboard, but also for (coated) textile materials (Fig. 10.13).

In the two-point bending test, a specimen is clamped on one side, while the other end of the sample is subject to a vertical force. The loading pin transferring the force is not fixed on a certain position of the textile but can glide over it.

This method can also be used to examine the influence of folding a textile material with a defined angle using a defined force.

The three-point bending test is described in ISO 178 and ASTM D790 and sketched in Fig. 10.14. The pins are not fixed to the specimen but can horizontally glide over it. This test is normally used for rigid and semirigid plastic materials, such as textile composites. It can be used to characterize the flexural E-modulus as

Fig. 10.13 Two-point bending test on a composite
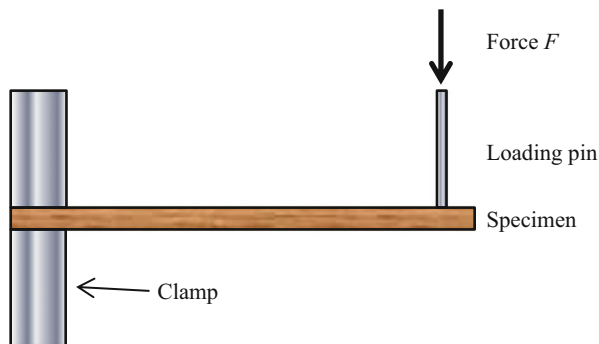
Fig. 10.14 Three-point bending test on a composite
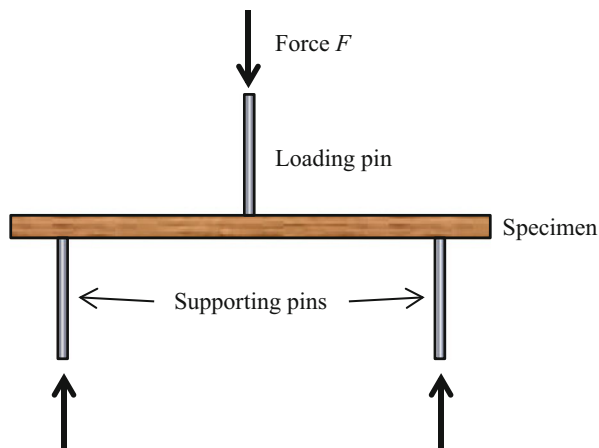
well as stress-strain relations until the specimen breaks. The three-point bending test is often carried out using a universal testing machine which exerts a force on the specimen.

In this test, the elongation of the surface is significantly greater than in the tensile tests described above, while the core of a symmetric sample stays unaltered.

In the four-point bending test (Fig. 10.15), the bending moment between both pressure points is constant, which is an advantage compared to the usual three-point bending test. On the other hand, the setup is slightly more complicated due to the second loading pin. Like in the three-point bending test, the distances between all pins are defined, but the fabric is not fixed to them.

Another method of investigating the bending stiffness of a textile fabric is given by joining two opposite sides of a rectangular sample to obtain a tubular specimen and compressing this tube using a universal testing machine (Pan et al. 1993).

For all of these methods, it should be mentioned that specifying the method used, either by indicating the respective standard or describing the experiment, is important to allow generating reliable and reproducible results.

Fig. 10.15 Four-point
bending test on a composite
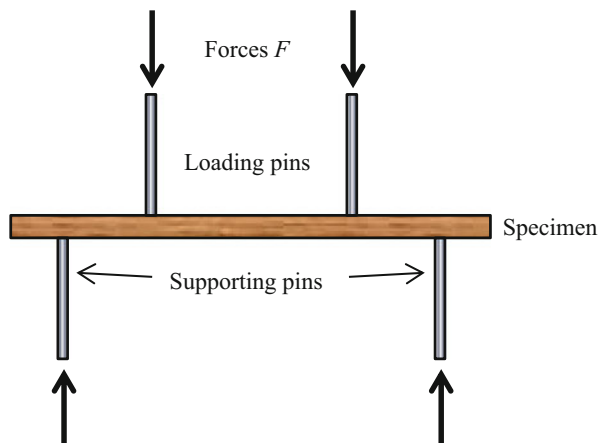
While the aforementioned methods concentrate on textile fabric or composites, the bending behavior of yarns is usually measured by clamping the yarn horizontally, as in the two-point bending stiffness experiment, and analyzing the shape of the curvature which is formed due to its own weight. This procedure can be performed for different yarn lengths, resulting in different relations between load and deflection due to a strongly nonlinear bending behavior (Cornelissen and Akkerman 2009).

10.5   Drape and Drapability of Textile Fabrics

The drapability of textile is defined as the possibility to apply fabrics wrinkle-free on free-dimensional geometries (Denninger 2009). Depending on the planned application of the textiles, the test methods can differ. The picture frame test is often used to detect the critical shear angle characterizing the start of undesired wrinkling (Christ et al. 2012). Especially for architectural textiles, e.g., a test setup was developed using curved bowls of radii 300 mm or 1000 mm, respectively, in which test fabrics were positioned and examined for wrinkles (Eckers et al. 2012). Simulations have shown the influence of the fabric weave on the drapability (Hübner et al. 2012).

Drape can also describe the way that textile fabrics hang under their own weight which is an important parameter for the "look" of a garment and also often interesting to know for technical textiles. Besides the apparent difference in drape between woven and knitted fabrics, testing the drape can give more information about the ability of a fabric to fall freely, under its own weight.

Drape is strongly correlated with the bending stiffness of textiles and can be tested, e.g., by the Cusick drape tester which is sketched in Fig. 10.16. A sample of defined dimensions – chosen after a pretest in dependence on its drape properties – is clamped between two horizontal disks of defined diameter. The sample's shadow
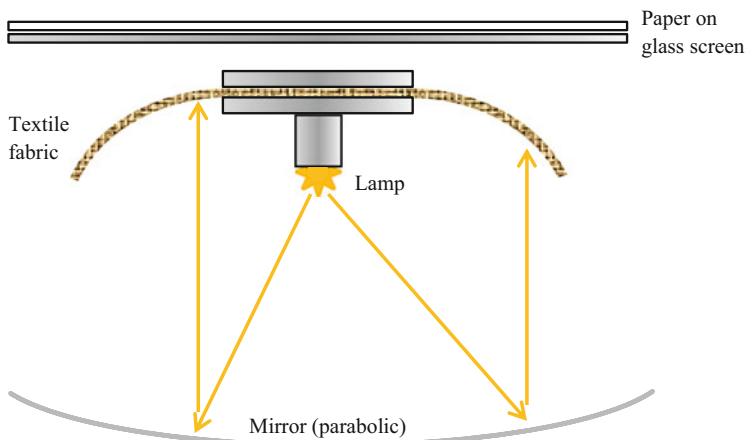
Fig. 10.16 Drape tester according to EN ISO 9073-9

due to illumination with parallel light is projected onto a piece of paper where the ratio of dark and light areas is calculated, either using a planimeter, cutting and weighing the shadow ring (Cusick 1968), or using an optical system and image analysis software (Behera and Pangadiya 2003). Details are described in EN ISO 9073-9. However, in all cases the method used must be mentioned since different definitions of the drape coefficient exist (Jeong 1998; Frydrych et al. 2003).

10.6 Compressibility of Textile Materials

Textile fabrics are often compressible. This means that they change their thickness, dependent on the vertical force applied on them.

The thickness of a textile material, however, is an important parameter often used for its description, similar to the mass per unit area. Thus, several thickness measurement devices are commercially available, testing textile thickness according to (or based on) EN ISO 5084. In this standard, a stamp with diameter 50.2 mm is used to impose a pressure of 1 kPa on the textile under examination. Special textiles, such as certain warp knitted fabrics or roughened woven fabrics, are suggested to be loaded with only 0.1 kPa.

The compressibility is described, e.g., in DIN 53885 as the difference of the thicknesses, measured using pressures of 0.2 and 2 kPa. It occurs in literature especially with respect to spacer fabrics (weft or warp knitted) (Rieder et al. 2009; Sheikhzadeh et al. 2010; Haupt et al. 2011; Liu et al. 2012a, b), but also to usual knitted fabrics (Chung et al. 2013) or even yarns (Jaouadi et al. 2009) and fiber assemblies (van Wyk 1946; Eggert and Eggert 1925; Beil and Roberts 2002).

The influence of the pressure on the measured thickness is depicted in Fig. 10.17 for two weft knitted samples of different thickness. Even in such "normal" fabrics, a

Fig. 10.17 Thickness
measurements performed
using a device according to
EN ISO 5084 under
different pressures
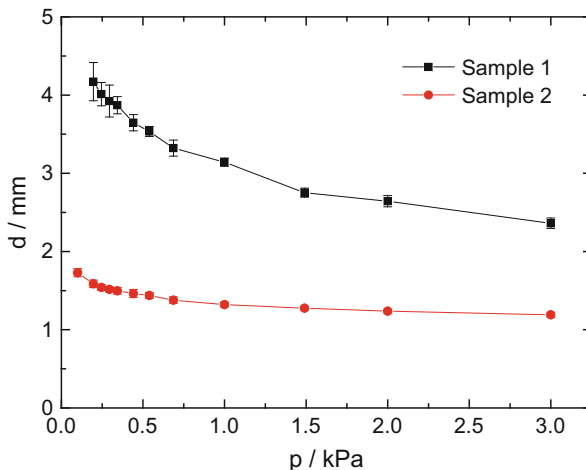
significant dependence of the measured thickness on the pressure is visible. For
thicker – and more open-pore – fabrics, this effect is stronger. Here, nearly a factor
of two between the thickness values measured with highest and lowest pressure is
visible for the relatively thick fabric "sample 1"; however, even for the thinner and
more compact fabric "sample 2," the thickness measured using a typical pressure of
1 kPa is significantly reduced in comparison with the thickness extrapolated to a
pressure of 0 kPa.

Apparently, examination of fabric thickness according to EN ISO 5084 can still
cause misleading results.

A special case occurs if measurements of the textile fabric thickness are
performed on the one hand with a textile testing instrument based on EN ISO
5084 and on the other hand with a simple micrometer gauge, as it is used for
examinations of the thickness of rigid materials.

Figure 10.18 depicts both processes and the measured thicknesses: While the
textile testing device measures a fabric thickness of 0.95 mm (this value is reduced
to ~0.88 mm using an additional load), the micrometer gauge measures only
0.54 mm. Using both instruments on rigid samples, such as a piece of paper or a
metal sheet, they give identical values.

Apparently the distinctly smaller measurement area of the micrometer gauge
results in examination of a "local" thickness which may be significantly smaller
than the "global" thickness since the latter may be influenced by the fabric stiffness,
small knobs, etc.

In most cases, this means that a micrometer gauge is no adequate alternative for
a textile thickness measurement instrument. Nevertheless, there are situations in
which the micrometer gauge results make more sense to be used: if the thickness
value is necessary for a finishing process on the respective textile which also works
only on small spots of the fabric, such as 3D printing on a textile, then adjusting the

Fig. 10.18 Thickness measurements on the same fabric using a device based on EN ISO 5084 (*left panel*) and a usual micrometer gauge (*right panel*)

nozzle height with respect to the fabric height should be based on the micrometer gauge value.

Literature

Ajeli, S., Jeddi, A.A.A.: Geometrically Poisson's ration of the polyester double-bar warp-knitted structures on the jamming point. J. Text. Polym. **2**, 24 (2014)

Behera, B.K., Pangadiya, A.: Drape measurement by digital image processing. Text. Asia **34**, 45–50 (2003)

Beil, N.B., Roberts Jr., W.W.: Modeling and computer simulation of the compressional behavior of fiber assemblies: Part 1: Comparison to van Wyk's theory. Text. Res. J. **72**, 341–351 (2002)

Christ, M., Sköck-Hartmann, B., Krieger, H., Hoffmeister, C., Herrmann, A.S., Gries, T.: Prüfverfahren und Methoden zur Charakterisierung der Drapierbarkeit von technischen Textilien. In: Proceedings of 13th Chemnitzer Textiltechnik-Tagung, 14–15 Mar, pp. 250–257 (2012)

Chung, S.-A., Ehrmann, A., Weber, M.O.: Accuracy of thickness measurements on knitted fabrics. Melliand Int. **19**, 32–33 (2013)

Cornelissen, B., Akkerman, R.: Analysis of yarn bending behaviour. In: Proceedings of the 17th International Conference on Composite Materials (ICCM 17). Edinburgh (2009)

Cusick, G.E.: The measurement of fabric drape. J. Text. Inst. **59**, 253–260 (1968)

Denninger, F. (ed.): Lexikon Technische Textilien. Deutscher Fachverlag, Frankfurt Main (2009)

Eckers, V., Janetzko, S., Gries, T.: Drape study on textiles for concrete applications. AUTEX Res. J. **12**, 50–54 (2012)

Eggert, M., Eggert, J.: In: Mark, H. (ed.) Beiträge zur Kenntnis der Wolle und ihrer Bearbeitung. Verlag Gebr. Borntraeger, Berlin (1925)

Frydrych, I., Dziworska, G., Matusiak, M.: Influence of the kind of fabric finishing on selected aesthetic and utility properties. Fibres Text. East. Eur. **11**, 31–37 (2003)

Gao, X., Wang, L.: Finite element modelling for tensile behavior of thermally bonded nonwoven fabric. AUTEX Res. J. **15**, 48 (2015)

Haupt, M., Janetzko, S., Berger, L., Diestel, O., Cherif, C., Gries, T., Eckstein, L.: Improvement of compressive strength of weft-knitted spacer fabrics. In: Proceedings of the Aachen-Dresden International Textile Conference (2011)

Hübner, M., Diestel, O., Sennewald, C., Gereke, T., Cherif, C.: Simulation of the drapability of textile semi-finished products with gradient-drapability characteristics by varying the fabric weave. Fibres Text. East. Eur. **20**, 88–93 (2012)

Jaouadi, M., Msahli, S., Sakli, F.: Contribution to measurement of real yarn diameter. J. Text. Inst. **100**, 158–164 (2009)

Jeong, Y.J.: A study of fabric drape behaviour with image analysis Part I: Measurement, characterisation, and instability. J. Text. Inst. **89**, 59–69 (1998)

King, M.J., Jearanaisilawong, P., Socrate, S.: A continuum constitutive model for the mechanical behavior of woven fabrics. Int. J. Sol. Struct. **42**, 3867 (2005)

Liu, Y., Hu, H., Lam, J.K.C., Liu, S.: Negative Poisson's ratio weft-knitted fabrics. Text. Res. J. **80**, 856 (2010)

Liu, Y., Hu, H., Long, H., Zhao, L.: Impact compressive behavior of warp-knitted spacer fabrics for protective applications. Text. Res. J. **82**, 773–788 (2012a)

Liu, Y., Hu, H., Zhao, L., Long, H.: Compression behavior of warp-knitted spacer fabrics for cushioning applications. Text. Res. J. **82**, 11–20 (2012b)

Ning, P.: Analysis of woven fabric strengths: prediction of fabric strength under uniaxial and biaxial extensions. Compos. Sci. Technol. **56**, 311 (1996)

Pan, N., Zeronian, S.H., Ryu, H.-S.: An alternative approach to the objective measurement of fabrics. Text. Res. J. **63**, 33–43 (1993)

Penava, Ž., Penava, D.Š., Knezić, Ž.: Determination of elastic constants of plain woven fabrics by a tensile test in various directions. Fibers Text. East. Eur. **22**, 57 (2014)

Rant, D., Rijavec, T., Pavko-Cuden, A.: Auxetic textiles. Acta Chim. Slov. **60**, 715–723 (2013)

Rant, D., Ciobanu, R., Blaga, M., Pavko-Cuden, A.: Compression of foldable links-links knitted structures. Tekst. Konfeksiyon **24**, 349–355 (2014)

Rieder, O., Wiedmaier, O., Möck, W., Planck, H.: Spacer circular knit fabrics with specific physical properties. Tech. Text. **52**, E126–E127 (2009)

Sheikhzadeh, M., Ghane, M., Eslamian, Z., Pirzadeh, E.: A modeling study on the lateral compressive behavior of spacer fabrics. J. Text. Inst. **101**, 795–800 (2010)

Sun, H., Pan, N.: Shear deformation analysis for woven fabrics. Compos. Struct. **67**, 317 (2005)

Sun, H., Pan, N., Postle, R.: On the Poisson's ratios of a woven fabric. Compos. Struct. **68**, 505 (2005)

Szewczyk, W.: Determination of Poisson's ratio in the plane of the paper. Fibers Text. East. Eur. **16**, 117 (2008)

Ugbolue, S.C., Kim, Y.K., Warner, S.B., Fan, Q., Yang, C.-L., Kyzymchuk, O., Feng, Y., Lord, J.: Engineered warp knit auxetic fabrics. J. Text. Sci. Eng. **2**, e103 (2012)

van Wyk, C.M.: Note on the compressibility of wool. J. Text. Inst. **37**, T285–T292 (1946)

Zhou, M., Du, Z., Lu, G.: Textile materials and structures with negative Poisson's ratio – an overview. J. Fiber. Bioeng. Inform. **6**, 349 (2013)

Chapter 11
Stab and Cut Resistance

Nowadays attacks or threats with knives are being reported regularly. Special occupational groups, such as taxi or bus drivers and teachers, must be aware of the danger to experience such an assault themselves. Even children and young adults often use knives as weapons. Additionally, knives are also dangerous when being used as tools. Nearly half of all accidents with hand tools are stab or cut injuries due to weapons (Winkler 2005).

This is why stab- and cut-resistant textiles are typical parts of the personal body armor. This chapter gives an overview of new developments in this research area and typical measurement methods.

11.1 Stab- and Cut-Resistant Body Armor

The protective textile used to prevent people from damage caused by either weapons, i.e., knives or projectiles, or by a potentially dangerous action or environment is called personal body armor. This means that body armor has to stop knives or projectiles before hurting a person, and additionally the impact energy has to be distributed over a large area to reduce its effect on a small point on the body.

Typical body armor used by military or police is still heavy, stiff, and relatively thick and thus reduces the wearer's movements. Common cut- and stab-resistant garments to secure people from attacks and accidents are often produced from metal ring fabrics or aluminum scales (Anonymous 2003b; Mehler 2016; Heilemann 2016; Münch 2016). Especially in vests, the resistance to stab and projectile impact is often increased using inserted protective plates or multilayer aramid (Security Equipment Service 2016; Securitywelt 2016; POLAS 2016; Dagdas Projects 2016; SafeGuard Clothing 2016).

This is why recent developments concentrate on high-tenacity yarns such as aramid, ultra-high molecular weight polyethylene (UHMWPE) or glass (Alpvildiz et al. 2011; Flambard and Polo 2000; Flambard and Polo 2001, 2004;

Vidzem et al. 2013), metal wires (Anonymous 2000, 2003a, b, 2007, 2008; Rebouillat et al. 2010), or multilayer systems from different materials (Annand 2009; Thilagavathi et al. 2010).

Such textile fabrics, however, mostly aim at being integrated in gloves or are recently being investigated in basic research projects. Recent research approaches are based, e.g., on combinations of UHMWPE with shear-thickening fluid (Sun et al. 2013), optimized stacking orders (Horsfall et al. 2013), or laser sintering textile-like structures (Johnson et al. 2013).

11.2   Testing Stab and Cut Resistance

While attacks by knives are often being reported in the news and in blogs (Anonymous 2009, 2010, 2011, 2015, 2016), the details of such assaults are only given scarcely. In some cases, the impact area is depicted, e.g., the heart, back, or belly (Anonymous 2006a, b). The movement patterns or estimated forces during the attack are usually not given. Similarly, for accident-prone situations, full-body garments from metal ring fabrics are recommended (BGN 2016), while no statistical information can be found about typical cut directions and forces.

This is why cut- and stab-resistant properties of fabrics are tested according to several standards, taking into account various garments and situations of use. Stab resistance, e.g., is defined and measured differently, depending on whether gloves or jackets are tested. The following subchapters give an overview of various test procedures for different applications and their advantages and drawbacks.

11.3   Testing Gloves

Cut-resistant gloves are used to prevent the hand and fingers from cuts due to sharp tools. Most cut-resistant gloves are either prepared from metal rings or knitted from cut-resistant yarn. For the latter, para-aramid or UHMWPE yarns can be used as well as glass or steel yarns. Combinations of common knitted gloves with protective materials in the most endangered areas of the hand are also possible. Often the gloves are finally coated with polyurethane, nitrile, or other materials.

For textile gloves, the standard EN 388 integrates four different test procedures, dealing with different possible hazards, depicted by a pictogram with four numbers below given on the glove. This test is also known as coup test. The resistance to abrasion is tested using sandpaper which is abrading the material under examination with a defined pressure. The cut resistance is defined by the number of cutting cycles of a circular blade with diameter 40 mm rotating against the lateral movement at constant speed which is necessary to cut through the fabric. The tear resistance describes the necessary force to tear the sample. The puncture resistance, finally, is given by the required force to pierce the sample with a thin pin. The

highest possible rating would be 4544, with only the cut resistance being rated from 1 to 5 and the other three values from 1 to 4.

Alternatively, the ISO 13997 uses a razor blade under increasing pressure which is pushed over the sample. The distance before the blade impinges through the fabric is recorded. The blade cut tester consists of a straight blade which is drawn across the sample mounted on a curved surface. This method is similar to the US standard F1790 developed by ASTM.

While all three mentioned methods are often used, the EN 388 is most common in Europe. This can be problematic especially for hard and cut-resistant materials which tend to dull the blade, resulting in an overestimation of the test values (Vanerman 2010). It should be mentioned that not only the metallic chain mail is inappropriate for this test but also glass fabrics and other hard technical yarns, so that the ISO 13997 is mostly regarded as more accurate for high-level cut-resistant gloves.

This is one of the reasons why testing fabrics for gloves according to ISO 13997 may be better than using the EN 388. The other reason is the relative ease to build a respective test stand on one's own. The drawback, however, is the necessity to carry out a large number of different cuts, always using new blades.

In a test according to ISO 13997, a straight blade of known sharpness is fixed in a carriage which is moved horizontally over the bent fabric until the first cut is going through (Fig. 11.1). This is usually measured as an electrical contact between blade and sample holder. The pressure/force between blade and fabric can be varied. Usually, five cuts are performed using forces resulting in cut lengths between 30 and 50 mm, between 15 and 30 mm, and between 5 and 15 mm. The resulting 15 values are plotted in a graph, and an exponential fit is used to interpolate the necessary force for a cut length of 20 mm. After executing five cuts with this force, the results are added to the graph. If their average is inside the allowed value of (20 ± 2) mm, this force is the final result; else the procedure has to be repeated using the extended graph for a new estimation of the necessary force. The result of a cut test according to ISO 13997 thus is the force necessary to create a cut length of 20 mm.

Independent of the aforementioned test standards, it may make sense to develop own measurement procedures for gloves used for special applications. A universal
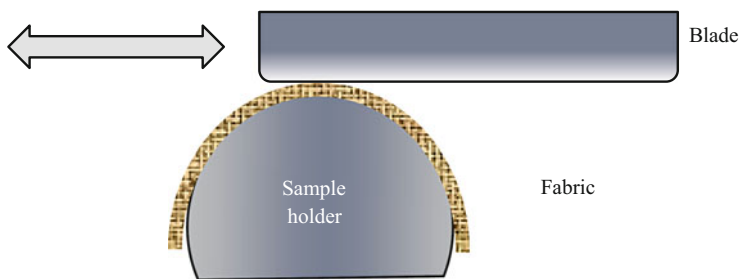
Fig. 11.1 Blade cut test according to ISO 13997, using a so-called tomodynamometer

testing machine, e.g., can be equipped with either a blade or a pair of scissors to measure force-displacement curves, showing which force is necessary to cut a fabric by a special blade or using scissors.

11.4   Testing Garments

Although mostly known for tests of gloves, both standards ISO 13997 and ASTM F1790 can also be used for other protective clothing materials, while the EN 388 is explicitly meant for gloves.

Stab resistance of garments, however, is tested by other standards which differ in some aspects. One of them is the HOSDB Body Armour Standards for UK Police (Croft and Longhurst 2007a, b, c). The HOSDB test standard aims at describing a reproducible test of stab resistance of body armor. The three parts of the standard refer to general requirements (part 1), ballistic resistance (part 2), and knife and spike resistance (part 3), the latter mostly being of interest with respect to stab resistance measurements.

Figure 11.2 depicts the general setup of the HOSDB test. The sample under examination is mounted on a composite backing material (dark gray) which is placed on an even, rigid surface (light gray). The blade (or spike) falls down onto the sample, driven by a defined weight. Knife and knife holder have a mass of 650 g and are embedded in a nylon case of 1.25 kg which decreases the friction between the falling weight and the drop tube, the latter ensuring that the knife impinges on the sample without canting or rotating. The knife holder can slide vertically inside the nylon case. In the moment of impact, it is pressed back into the case, compressing a foam disc at the upper end of the nylon case which forces it into the sample again. This damping foam has to be renewed regularly.

During falling onto the sample, the velocity of the missile is measured at 25 mm before the impact using light screens. The dimensions and tip sharpness of the blade (Fig. 11.3) are exactly defined, as well as the composite backing material which consists of a number of layers of neoprene, special foam, and rubber. Especially for preformed armor, Plasticine should be used instead. Both backing materials have to be prepared by being placed in a standard climate for 12 h.

Before testing a sample using the composite backing material, a sheet of paper can be placed between sample and backing material to enable cut length measurements. The test is performed 40 times per material, with a maximum allowed penetration of 7 mm for the lower energy used in each protection level (30 tests) and 20 mm for the higher energy of the same protection level (10 additional tests). The desired energies are reached by keeping the mass of the missile constant and changing the impact velocity by varying the falling height.

Additional tests should be performed at especially week points, such as seams, as well as at female armor. Tests using other impact angles can be added.

The Stab Resistance of Personal Body Armor NIJ Standard-0115.00 was developed jointly by the Police Scientific Development Branch of the United Kingdom

Fig. 11.2 Stab test according to the HOSDB Body Armour Standards for UK Police
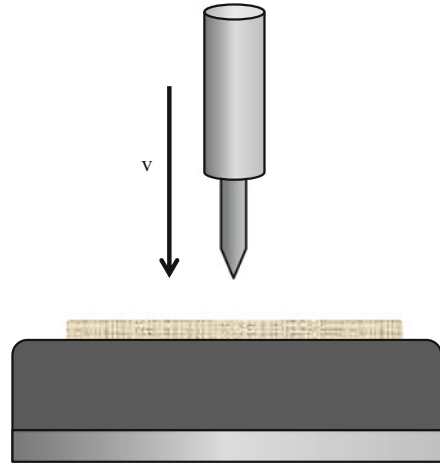
Fig. 11.3 Standard blade according to VPAM test standard KDIW 2004 and HOSDB Body Armour Standards for UK Police, placed on Plasticine backing material. From Weber et al. (2014)

and the Technical Support Working Group in the United States (NIJ 2000). Being based on the PSDB Stab Resistant Body Armor Test Procedure (Pettit and Croft 1999) which is also used as a base of the HOSDB Body Armour Standards for UK Police, the NIJ standard is quite similar to the HOSDB test procedure.

While in both aforementioned standards the backing behind the sample is usually a composite from rubber, foam, and neoprene, the VPAM test standard KDIW 2004 uses Plasticine as backing material (VPAM 2011). Additionally, the blade is fixed in a rigid metal block of a defined weight, opposite to the bicomponent missile of NIJ and HOSDB test standards (Fig. 11.4). This means that tests according to VPAM do not take into account the possible recoil of a knife during an attack, followed by a second impact, which is simulated by NIJ and HOSDB test conditions. Other parameters, such as the blades, are identical in these standards (Fig. 11.3).

Fig. 11.4 VPAM-KDIW
2004 test stand with knife in
knife holder, the latter being
mounted below an
electromagnet which holds
or releases the missile
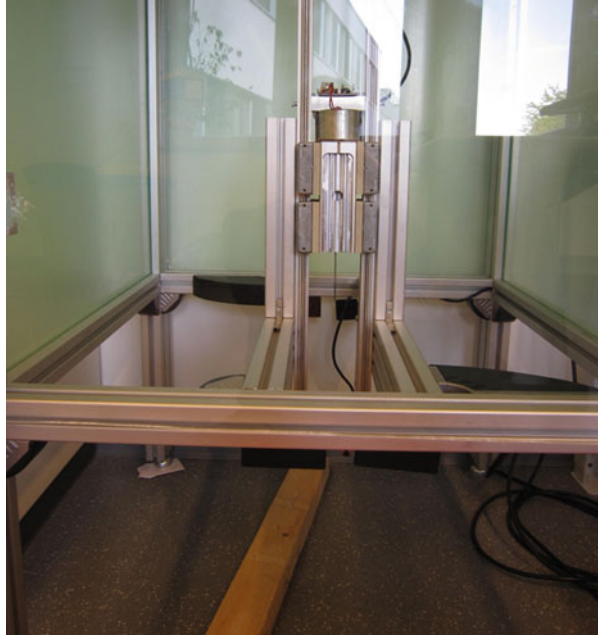
The VPAM test instructions are often used in German-language countries where most VPAM members are located (VPAM 2016).

Building a VPAM test stand on your own is easier than building a standard-conform HOSDB test stand due to the simpler construction of the missile/blade holder. On the other hand, evaluation of the test results is more time-consuming and error prone for the VPAM test. Here, it is necessary to measure the penetration depth by more sophisticated methods than in the HOSDB standard with composite backing.

The cut depth in the Plasticine cannot be measured reliably by putting a blade into the channel until a stronger resistance is detectable, as suggested in the HOSDB standard for the composite backing. In the Plasticine block, the friction between blade and backing material is too high, resulting in significant changes of the stab channel.

Grouting the channel with a fast-drying resin is in principle possible but results in potential contamination of the Plasticine. Additionally it cannot be guaranteed that the resin depicts the complete penetration channel since filling the channel may be hampered by small Plasticine lumps inside.

A more reliable procedure is digging out the penetration channel. For this, after the test, a large hole is cut into the Plasticine with a knife, and the channel is excavated by cutting further thin layers away until the mark of the tip of the blade becomes visible (Fig. 11.5). In this way, the whole penetration channel is observable, and possible contaminations (e.g., by undesired air bubbles in the Plasticine)

Fig. 11.5 Digging out the penetration channel in the Plasticine after a VPAM-KDIW test
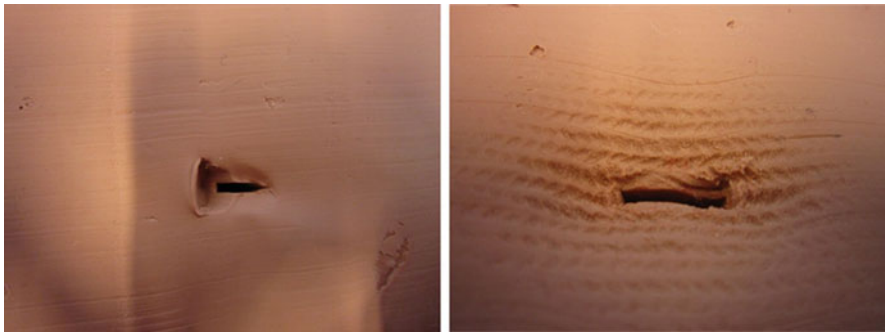
Fig. 11.6 Cuts in Plasticine surface after VPAM-KDIW tests with paper (*left panel*) and a knitted fabric (*right panel*)

can be detected. The length of the stab channel can now be measured between Plasticine surface and tip mark.

While the HOSDB uses a "witness paper" between sample and composite backing to verify the measured penetration depth by comparison with the cut length, the length of the cut on the Plasticine surface is not suggested to be measured in the VPAM-KDIW 2004.

Figure 11.6 depicts cuts in the Plasticine surface after VPAM-KDIW tests with paper and a knitted fabric, respectively. While the relatively rigid bundle of paper sheets shifts the knife laterally during the stab test which can be recognized by the displaced material on the left side of the cut, cutting through the knitted fabric results in a slight deformation of the surface. In both cases it is nevertheless possible to measure the cut length. More complicated situations can arise when the fabrics

under investigation are strongly elongated during the test, resulting in a deep trauma ("valley" in the Plasticine) before the actual penetration channel starts.

Former investigations, however, have shown that also for measurements with Plasticine as backing material, it can be helpful to measure the cut length in addition to the penetration depth. In this way, strong deviations due to misinterpretations of the stitch channel can be recognized easily (Aumann et al. 2013).

The former ISO/DIS 14876-3:1999 (Protective clothing-Body armour-Part 3: Knife stab resistance) and ISO/DIS 14876-4:1999 (Protective clothing-Body armour-Part 4: Needle and spike stab resistance) were firstly replaced by ISO/DIS 14876-3:2002 and afterward withdrawn; thus they cannot be used anymore. These standards were more similar to the VPAM test standard while also containing several ideas of HOSDB and NIJ standards.

Literature

Alpvildiz, T., Rochery, M., Kurbak, A., Flambard, X.: Stab and cut resistance of knitted structures: a comparative study. Text. Res. J. **81**, 205–214 (2011)

Annand, S.: Knitted fabrics to resist slashes. Knitting Int. **1375**, 36–39 (2009)

Anonymous: Insert deflects stabs. High Performance Text., 4–5 Feb 2000

Anonymous: Safer from cuts. Adv. Text. Techn., April (2003a)

Anonymous: Berufsgenossenschaftliche Regeln für Sicherheit und Gesundheit bei der Arbeit, BGR 196: Benutzung von Stechschutzbekleidung (2003b)

Anonymous: Täter nach Messerattacke noch flüchtig, ORF.at 29.1.2006. http://ooe.orf.at/stories/86105/. Last Accessed 2 July 2016 (2006a)

Anonymous: 20 Jahre Haft nach tödlicher Messerattacke, ORF.at 19.6.2006 (a). http://noe.orf.at/stories/116832/. Last Accessed 2 July 2016 (2006b)

Anonymous: Composite yarn offers more comfortable cut-resistance. Adv. Text. Tech., Juli 2007, 6–7

Anonymous: Latest cut-resistant gloves push quality standards to the limits. Tech. Text. Int. **17**, 29 (2008)

Anonymous: Mann verletzt aufgefunden, BZ Berlin 3.5.2009. http://www.bz-berlin.de/bezirk/neukoelln/mann-verletzt-aufgefunden-article445524.html

Anonymous: Mann sticht in Suchtklinik drei Menschen nieder, News.de 9.7.2010 http://www.news.de/schlaglichter/855064609/mann-sticht-in-suchtklinik-drei-menschen-nieder/1/. Last Accessed 2 July 2016

Anonymous: Mann schleppt sich mit Stichverletzungen in Haus, Berliner Morgenpost 2.7.2011. http://www.morgenpost.de/berlin/polizeibericht/article1689502/Mann-schleppt-sich-mit-Stichverletzungen-in-Haus.html. Last Accessed 2 July 2016

Anonymous: Der Mann, der den Attentäter von Köln stoppte. http://www.welt.de/politik/deutschland/article147770143/Der-Mann-der-den-Attentaeter-von-Koeln-stoppte.html. Last Accessed 2 July 2016, 19.10.2015

Anonymous: Haftbefehl nach Messerattacke in Dortmunder Kaufhof, 21-05-2016. http://www.derwesten.de/staedte/dortmund/haftbefehl-nach-messerattacke-in-dortmunder-kaufhof-id11846298.html. Last Accessed 02-07-2016

Aumann, S., Ehrmann, A., Vidzem, B., Brücken, A., Weber, M.O., Bache, T.: Comparison of penetration depth and cutting width in stab protection measurements according to VPAM. In: Proceedings of Aachen-Dresden International Textile Conference, Aachen, 28–29 Nov 2013

BGN – Berufsgenossenschaft Nahrungsmittel und Gastgewerbe: BGN-Sicherheitstipp: Sicherer Umgang mit Messern. https://www.bgn.de/446/54781/1. Last Accessed 02-07-2016

Croft, J., Longhurst, D.: HOSDB Body Armour Standards for UK Police (2007), Publication No. 39/07/A, Home Office Scientific Development Branch, ISBN: 978-1-84726-424-4 (2007a)

Croft, J., Longhurst, D.: HOSDB Body Armour Standards for UK Police (2007), Publication No. 39/07/B, Home Office Scientific Development Branch, ISBN: 978-1-84726-425-1 (2007b)

Croft, J., Longhurst, D.: HOSDB Body Armour Standards for UK Police (2007), Publication No. 39/07/C, Home Office Scientific Development Branch, ISBN: 978-1-84726-426-8 (2007c)

Dagdas Projects – Polizeibedarf. http://polizeibedarf-dagdas.de/artikeldetails/kategorie/einsatzwesten-chest-rigs-zubehoer/artikel/ballistische-sk1-einlagen-schutzplattengroesse.html. Last Accessed 03-07-2016

Flambard, X., Polo, J.: Stab resistance of multi-layers knitted structures – (Comparison between para-aramid and PBO fibers). J. Adv. Mater. 36, 30–35 (2004)

Flambard, X., Polo, J.: Fibres for facing sharp and pointed weapons in textile structures (Comparison between para-aramid and PBO fibres), Sustainability and Recycling of Textile Materials. In: Proceedings of the Spring Meeting of Fibre Society, University of Minho/Portugal 17–19 May 2000

Flambard, X., Polo, J.: Stab resistance of knitted structures for protective clothing applications (Comparison between para-aramid and PBO fibres), Techtextil Symposium 2001. 2. New Textiles – New Technologies, Frankfurt am Main 23–26 Apr 2001

Friedrich Münch GmbH & Co. KG: Niroflex. http://www.niroflex.de/index.php?page=schuerzen-boleros-2. Last Accessed 02-07-2016

Heilemann Sicherheitstechnik GmbH: Euroflex-Products. http://www.euroflex-safety.de/en/Produkte/. Last Accessed 02-07-2016

Horsfall, I., Watson, C.H., Champion, S.M.: Optimizing the stacking sequence in dual-purpose body armors. J. Appl. Mech. – Trans. ASME 80, 031901 (2013)

Johnson, A., Bingham, G.A., Wimpenny, D.I.: Additive manufactured textiles for high-performance stab resistant applications. Rapid Prototyping J. 19, 199–207 (2013)

Mehler Law Enforcement. http://www.mehler-law-enforcement.de/index.php?id=85&L=1. Last Accessed 02-07-2016

NIJ – National Institute of Justice: Stab Resistance of Personal Body Armor, NIJ Standard–0115.00 (2000)

Pettit, M.J., Croft, J.: PSDB Stab resistance standard for body armour (1999). Police Scientific Development Branch, Publication No 6/99 (1999)

POLAS Polizeiausrüstung und Sicherheitsbedarf: http://www.polasonline.de/Schutzwesten-ballistische-Schutzausruestung/Stichschutz. Last Accessed 03-07-2016

Rebouillat, S., Steffenino, B., Miret-Casas, A.: Aramid, steel, and glass: characterization via cut performance testing, of composite knitted fabrics and their constituent yarns, with a review of the art. J. Mat. Sci. 45, 5378–5392 (2010)

SafeGuard Clothing: http://www.safeguardclothing.de/27-stichschutzweste-body-armor. Last Accessed 03-07-2016

Security Equipment Service: http://police-shop.com/shop/de/Schutzwesten/Stichhemmende-Unterziehweste. Last Accessed 03-07-2016

Securitywelt: https://www.securitywelt.de/Westen. Last Accessed 03-07-2016

Sun, L.L., Xiong, D.S., Xu, C.Y.: Application of shear thickening fluid in ultra high molecular weight polyethylene fabric. J. Appl. Polym. Sci. 129, 1922–1928 (2013)

Thilagavathi, G., Rajendrakumar, K., Kannajan, T.: Development of textile laminates for improved cut resistance. J. Eng. Fib. Fabrics 5, 40–44 (2010)

Vanerman, S.: Cut Resistance: What's in a Level 5 Glove? EHS Today 01-02-2010. http://ehstoday.com/ppe/news/cut-resistance-whats-level-glove-7862. Last Accessed 03-07-2016

Vidzem, B., Aumann, S., Heimlich, F., Werner, R., Ehrmann, A., Obermann, M., Brücken, A., Weber, M.O., Bache, T.: Comparison of penetration depth and cutting width in stab protection

measurements according to VPAM. In: Proceedings of Aachen-Dresden International Textile Conference, Nov 28–29 2013

VPAM – Vereinigung der Prüfstellen für angriffshemmende Materialien und Konstruktionen: Prüfrichtlinie Stich- und Schlagschutz, VPAM-KDIW 2004 (2011)

VPAM – Vereinigung der Prüfstellen für angriffshemmende Materialien und Konstruktionen: Website http://www.vpam.eu/. Last Accessed 09-07-2016

Weber, M.O., Aumann, S., Brücken, A., Ehrmann, A., Bache, T.: Stab resistant knitted clothing. In: Proceedings of 8. Aachen Dresden Textile Conference, Dresden 27–28 Nov 2014

Winkler, F.-G.: Neue BG-Regeln zu Stechschutz – Hilfestellungen und Nutzen für die Praxis, sicher ist sicher – Arbeitsschutz aktuell 9, pp. 380–381 (2005)

Index